UNIVERSITY OF ST. ANDREWS

Thesis Copyright Declaration Form.

A UNRESTRICTED

"In submitting this thesis to the University of St. Andrews I understand that I am giving permission for it to be made available for public use in accordance with the regulations of the University Library for the time being in force, subject to any copyright vested in the work not being affected thereby. I also understand that the title and abstract will be published, and that a copy of the work may be made and supplied to any bona fide library or research worker."

B RESTRICTED

"In submitting this thesis to the University of St. Andrews I wish access to it to be subject to the following conditions:

for a period of years [maximum 5] from the date of submission the thesis shall be

a) withheld from public use.

b) made available for public use only with consent of the head or chairman of the department in which the work was carried out.

I understand, however, that the title and abstract of the thesis will be published during this period of restricted access; and that after the expiry of this period the thesis will be made available for public use in accordance with the regulations of the University Library for the time being in force, subject to any copyright in the work not being affected thereby, and a copy of the work may be made and supplied to any bona fide library or research worker."

Declaration

I wish to exercise option A [i.e. A, Ba or Bb] of the above options.

Signature DOROTHY A. GRAHAM Date 7/8/1982

To Dad.

Studies of the Temperature Dependence of Phosphorescence of Molecules in Rigid Systems.

A thesis

presented for the degree of

DOCTOR OF PHILOSOPHY

in the Faculty of Science of the

University of St. Andrews

by

Dorothy A. Graham

October 1981

University of St. Andrews

DECLARATION

I declare that this thesis is my own composition, that the work of which it is a record has been carried out by me, and that it has not been submitted in any previous application for a Higher Degree.

This thesis describes results of research carried out at the Department of Chemistry, University of St. Andrews, under the supervision of Dr. T. M. Shepherd since October 1st 1978.

Dorothy A. Graham

CERTIFICATE

I hereby certify that Dorothy A. Graham has spent eleven terms of research work under my supervision, has fulfilled the conditions of Ordinance No. 12 (St. Andrews) and Resolution of the University Court, 1967, No. 1 and is qualified to submit the accompanying thesis in application for the degree of Doctor of Philosophy.

T. M. Shepherd

Director of Research

ACKNOWLEDGEMENTS

I would like to thank Dr. T. M. Shepherd for his help and encouragement during the course of this work, Mr. Alistair J. Cairns for his patience and assistance with the microcomputer and the technicians in the department who have always been efficient, friendly and reliable.

I am indebted to the Science Research Council for a grant to finance this work and to Professor Lord Tedder and Professor P. A. H. Wyatt for providing the research facilities.

Finally I thank my family and all my friends for their loyalty and for the help they have given me on so many occasions.

CONTENTS

ABSTRACT

The phosphorescence decays of 1-bromonaphthalene, 2-bromonaphthalene, 9-bromophenanthrene and benzil in poly(methylmethacrylate), PMMA, matrices are shown to be non-exponential at temperatures above 300K. The temperature dependence of the second order of the decay is interpreted in terms of triplet-triplet annihilation caused by triplet energy transfer between the repeat units of the polymer chain. The temperature dependence of the first order component is shown to be independent of the nature of the solute molecule.

The possibility of photoreduction of the aromatic ketones, benzil, benzophenone and anthraquinone in PMMA matrices is investigated and mechanisms are proposed for the reactions, supported by phosphorescence decay data. In all cases emission from a photoproduct could explain the non-exponential decay above 190K.

The temperature dependence of the ^5D_o Eu^{3+} level in crystalline hexafluoroacetylacetonate and benzoyltrifluoroacetylacetonate chelates is rationalized by thermal depopulation to a lowlying ligand level. Evidence in support of energy transfer to both singlet and triplet ligand levels, depending on the nature of the cation, is presented in this thesis.

CHAPTER 1

INTRODUCTION

A useful definition of photochemistry has been given by Wayne[1] which states, "Photochemistry is the study of interaction between light and matter and is concerned both with chemical changes brought about by the absorption of light and with emission of radiation from energy rich species."

The present understanding of photochemistry owes much to Grotthus and Draper who, in the 19th century, realized that only light absorbed by a species could be effective in producing a photochemical change.

Another concept of major importance, which was introduced by Einstein, is that of quantum yield or quantum efficiency, ϕ. Since photochemistry has become so diversified ϕ has obtained a variety of definitions which are discussed in books by Wayne[1], Parker[2] and Calvert[3]. To avoid confusion one should always indicate the type of quantum yield which is being discussed, emission, decomposition, rearrangement etc. For example the quantum yield of emission is given by:-

$$\phi = \frac{\text{number of quanta emitted by a particular state}}{\text{number of quanta absorbed by the ground state}}$$

Development of atomic and molecular orbital theory made it

possible to rationalize many of the photochemical concepts which had been developed experimentally. Indeed the majority of current photochemical theory has been derived from consideration of atomic and molecular orbitals.

Atomic orbitals and energy levels

The wavefunctions, Ψ , of the atomic orbitals of a single-electron atom (or ion) can be determined by solving the Schrodinger equation,

$$H\Psi = E\Psi$$

where E = the energy of the particular wavefunction and H = the Hamiltonian operator. The Hamiltonian operator for the internal energy of the hydrogen atom is:-

$$H = -\frac{\hbar^2}{2m}\left(\frac{\partial^2}{dx^2} + \frac{\partial^2}{dy^2} + \frac{\partial^2}{dz^2}\right) - \frac{e^2}{r}$$

$$= -\frac{\hbar^2}{2m}\nabla^2 - \frac{e^2}{r}$$

and the Schrodinger equation has the form:-

$$\left(\frac{\hbar^2\nabla^2}{2m} + \frac{e^2}{r}\right)\Psi = -E\Psi$$

where m = the reduced mass of the hydrogen atom and r = the distance between the nucleus and the electron.

Only certain values of E permit solution to this equation and

these are given by:-

$$E_n = - \frac{2\pi^2 m\ e^4}{n^2 h^2}$$

where n = 1,2,3... the most stable state has n = 1 and an energy of -13.53 electron volts - the ionization potential of the hydrogen atom. As n increases the spacing between the energy levels approaches zero.

These energy levels are consistent with relationships which were previously derived empirically by spectroscopists who had investigated the emission lines in the spectrum of atomic hydrogen. For example, in 1885 Balmer observed a set of lines which obeyed the relationship:-

$$\frac{1}{\lambda} = R\left(\frac{1}{2^2} - \frac{1}{n^2}\right)$$

where λ = the wavelength of the line, n = an integer and R is known as the Rydberg constant. The lines correspond to transitions from levels $E_{n>2}$ to E_2. Other series were discovered by Lyman, Paschen, Brackett and Pfund which have been shown to be due to transitions from higher levels to E_1, E_3, E_4 and E_5 respectively.

Solution of the Schrodinger equation also shows that, with the exception of E_1, the energy levels are degenerate and provides information on the radial distribution of the electrons. This provides the basis for atomic quantum numbers. In a hydrogen-like atom the electron can be described using three quantum numbers:-

n - the principal quantum number, values 1,2,3...

ℓ - the azimuthal quantum number, values 0,...n

m_l - the magnetic quantum number, values $-l....+l$.

n represents the shell in which the electron is to be found; l defines the orbital angular momentum of the electron (which has the value $\sqrt{l(l+1)}h/2$) and hence the type of orbital. l=0,1,2,3 correspond to s,p,d and f electrons respectively; m_l defines the quantized direction of the orbital angular momentum vector in space.

A further electronic quantum number arises, not from the Schrodinger equation, but from relativistic quantum mechanics. This is the spin quantum number, m_s, which defines the two possible spin states of an electron.

m_s - the spin quantum number, values $\pm 1/2$

The Pauli exclusion principle states that no two electrons in a given atom may have the same four quantum numbers (n,l,m_l,m_s).

In atoms with more than one electron the Schrodinger equation cannot be solved exactly because of the introduction of interelectronic repulsion terms. The nature of the various energy levels which may arise from a multielectron atom may, in many cases, be simply derived using the Russell-Saunders coupling approximation. This introduces the concept of quantum numbers for the entire atom which are derived from the electronic quantum numbers of the individual electrons. The approximation is the premise that the individual electronic quantum numbers remain good for a multielectron atom. This is acceptable for atoms with atomic number, Z, $\leq$ 30.

In this approximation the values of the individual spin and angular momenta of the electrons are combined to give atomic spin and angular momenta. They are denoted as follows:-

L - the total orbital angular momentum, which is the vector sum of l for the individual electrons.

S - the total spin angular momentum, which is the vector sum of m_s for the individual electrons.

Conventionally both L and S only take positive integer values. Since these momentum vectors are spacially quantized the atomic quantum numbers, M_L and M_S, are used to indicate the direction of the vectors

M_L - takes integer values -L,...,+L

M_S - takes integer values -S,...,+S

States with L = 0,1,2,... are known as S,P,D... states analogous to atomic orbitals.

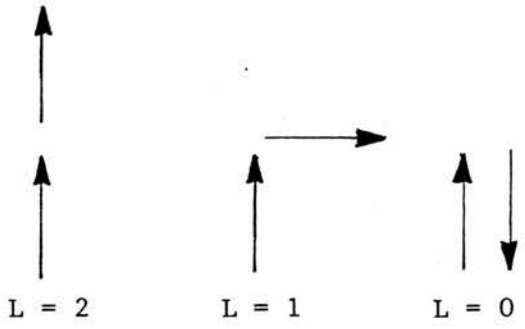

Figure 1.1 Combination of orbital angular momentum of two electrons each with l = 1 to give total angular momentum L.

The energy states defined by L and S can be further split by interactions between the magnetic fields due to the spin momentum of one electron and the orbital momentum of another. This is spin-orbit coupling and requires the use of a further atomic quantum number, J.

J takes the value of the vector sum of L and S i.e. L+S, L+S-1,...,L-S.

The extent of the splitting caused by spin-orbit coupling is dependent upon the nature of the nucleus and increases with Z, the atomic number. Generally for atoms with $Z \leq 30$ this splitting is small in comparison with the differences in the energy states caused by interelectronic repulsion.

The energy states of an atom are defined by the nomenclature:-

$$^{2S+1}L_J \quad \text{e.g.} \; ^3F_2$$

where 2S+1 is the spin multiplicity.

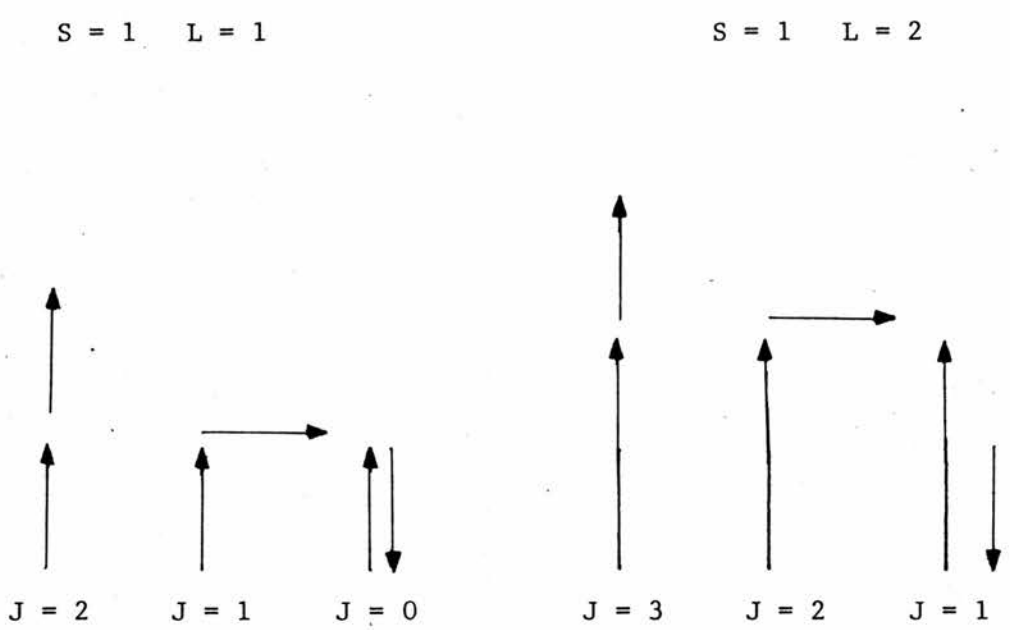

Figure 1.2 Combination of spin and orbital angular momentum to give total angular momentum J.

The individual J levels can be further split into a maximum of 2J+1 levels by magnetic (Zeeman effect) or electric (Stark effect) fields.

The ground state for a particular electronic configuration can be readily determined by the use of Hund's rules. These rules must be applied consecutively and require the ground state to have:-

(i) the maximum possible spin multiplicity.

(ii) the maximum possible orbital angular momentum

(iii) the maximum possible value of J when the shell is more than half-filled

(iv) the minimum value of J when the shell is less than half-filled.

For example, the Eu^{3+} ion has a $4f^6$ configuration outside a closed shell. The maximum spin multiplicity occurs with all the electrons unpaired i.e. $2S+1 = 7$ and the maximum orbital angular momentum in these circumstances is $L = 3$ i.e. a ^7F state. Since the shell is less than half-filled the ^7F_o multiplet is the ground state.

Empirically derived selection rules for the electronic transitions in atoms have been rationalized by quantum mechanics. For a fully allowed transition the following conditions are necessary:-

$\triangle L = \pm 1$ if there is only one unpaired electron.

$\triangle L = 0, \pm 1$ if there are several unpaired electrons.

$\triangle J = 0, \pm 1$ except for J=0 to J=0 which is forbidden.

$\triangle S = 0$.

Molecular orbitals

The molecular orbital theory of the electronic structure of molecules is an extension of the atomic orbital theory to molecules.

In molecular orbital theory it is assumed that the electrons in molecules occupy orbitals which extend around all the atoms in the molecule. In the ground state of the molecule the available electrons are allocated to the molecular orbitals of lowest energy. No more than two electrons can occupy each orbital. This is analogous to the Aufbau principle used to explain atomic structure.

Molecular orbital theory is largely based on the linear combination of atomic orbital (LCAO) approximation which is generally attributed to the work of Hund, Mulliken and Lennard-Jones (1927-1929). In this approximation it is assumed that a molecular orbital can be obtained from a linear combination of the atomic orbitals of each atom in the molecule. Thus if ϕ_i is one of the relevant atomic orbitals, the molecular orbital may be written as:-

$$\Psi = \sum c_i \phi_i$$

where c_i are the coefficients, which must be determined. Provided sufficient atomic orbitals are included in the expansion a good molecular orbital may be obtained.

The simplest molecule is H_2^+ and within the limitations of the Born-Oppenheimer approximation i.e. the total wavefuntion can be separated into electronic and nuclear parts, the Schrodinger equation can be solved exactly for this molecule. In this respect it resembles the hydrogen atom.

The lowest energy atomic orbital of the hydrogen atom is the 1s orbital and the lowest molecular orbital, Ψ, of the H_2^+ can be written using the LCAO approximation as:-

$$\Psi = c_a 1s_a + c_b 1s_b$$

The probability density of an electron in Ψ is

$$\Psi^2 = c_a^2(1s_a)^2 + c_b^2(1s_b)^2 + 2c_a c_b(1s_a 1s_b)$$

Since atoms a and b are identical in this case the electron densities around each nucleus must be identical and therefore $c_a^2 = c_b^2$. Only two molecular orbitals satisfy these conditions,

$$\Psi_g = N_g(1s_a + 1s_b)$$
$$\Psi_u = N_u(1s_a - 1s_b)$$

where N_g and N_u are normalizing constants. Ψ_g is a bonding molecular orbital and Ψ_u is an anti-bonding molecular orbital. The probability densities of these orbitals are shown in Figure 1.3.

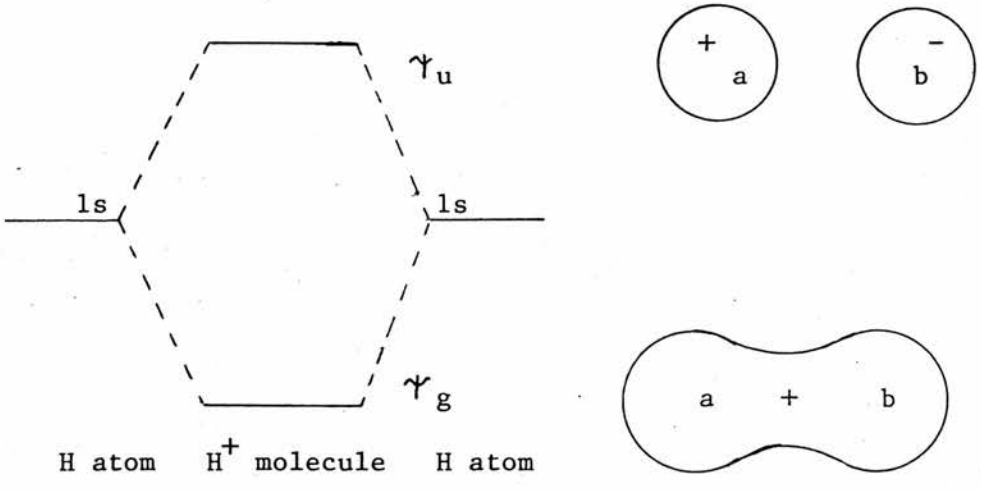

Figure 1.3. The molecular orbitals of H_2^+.

Other atomic orbitals can be combined, subject to symmetry restrictions, in a similar way. For example two sets of 2p orbitals may be overlapped to give six molecular orbitals, three bonding and three anti-bonding orbitals. These are represented in Figure 1.4, where the internuclear axis is taken to be the z axis. The $2p_{za}$ and $2p_{zb}$ orbitals combine to give a σ-bonding and σ^*-antibonding orbital. The $2p_x$ and $2p_y$ atomic orbitals combine to give π-type molecular orbitals.

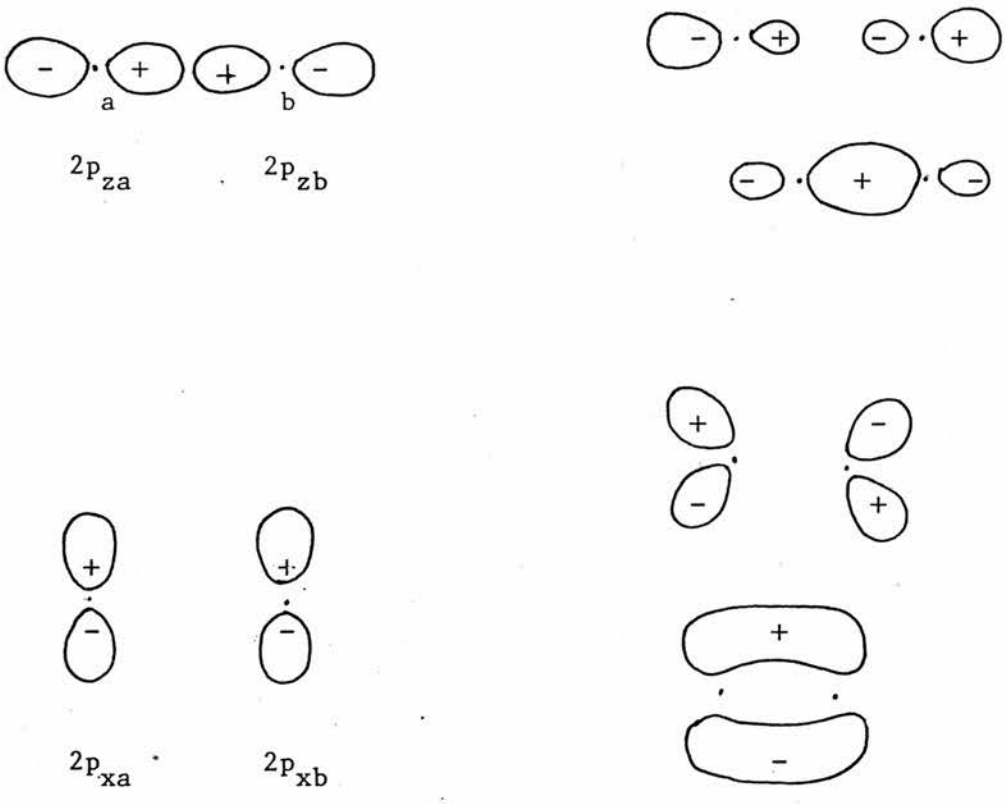

Figure 1.4. Molecular orbitals formed by 2p atomic orbitals in a homonuclear diatomic molecule (the $2p_y$ orbitals overlap analogously to the $2p_x$ orbitals)

In the homonuclear molecules discussed above the charge density

distributions are symmetrical. In the bonding molecular orbitals the density is increased between the nuclei whereas it is decreased in the antibonding orbitals.

In general, atomic orbitals may be linearly combined to form molecular orbitals only if they have the same symmetry. For significant bonding to occur it is necessary that the two orbitals have similar energies (in the specific cases discussed above they have identical energies) and the relevant atoms must be close together to allow overlap.

This can be illustrated by examining the molecular orbital representation of the carbonyl group in a molecule such as R_2CO. Overlap of s atomic orbitals of the C and O atoms gives a σ-bonding and σ^*-antibonding orbital; overlap of a p atomic orbital of each atom gives π-bonding and a π^*-antibonding orbital (Figure 1.4). In addition there remains a non-bonding molecular orbital largely localized on the oxygen atom which contains the lone-pair of electrons.

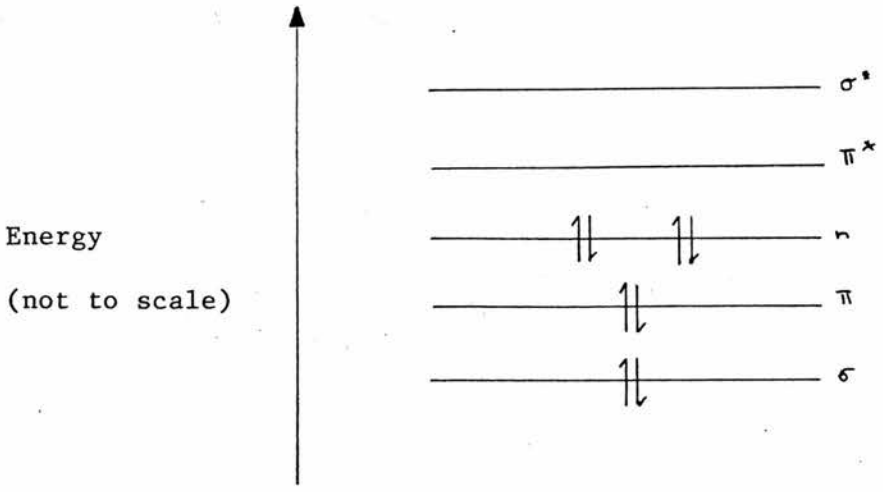

Figure 1.5. The molecular orbitals assosiated with a carbonyl group. The ground state configuration is shown.

Figure 1.5 shows the π-bonding to be less strong than the σ-bonding component. In heteronuclear molecules, such as the carbonyl bond, the charge density distribution of the σ and π orbitals is not symmetrical and is biased towards the more electronegative atom, the oxygen atom.

From the energy level diagram shown in Figure 1.5 it may be seen that promotion of an electron from the bonding or non-bonding orbitals gives rise to excited states of the molecule. These are discussed in more detail later.

Various semi-empirical and ab-initio self consistent field methods have been employed to calculate the molecular orbital wavefunctions and currently these give acceptable results for relatively small ground state molecules. Calculations involving excited state molecules have, in general, been less successful and determination of the energy of excited molecular states relies very heavily on experimental measurements.

In contrast to atoms, molecules may also possess vibrational and rotational energy. The rotational and vibrational energy levels are quantized and can be derived from the Schrodinger equation using the appropriate Hamiltonian operators.

Vibrational Energy Levels

Diatomic molecules may be considered as simple harmonic oscillators in which case the potential energy, PE, of a bond with length r is given by

$$PE = \frac{1}{2} k(r - r_e)^2$$

where k is the force constant of the bond and r_e is the equilibrium bond length. The Schrodinger equation then takes the form

$$\frac{\partial^2}{\partial x^2} + \frac{8\pi^2 m}{\hbar} E - \frac{1}{2} k(r - r_e)^2 = 0$$

and the permitted energy levels are:-

$$E_v = h\nu(n + \frac{1}{2})$$

where $\nu = (k/m)^{\frac{1}{2}}$ and n = 0,1,2,...

This simple model does not predict the convergence of the energy levels and is only a good approximation for bond lengths close to the equilibrium bond length.

The Morse potential energy function is more useful for predicting the vibrational energy levels in diatomic molecules:-

$$PE = De(1 - \exp(-a(r - r_e))^2)$$

where De is the dissociation energy of the bond which can be determined spectroscopically and $a = \frac{1}{2}\left[\frac{2m}{De}\right]^{\frac{1}{2}}$

The permitted energy levels are given by

$$E_v = (n + \frac{1}{2})h\nu - (n + \frac{1}{2})^2 h\nu x_e + (n + \frac{1}{2})^3 h\nu y_e \ldots$$

where x_e and y_e are anharmonicity constants and it is a good

approximation for bond lengths between 0.04 and 0.16nm but less satisfactory outside these limits.

In contrast to diatomics, which only have one mode of vibration, non-linear polyatomic molecules have 3N - 6 independent modes of vibration (3N - 5 if the molecule is linear). These particular modes can be independently excited.

Rotational Energy Levels

For diatomic molecules the permitted solutions of the Schrodinger equation are:-

$$E_j = -\frac{h^2}{8\pi^2 cI} J(J+1) \quad cm^{-1}$$

where I is the moment of inertia which is given by mr^2 where m is the reduced mass and r is the internuclear distance. J is the rotational quantum number and takes values 0,1,2,....

$-\frac{h^2}{8\pi^2 cI}$ is often referred to as the spectral constant B, and for a given molecule,

$$E_j = BJ(J+1) \quad cm^{-1}$$

This relationship also holds for linear molecules e.g. CO_2 and C_2H_2, and for molecules in which the moment of inertia in all directions is the same (spherical top molecules such as CH_4).

Calculation of the rotational energy levels becomes more complicated if the moments of inertia are not the same in each direction; a general expression has been derived where the moments of

inertia in two directions are equal but different from the third, (spherical top molecules such as NH_3 and CH_3Cl). In these circumstances a further quantum number K, which describes the angular momentum about a particular axis is required; permitted energy levels are

$$E_j = BJ(J + 1) + (\alpha - \beta)k^2$$

where α and β are related to the moments of inertia parallel and perpendicular to the axis respectively.

$$\alpha = \frac{h^2}{2I_{\parallel}} \quad ; \quad \beta = \frac{h^2}{2I_{\perp}}$$

The calculation of the rotational energy levels in asymmetric molecules is very complex and no general expression has been derived.

The vibrational and rotational energy levels of the electronic ground state may be observed by infra-red spectroscopy but the vibrational fine structure is usually only clearly resolved for molecules in the gaseous phase. In the solid state, rotation is sterically restricted and in solution collisions cause frequent changes in the rotational states and the spectra consists of broad unresolved lines corresponding to the vibrational transitions.

Transitions between the various energy levels are often discussed with reference to a Jablonski diagram. Figure 1.6 illustrates the energy levels present in a diatomic molecules and shows some of the allowed transitions between them; typical spacings between vibrational, rotational and electronic energy levels are shown below.

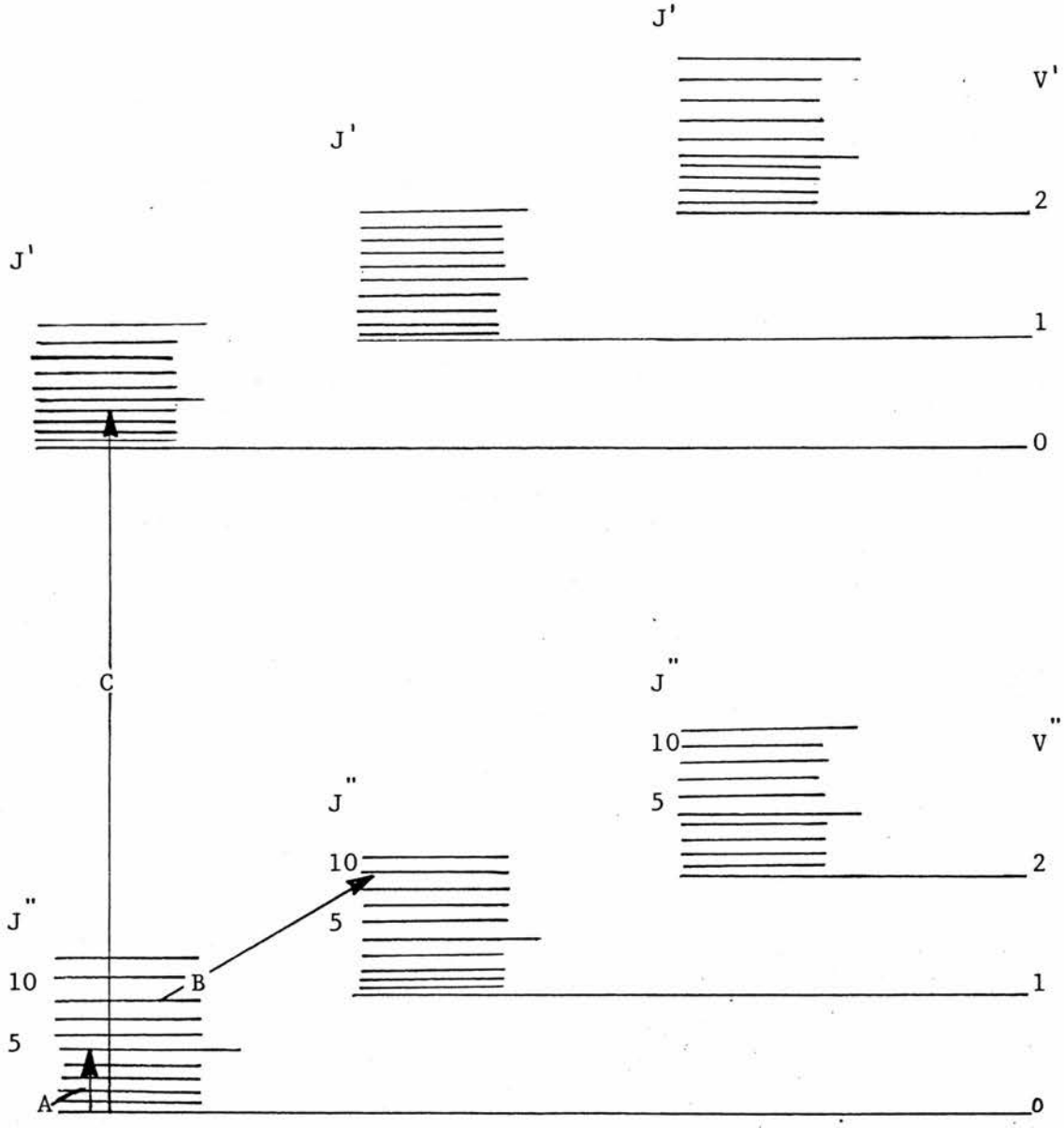

Figure 1.6. Jablonski Diagram

A Pure rotational (far infrared)

B Vibrational-rotational (near infrared)

C Electronic (u.v. visible)

Rotational	0.4 kJ mol^{-1}
Vibrational	4 - 40 kJ mol^{-1}
Electronic	160 - 1000 kJ mol^{-1}

It can be seen that the energy between the rotational states is very small compared to electronic levels and consequently when considering electronic transitions the rotational energy levels are frequently ignored.

Intermolecular Energy Transfer

Intermolecular energy transfer from a donor D, to an acceptor A, has been observed in gaseous, liquid and solid phases and it competes with emission to deactivate an excited state. This process, the mechanism of which is obviously dependent on the conditions, results in quenching of the donor emission and may be represented as:-

$$D^* + A \text{ -----> } D + A^*$$

where D^* and A^* are excited states of D and A respectively.

Any ground state or excited species, in the system by design or as an impurity, which has energy levels compatible with the donor, may accept energy from the donor. Rapid deactivation of the triplet state by molecular oxygen is well known and quenching of a reaction path by oxygen is often used to detect triplet state intermediates. Care must be taken when observing phosphorescence to exclude oxygen.

Experimentally, energy transfer may manifest itself in several ways including concentration depolarization of fluorescence and sensitized emission of fluorescence or phosphorescence. Several

mechanisms, both radiative and non-radiative, have been proposed to rationalize intermolecular energy transfer and some of these are discussed below.

Radiative Energy Transfer

Radiative energy transfer involves emission of a photon by the donor and subsequent absorption by the acceptor in a process where the efficiency is dependent upon the extent of overlap between the emission spectrum of the donor and the absorption spectrum of the acceptor: it may be represented as follows:-

singlet-singlet $\quad {}^1D^* \text{-----}> {}^1D + h\nu_f \qquad {}^1A + h\nu_f \text{-----}> {}^1A^*$

triplet-singlet $\quad {}^3D^* \text{-----}> {}^1D + h\nu_p \qquad {}^1A + h\nu_p \text{-----}> {}^1A^*$

where the superscripts ^{1} and ^{3} denote the singlet and triplet states respectively.

Normally triplet-triplet radiative transfer is negligible because of the low transition probability of the forbidden $S_o \text{---}> T_1$ transition in the acceptor.

Non-radiative Energy Transfer

Energy absorbed by one molecule may be transferred non-radiatively to another molecule if there is interaction between an excited donor and an acceptor within the lifetime of the donor.

The concept of non-radiative energy transfer between atoms was first advanced by Franck in 1922 and his predictions were confirmed experimentally by Cario and Franck[4] when they observed emission from

thallium vapour which was sensitized by excited mercury atoms.

Franck's concept was extended to polyatomic molecules by Perrin[5,6] to explain the concentration dependent depolarization of fluorescence from certain dyes.

Terenin and Ermolaev[7,8] elucidated the general aspects of intermolecular energy transfer between triplet states with the help of spectroscopic evidence. Their experiments in frozen binary solutions of aromatic molecules showed that sensitized emission was identical with emission produced by direct excitation. A good illustration of this comes from the emission from an E.P.A. solution of naphthalene and benzophenone at 77K which is characteristic of naphthalene when irradiated at 360nm where only benzophenone absorbs.

The major feature of their conclusions indicates that sensitized phosphorescence can be interpreted as relatively short-range exchange resonance interaction.

In the case of interatomic energy transfer a very close resonance between the donor and acceptor electronic energy levels is required because any excess energy can only be lost as translational energy; this is reflected by a very marked decrease in the efficiency of energy transfer with increase in the energy gap, ΔE, between the states involved.

Although exact resonance is not critical for polyatomic molecules, because excess energy may be dissipated by vibrational relaxation as well as translation, a fairly close resonance is required for significant transfer to occur.

Non-radiative energy transfer may involve one or more of the following processes:-

(i) Coulombic, or dipole-dipole, interaction.

(ii) Exchange interaction.

(iii) Collisional interaction.

Coulombic Energy Transfer

A theoretical analysis for coulombic interaction, involving dipole-dipole and dipole-quadrupole interactions between the donor and acceptor, was chiefly developed by Forster[9]. Energy transfer of this type is effective over 5-10nm and is governed by a very restrictive selection rule which forbids a change in multiplicity in either the donor or the acceptor. As with radiative energy transfer there must be overlap between the emission spectrum of the donor and the absorption spectrum of the acceptor and the allowed transitions include:-

singlet-singlet $^1D^* + {}^1A \longrightarrow {}^1D + {}^1A^*$

triplet-singlet $^3D^* + {}^1A \longrightarrow {}^3D + {}^1A^*$

Exchange Energy Transfer

Dexter[10] gave Forster's theory a more general treatment to include energy transfers involving forbidden transitions and exchange effects.

Physical overlap between the electron clouds of a donor and an acceptor whose energy levels fulfil the resonance conditions may result in exchange energy transfer. The exact mechanism by which this process occurs is uncertain but, as the name suggests, it is thought to involve an exchange of electrons between the donor and the acceptor.

Since a physical overlap of the electron clouds is required the exchange interaction is effective over a short range, 0.6 - 1.5nm.

Rules for the transitions are less restrictive than for Coulombic interaction. The Wigner spin rule requires the total spin momentum of the system is conserved. For example, the following transitions are allowed:-

singlet-singlet $^1D^* + {}^1A \text{ -----> } {}^1D + {}^1A^*$

triplet-triplet $^3D^* + {}^1A \text{ -----> } {}^1D + {}^3A^*$

Energy Transfer in Collisions

Energy transfer can occur as the result of collisions between donor and acceptor molecules. Collisional energy transfer takes place via exciplex formation, and the conditions for transfer are similar to those for the exchange mechanism; the allowed transitions can be represented as:-

singlet-singlet $^1D^* + {}^1A \text{ ----> } {}^1(D.A)^* \text{ ----> } {}^1D + {}^1A^*$

triplet-triplet $^3D^* + {}^1A \text{ ----> } {}^3(D.A)^* \text{ ----> } {}^1D + {}^3A^*$

Energy Migration

Interaction of excited states with neighbouring molecules can lead to rapid multi-step transfer of electronic energy over large distances through a crystal or rigid medium; this is energy migration.

In pure crystals the mechanism for energy migration is considered

to involve excitons which are generated by absorption and then move through the lattice before becoming trapped or localized. Experimental evidence suggests that a large number of lattice sites may be visited by an exciton during its lifetime. Terenin et al.,[80] pointed out that the small interatomic distances in a crystal lattice facilitates the triplet-triplet exchange process and that triplet energy may be "handed over and propagated along an array of closely packed molecules".

This process is demonstrated by impure anthracene crystals; the observable green fluorescence is, in fact, sensitized emission from naphthalene which is present as an impurity. This green fluorescence disappears if the crystals are dissolved in fluid or solid solution.

Energy transfer in polymer matrices

Rigid matrices have often been used in photochemistry to effectively isolate the substrate molecules and prevent collisions. Consequently short-lived species are stabilized and this is reflected by the phosphorescence lifetimes in rigid solutions which are generally lower than in fluid solution[11,12].

The matrix does not actually prevent diffusion but greatly reduces the rate at which it occurs; molecular oxygen may take several months to diffuse into a polymer matrix and can be monitored by the amount of quenching of the phosphorescence of an aromatic molecule. Benzene has been shown to diffuse through PMMA with an activation energy of 70-180kJ/mol[13] depending on the concentration.

In many cases the matrix is not inert for example poly methylmethacrylate (PMMA) has been shown to participate in some energy

transfer processes. For example Oster and Oster[14] observed benzophenone - sensitized phosphorescence of naphthalene in PMMA and also emission from the pyrene dimer in polycarbonate; the conditions they used ruled out the possibility of material diffusion and they concluded that the polymer must be involved in the transfer process.

Kellog[15] reported triplet triplet interaction over large distances in a cellulose acetate film[16] and showed that energy absorbed by a co-polymer can transfer from the absorption site to an excimer site which can then emit.

Triplet energy transfer has been well established in solid solution by Fox and Couzzins[17]. MacCallum[18] claims that in fact there is no evidence for singlet energy migration as a common phenomenon in aromatic containing polymers and also that there is no reason to differentiate between aromatic chromophores attached to polymer molecules and a concentrated solution of the analogous small molecule in a matrix.

One manifestation of triplet energy migration is the emission of delayed fluorescence resulting from triplet-triplet annihilation; unequivocal assignment of electronic transitions is extremely difficult even for small molecules. Theoretical calculations are, at present, of limited value so empirical or semi-empirical criteria must be used to assign transitions to particular molecular orbitals.

General terms for the excited states were introduced by Terenin[20] and Kasha et al.[21] By their convention electronic configurations with a spin multiplicity of unity are singlet states, S, and those with spin multiplicity of three are triplets, T.

The ground states of most organic molecules are singlet ground states, S_o and the excited singlet states are denoted S_1, S_2, S_3...

where $S_n > S_{n-1}$. For every excited singlet state there is a corresponding electronic configuration involving two unpaired electrons. These are the excited triplets and are denoted T_1, T_2, T_3....

Although the spin conservation rule forbids electronic transitions between states with different spin multiplicities such transitions are often observed in polyatomic molecules because of spin-orbit coupling which mixes the triplet and singlet states to some extent. The mixed triplet wavefunction takes the form

$$\Psi_T = \Psi_T^o + \lambda_{TS}\Psi_S^o$$

where T^o and S^o are the pure zero-order states and λ_{TS} is a mixing coefficient. Mixing is greatly enhanced if there is a heteroatom in a polyatomic organic molecule.

Heavy Atom Effect

McClure[22] observed a regular decrease in the phosphorescence lifetime with increasing atomic weight of the halogen substituent (see Table 1.1) in a series of halogenated aromatic compounds at 77K. This decrease in lifetime was related to an enhancement of the spin-orbit coupling factor for the halogen; Miller et al.,[23] found that the relationship was with the square of the spin-orbit coupling factor and noted that as well as mixing the singlet and triplet states it also appeared to enhance the mixing of σ and π states.

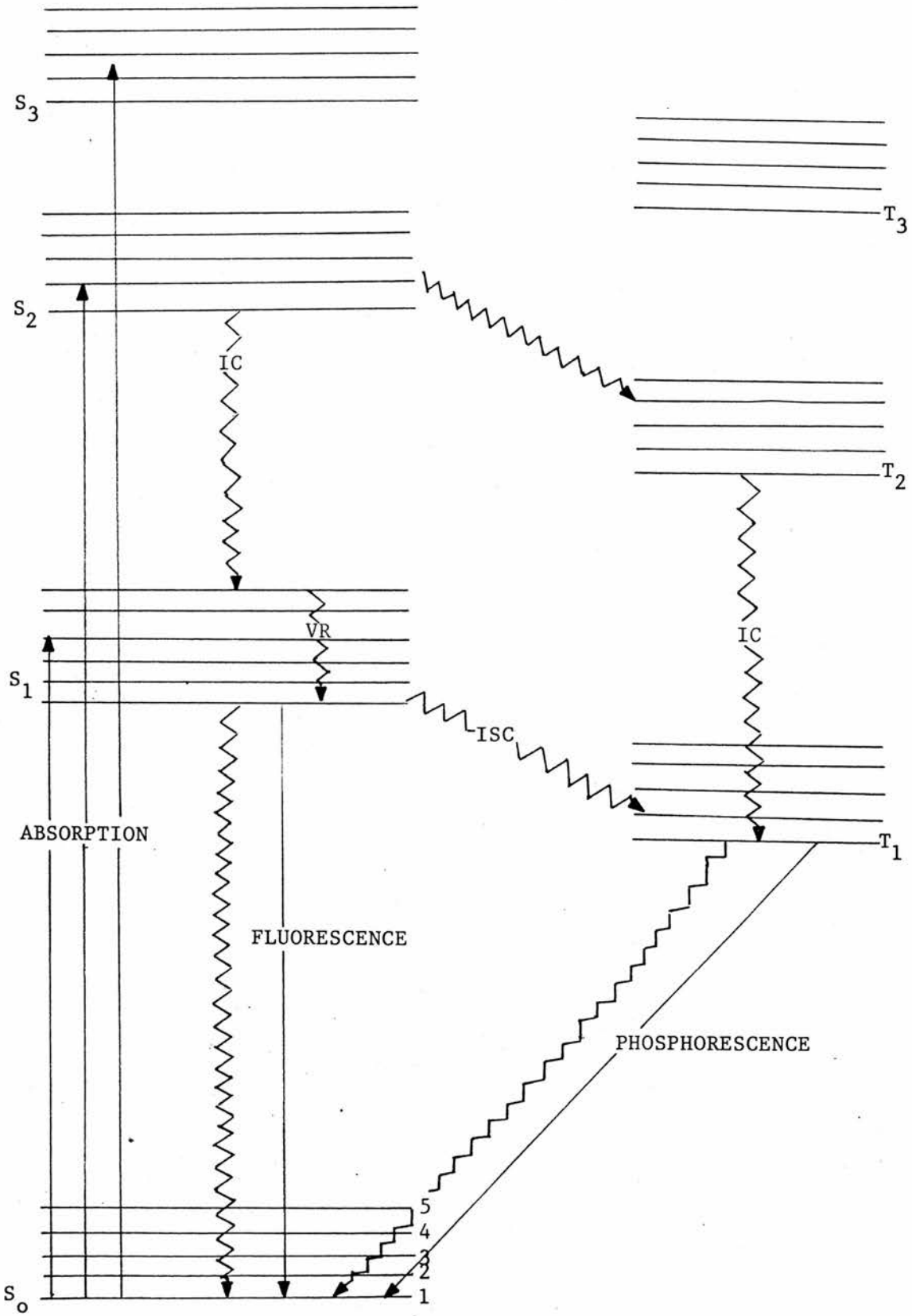

Figure 1.7. Jablonski Diagram

Process	Definition	Rate(s^{-1})
Absorption S_o ---> S_1	Promotion of an electron from the electronic ground state to an electronically higher level.	10^{15}
Internal conversion S_i ---> S_1 $i>1$	Non-radiative transition between two different electronic states of the same molecule which have the same multiplicity.	10^{11} - 10^{15}
Vibrational relaxation S_i^1 ---> S_i^o	Transitions from non - equilibrium vibrational energy distribution in a given electronic state to a thermally equilibrated vibration energy distribution relative to the zero point energy of the same state.	> 10^{12}
Intersystem crossing S_1 ---> T_1	Non-radiative transition from an electronic state of a given spin multiplicity to an electronic state of different multiplicity.	10^8
Internal conversion S_1 ---> S_o	Non-radiative transition between two electronic states of the same spin multiplicity.	10^5 - 10^7
Flourescence S_1 ---> S_o + $h\nu$	Radiative transition between two states of the same spin multiplicity.	10^7 - 10^9
Phosphorescence T_1 ---> S_o + $h\nu$	Radiative transition between two states of the same molecule which have different spin mulitplicities.	10^3 - 10^{-1}

Table 1.2. The primary photophysical processes.

SAMPLE	τ_p /s
naphthalene	2.3
1-chloronaphthalene	0.29
1-bromonaphthalene	0.018
1-iodonaphthalene	0.002

Table 1.1. Variation in τ_p with heavy atom substituent (Miller et al.[23])

The following effects usually accompany an increase in spin-orbit coupling:-

(i) enhancement of singlet-triplet absorption,

(ii) increase in the rate of S_1 ---> T_1 and T_1 ---> S_1,

(iii) decrease in phosphorescence lifetime,

(iv) decrease in fluorescence efficiency.

Intramolecular Energy Transfer

Electronic transitions can be illustrated by means of a Jablonski diagram[24] (Figure 1.7). The radiative transitions, both absorption and emission, are represented by solid lines and non-radiative transitions by wavy lines.

Absorption of a photon by a ground state molecule raises the molecule to an electronically, and usually vibrationally, excited state; the process is fast (10^{-15}s) relative to other photophysical processes and may occur to any of the excited singlet states S_1, S_2, S_3... In general singlet-triplet absorption has a very low transition probability.

An excited state molecule may undergo a photochemical reaction or it may lose its excess energy by photophysical processes. The primary photophysical processes summarized in Table 1.2 are discussed below.

Non-radiative Transitions

As indicated above the excited state reached by a molecule after absorption of a photon usually has additional vibrational energy. In most molecules the excess vibrational energy is rapidly lost (10^{-11} - 10^{-14}s) leaving the molecule in the zero vibrational level of the excited state. This process is called VIBRATIONAL RELAXATION (VR) (see Figure 1.7).

In comparison with the S_o and S_1 energy separation, the energy separation between the other excited states is relatively small and there is considerable overlap of the vibrational levels. One consequence of this overlap is an increase in probability of energy transfer between the excited states and a molecule raised to any state higher than S_1 will rapidly (10^{-11} - 10^{-15}s) lose energy and return to the S_1 state. This process is known as INTERNAL CONVERSION (IC) (see Figure 1.7).

Direct absorption from S_o to T_1 generally occurs with an extremely low transition probability because the transition is spin forbidden and the energy gap between the states is relatively large; ΔE is typically 240kJ mol^{-1} which minimises overlap between vibrational levels of the two states.

Population of the triplet state is usually achieved by transition from the corresponding singlet state where ΔE is typically 60kJ mol^{-1} which allows overlap between the vibrational levels. Such transitions, between states with different spin multiplicities, is

referred to as INTER-SYSTEM CROSSING (ISC) (see Figure 1.7), and because it involves a change in spin multiplicity it is relatively slow (10^{-8}s) compared to other radiationless processes.

Radiative Photophysical Processes

By the 1930's three types of luminescence had been observed:-

(i) a short-lived, temperature independent emission,

(ii) a longer-lived emission with the same spectrum as (i) but with temperature dependence and

(iii) a relatively long-lived emission at longer wavelengths than (i).

These three emissions have subsequently been characterized as fluoresence, delayed fluorescence and phosphorescence respectively.

Kasha formulated a general rule for emission from organic molecules which states that in condensed media the emitting level is the lowest excited level of that spin multiplicity. Although the majority of organic molecules obey this rule some exceptions have been found. For example, azulene is known to emit from the second excited singlet state S_2.

Fluorescence

Fluorescence is defined as a radiative transition between states of the same spin multiplicity, usually

$$S_1 \text{ -----> } S_o + h\nu$$

The transition is fully allowed and occurs in 10^{-7} - 10^{-10}s.

Phosphorescence

Phosphorescence is defined as a radiative transition between states with different spin multiplicity, usually

$$T_1 \text{ -----> } S_o + h\nu$$

These transitions are spin forbidden and are much slower (10^{-3} - 10s) than the corresponding fluorescence transitions.

Both fluorescence and phosphorescence intensities can be shown to decay according to first order kinetics i.e. the decay is exponential with time.

$$I(t) = I_o e^{-kt} \qquad (1)$$

$$\log I(t) = \log I_o - kt \qquad (2)$$

where I_o = initial intensity at some arbitrary time zero-time, I = the intensity at time t and k = the first order rate constant.

The time taken for the intensity of the emission to reach 1/e of its original intensity is called the lifetime of the emission (τ_f or τ_p) and takes the value

$$\tau = \frac{1}{k}$$

The relationship between the observed lifetime and the intrinsic (or natural) lifetime is

$$\tau_{obs} = \tau_o \phi_{f/p}$$

where $\phi_{f/p}$ is the quantum yield of the fluorescence or phosphorescence, and $\tau_{obs} = \tau_o$ only in the absence of any other deactivation process.

A more useful definition of the intrinsic lifetime takes into account the temperature independent radiationless processes which deactivate the excited state (see Figure 1.7), under these circumstances the rate of decay of the emission is:-

$$-\frac{d[A^*]}{dt} = k_r[A^*] + k_{nr}[A^*]$$

$$= k_o[A^*]$$

where k_o is the sum of the radiative and non-radiative rate constants, k_r and k_{nr} respectively. The intrinsic lifetime is then given by:-

$$\tau_o = \frac{1}{k_o}$$

Delayed Fluorescence

Although delayed fluorescence has an identical spectral distribution to normal fluorescence it exhibits a much longer lifetime and its intensity is temperature dependent. Two types of delayed fluorescence have been characterized by Parker[25,26].

E-type Delayed Fluorescence

E-type, or eosin-type, delayed fluorescence occurs as a result of thermally activated inter-system crossing from the triplet to singlet manifold and is therefore temperature dependent (see Figure 1.8). The intensity of the emission is proportional to the rate of absorption of

light and, since emission from S_1 is faster than inter-system crossing the lifetime is the same as that of the triplet state.

Activation energies for the inter-system crossing have been found, within experimental error to be the difference in energy between T_1 and S_1.

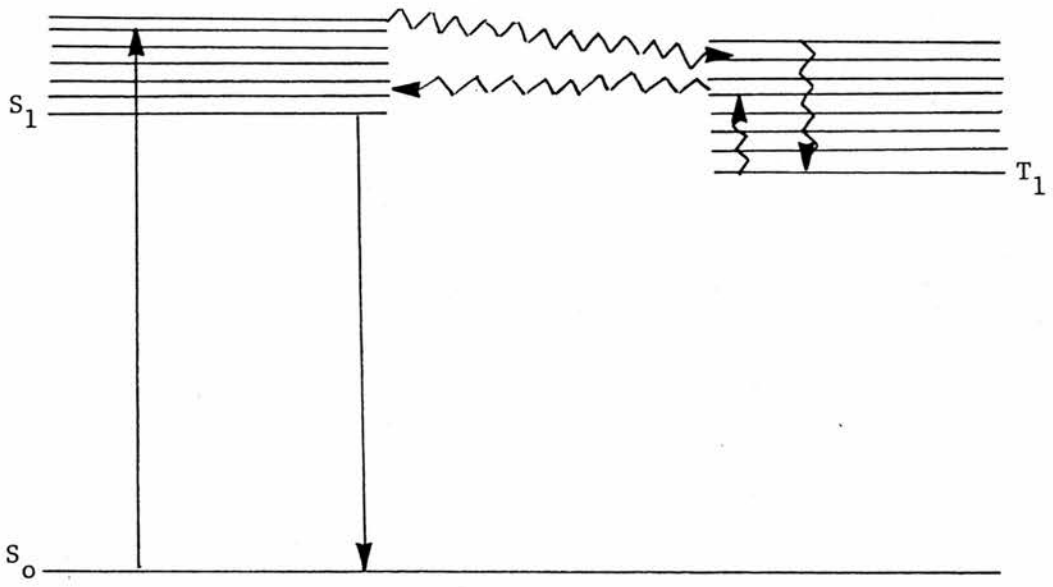

Figure 1.8. Thermally activated E-type delayed fluorescence.

P-type delayed fluorescence

Unlike E-Type delayed fluorescence, P-tpye delayed fluorescence is a bimolecular process and occurs as the result of interaction between two excited triplet molecules.

The net result of the interaction, which in solution may involve the formation of a very short-lived dimer, is the annihilation of the two triplets and the production of two singlet states one of which may be excited.

$$T_1 + T_1 \text{ -----> } S_1 + S_o$$

and/or $T_1 + T_1 \text{ -----> } 2S_o$

At low light intensities triplet-triplet annihilation does not alter the population of the triplet state significantly, hence the triplet concentration is proportional to e^{-kt}; the intensity of the delayed fluorescence is proportional to e^{-2kt} since the production of S_1 is dependent on the square of the triplet concentration.

Temperature dependence of the P-tpye delayed fluorescence in solution arises from the diffusive nature of the interaction between the triplet states.

As mentioned previously it is very difficult to assign electronic transitions to particular molecular orbitals, however certain photophysical and photochemical properties may be explained by considering the nature of the molecular orbitals involved in the excited state.

Although absorption of a photon can promote an electron from any molecular orbital the most common transitions involve electrons from the highest occupied molecular orbital, HOMO. In the case of organic polyatomic molecules the HOMO is usually n or π and the transitions, which are shown in Figure 1.9, give rise to $n - \pi^*$ and $\pi - \pi^*$ excited states. Transitions from lower energy molecular orbitals (e.g. σ) may occur if the exciting energy is sufficiently high.

Organic molecules containing a heteroatom are usually raised to $n - \pi^*$ excited states (although inter-electronic repulsion forces may invert the order of the energy levels) whereas unsaturated hydrocarbons generally achieve $\pi - \pi^*$ excited states.

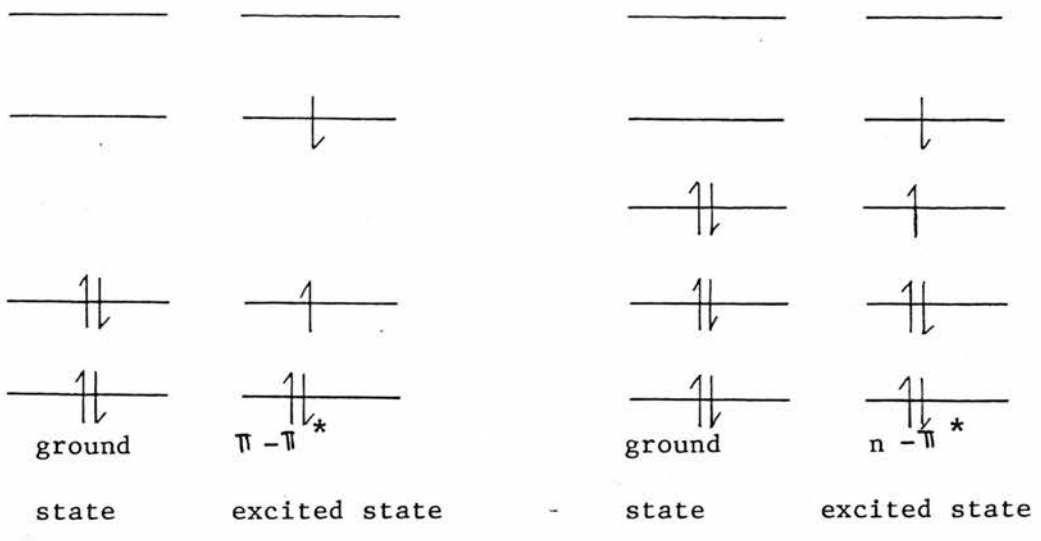

Figure 1.9. Molecular orbitals assosiated with transitions to n $-\pi^*$ and $\pi-\pi^*$ excited states.

There is considerable overlap between the π and π^* molecular orbitals, consequently there is a high transition probability for S_1 ---> S_o transitions and fluorescence competes favourably with inter-system crossing: fluorescence quantum yields for $\pi-\pi^*$ excited states are high compared to phosphorescence quantum yields.

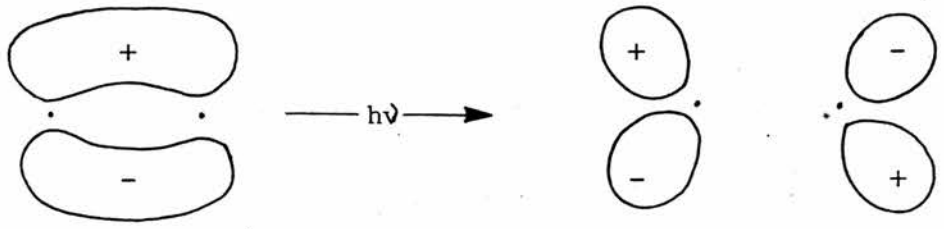

Figure 1.10. Molecular orbital representation of $\pi-\pi^*$ transition

In contrast to $\pi-\pi^*$ excited states there is little overlap between the n and π^* molecular orbitals and the n $-\pi^*$ excited singlet

states are relatively long-lived which enhances inter-system crossing to the triplet state.

In such molecules phosphorescence is often the predominant emission, for example in benzophenones the quantum yield of phosphorescence is often close to unity.[27,28]

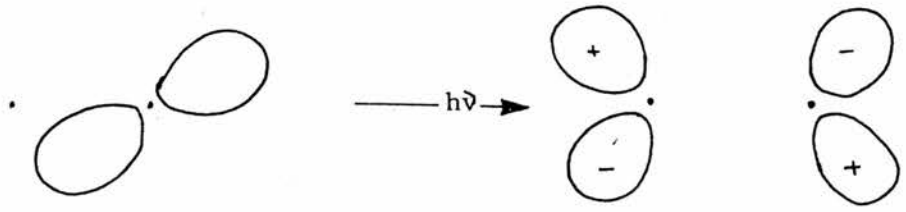

Figure 1.11. Molecular orbital representation of an $n - \pi^*$ transition.

Primary Photochemical Processes

Currently theoretical predictions of the nature and efficiency of photochemical reactions is not possible, however, quantitative theories have been developed using certain correlations between chemical structure and photochemical reaction paths as a basis. Such theories predict the photochemical reactions of a molecule by using data from structurally similar compounds. There are many photochemical reactions and the primary ones are summarized in Table 1.3.

Generally molecules with $\pi - \pi^*$ excited states differ significantly from those whose lowest excited states are $n - \pi^*$. In particular the natural lifetimes and degree of localization of excitation are greater and the $S_1 - T_1$ energy gaps are smaller for

$n - \pi^*$ states.

Pronounced differences in their photochemistry and photoreactivity exist and are due, in part, to these factors: for example the absorption bands of anthracene ($\pi - \pi^*$) and benzophenone ($n - \pi^*$) fall in the same region, at 26200 and 26000 cm^{-1} respectively, but irradiation of isopropyl alcohol solutions yield different products. Dianthracene is the photoproduct from the anthracene solution due to photodimerization (see Table 1.3);

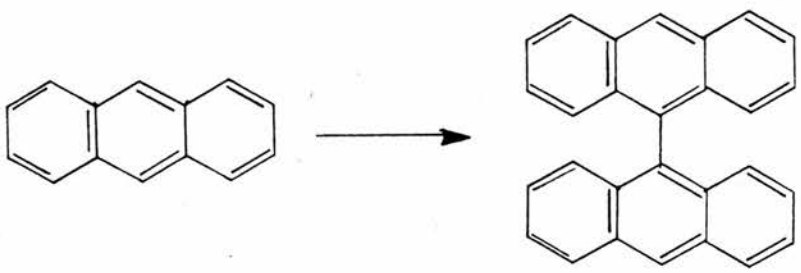

dianthracene

whereas hydrogen abstraction and photoreduction (see Table 1.3) produce benzopinacol and acetone from the benzophenone solution.

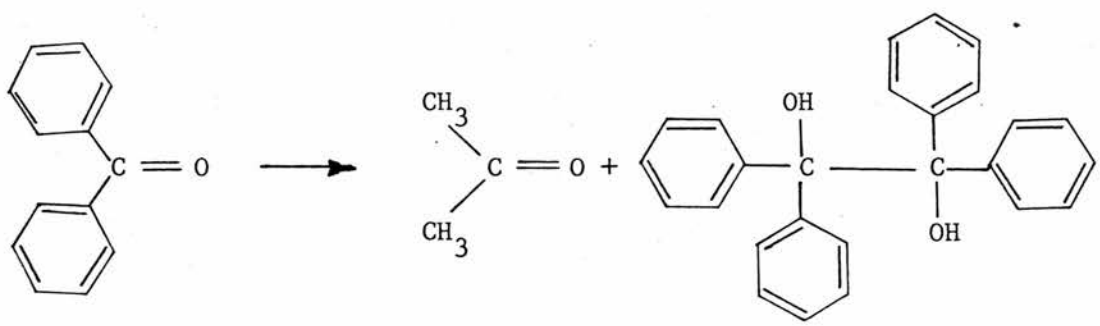

benzpinacol

These fundamental differences in the photochemistry of the two spectroscopic classes of organic molecules must be considered when evaluating photochemical systems; however, care must be taken to ensure that the observed differences are due to the electronic structure and not to differing light intensities or experimental conditions or simply to energy effects which do not alter the photochemistry of the system.

Excitation to the $\pi - \pi^*$ state does not necessarily mean that delocalization of the excitation will be an important factor in determining the photochemistry, for example benzophenone gives virtually the same products if it is excited to the $n - \pi^*$ or the $\pi - \pi^*$ state, presumably because the $\pi - \pi^*$ second excited state undergoes internal conversion to the $n - \pi^*$ first excited state before undergoing any photochemical reaction.

Process	Description
Dissosiation into radicals	---> $AB^{\bullet} + C^{\bullet}$
Intramolecular decomposition	---> E + F
Intramolecular rearrangement	---> ACB
Photoisomerism	$ABC(S_1)$ ---> ABC
Hydrogen-atom abstraction	or RH ---> $(ABCH)^{\bullet} + R^{\bullet}$
Photodimerisation	$ABC(T_1)$ ABC ---> $(ABC)_2$
Photosensitised reactions	D ---> ABC + products
Photoionization	---> $ABC^{+} + e^{-}$
"External" electron transfer	D ---> $ABC^{+} + D^{-}$
"Internal" electron transfer	---> $AB^{+} + C^{-}$

Table 1.3. Primary photochemical processes.

CHAPTER 2

EXPERIMENTAL METHODS

A. Materials

Preparation of europium(III) chloride

A measured quantity of 99.9% Eu_2O_3 (Koch-Light) was converted to the chloride by refluxing in 50% hydrochloric acid until it was completely dissolved; excess HCl was removed by repeatedly adding more water and either boiling or using a rotary evaporator until the pH approached 7. The cold neutral solution of $EuCl_3$ was diluted in a graduated flask with distilled water giving a stock solution of known concentration.

Ligands and amine bases

Ligands:- acetylacetone (Fisons), benzoyltrifluoroacetylacetone (Fluka), and hexafluoroacetylacetone (Koch-Light) and amine bases:- piperidine, pyridine, 2-aminopyridine, picoline (Fisons), tertiary butlyamine (BDH) and quinoline (H&W) were used without further purification.

Europium Chelates

(i) Tetrakis chelates

An aqueous solution of $EuCl_3$, prepared as above, was added dropwise to a 95% ethanol solution of the ligand and the amine base in the molar ratio 1:4:1 and the solution was boiled to remove most of

the ethanol. The crude product was precipitated by the addition of small amounts of water and was recrystallized from an ethanol/water mixture.

(ii)Tris chelates

The ligand and $EuCl_3$ were dissolved in a 50% ethanol solution in the molar ratio 3:1. The pH of the solution was slowly raised by dropwise addition of 0.5M ammonium nitrate solution until precipitation occurred at ca. pH 6.3. Care was taken not to allow the pH to rise further and precipitate the lanthanide hydroxide.

The C, N, H analyses of all the chelates prepared are given in Table 2.1.

Chelate	C	N	H	C	N	H
	Calculated			Experimental		
$Eu(btfa)_4pipH$	49.2	1.3	3.3	49.6	1.2	3.1
$Eu(btfa)_4pyH$	49.5	1.3	2.8	49.2	1.2	2.7
$Eu(btfa)_4quinH$	49.5	1.2	2.8	51.6	1.1	2.8
$Eu(btfa)_4Bu^tNH_3$	48.6	1.3	3.3	48.6	1.1	3.0
$Eu(hfaa)_4pyH$	49.5	1.3	2.8	49.1	1.2	2.7
$Eu(hfaa)_4\alpha picH$	27.9	2.6	1.0	27.7	2.5	1.0
$Eu(hfaa)_4Bu^tNH_3$	27.3	1.3	1.5	26.1	1.4	1.7
$Eu(aa)_3.3H_2O$	35.8	0.0	5.4	35.6	0.0	5.5

Table 2.1. C,N,H analysis of europium chelates.

Preparation of the PMMA samples.

The stabilizer was removed from commercial methyl methacrylate monomer(BDH) by washing with two volumes of 2M NaOH then with several volumes of distilled water. The destabilized monomer was dried and stored over sodium sulphate in a cool dark place, to minimise polymerization and used without further purification.

The benzil (Fisons), benzophenone (Fisons) , 2-bromonaphthalene (Aldrich), 9-bromophenanthrene (Aldrich) and anthraquinone (Fisons) were recrystallized from ethanol and the 1-bromonaphthalene (H&W) was redistilled before use. 10^{-3}M solutions of the solute in the destabilized monomer were prepared and 1mg of initiator (2,2-azobis-2-methylpropionitrile (Aldrich)) /5mls of solution was added. The samples were degassed using the freeze-thaw method and polymerized in a nitrogen atmosphere for about 18hrs at 340K. The sample tubes were evacuated after polymerization and sealed before annealing the sample by heating to 380K for two hours. The preparation of the samples was carried out in the dark. They were found to be strain-free after examination through a strain viewer.

Samples used in the absorption spectroscopy measurements were made in glass tubes of 1cm diameter and were not evacuated after polymerization. The samples were cut and polished in the dark, to prevent any photochemical reaction and were used within a week of being polymerized to minimise the extent of any diffusion of oxygen through the polymer matrix.

B. Apparatus

(i) Ground State Absorption Spectroscopy

Absorption spectra in the ultraviolet and visible regions were obtained using a Perkin-Elmer Ultraviolet Spectrophotometer model 402. This instrument has a wavelength range of 190 to 850nm, and an optical density range of 0 to 1.5. All measurements were carried out at room temperature using a polished polymer sample of path length ca. 1cm. Air was used as a reference in all the measurements in this thesis.

(ii) Excitation Spectroscopy

Perkin-Elmer Hitachi MPF-44A Spectrofluorimeter

This instrument can be used to determine the emission or excitation spectra of luminescent solids or solutions. Use of different cell compartments permits spectra to be obtained at temperatures ranging from 77K to room temperature and above.

The excitation light source is a 150 watt Xenon lamp, giving a near continuum from ca. 270nm to above 850nm. The excitation monochromator allows irradiation of samples in the range 200-700nm with monochromatic light. The emission monochromator selectively monitors the intensity of radiation emitted by the sample between 200 and 800nm. Both monochromators are of the Czerny-Turner grating variety (600 lines mm^{-1}). The gratings can be manually scanned, or motor driven.

Excitation spectra were obtained by setting the emission monochromator at, at or near to the emission maximum, and the intensity of the emission was monitored as the excitation wavelength

was scanned through the desired range. Emission spectra were measured by setting the excitation wavelength at, or near to the absorption maximum of the sample, and scanning the emission wavelength. Resolution of spectra depended on the excitation and emission slit widths, which can both be altered within the range 1 to 20nm.

Two modes of operation are possible with this instrument,

(a) Manual mode,

(b) Reference mode.

In the manual mode, no correction is made for any short or long term fluctuations which may occur in the intensity of the Xenon lamp, and which may be caused, for example, by changes in the lamp supply voltage.

In the reference mode, the excitation light passes through a beam splitter, and a small fraction of the light is focussed on to a reference photomultiplier, the output of which inversely controls the gain of the main photomultiplier. In this system, there is some compensation for fluctuations in excitation light intensity. This mode was used for all measurements reported in this thesis.

(iii) Phosphorescence Lifetime Apparatus

The apparatus described in this section was used to obtain and process emission decay data for both europium chelate (Chapter 6) and organic compounds in various matrices (Chapters 3,4 & 5).

The optical aspects of the apparatus are shown schematically in Figure 2.1. The light from the E.G. and G. FX-31 flash tube is focussed onto the sample which is contained in a purpose built clear Dewar sample compartment. The emission from the sample is focussed (right angled viewing) onto the slits of a Hilger and Watts prism

monochromator which is attached by a light tight seal onto the sample box. A black glass filter (pass band 300-390nm) was generally inserted in the excitation beam. The sample box is approximately 50cm square and 30cm high and the inside is painted matt black.

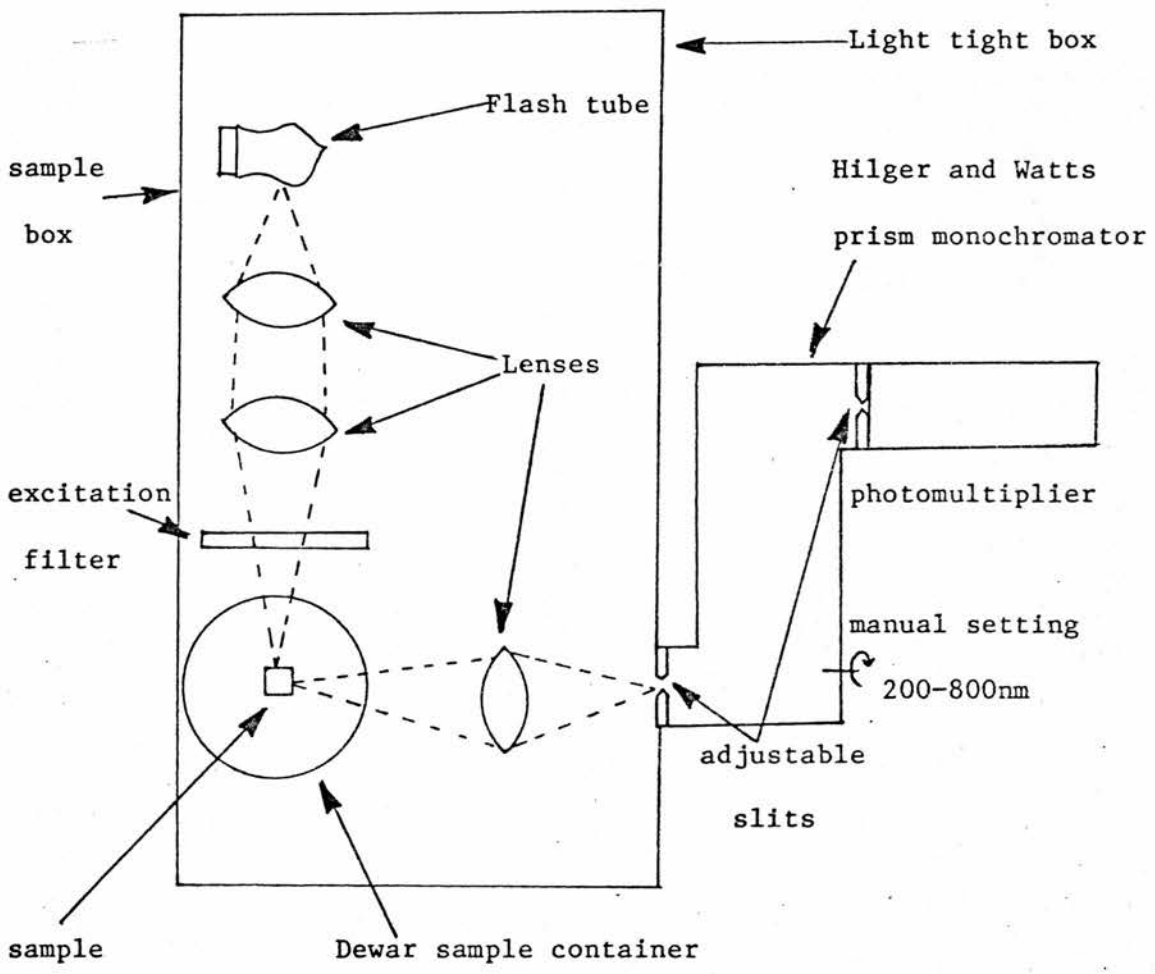

Figure 2.1. Basic optical arrangement (top view)

Optical baffles, not shown in Figure 2.1 are used to minimise scattered light within the sample box.

The Dewar sample compartment was designed to allow hot or cold nitrogen gas to be circulated through it and hence give control of the sample temperature over the range 130-400K. The compartment can also

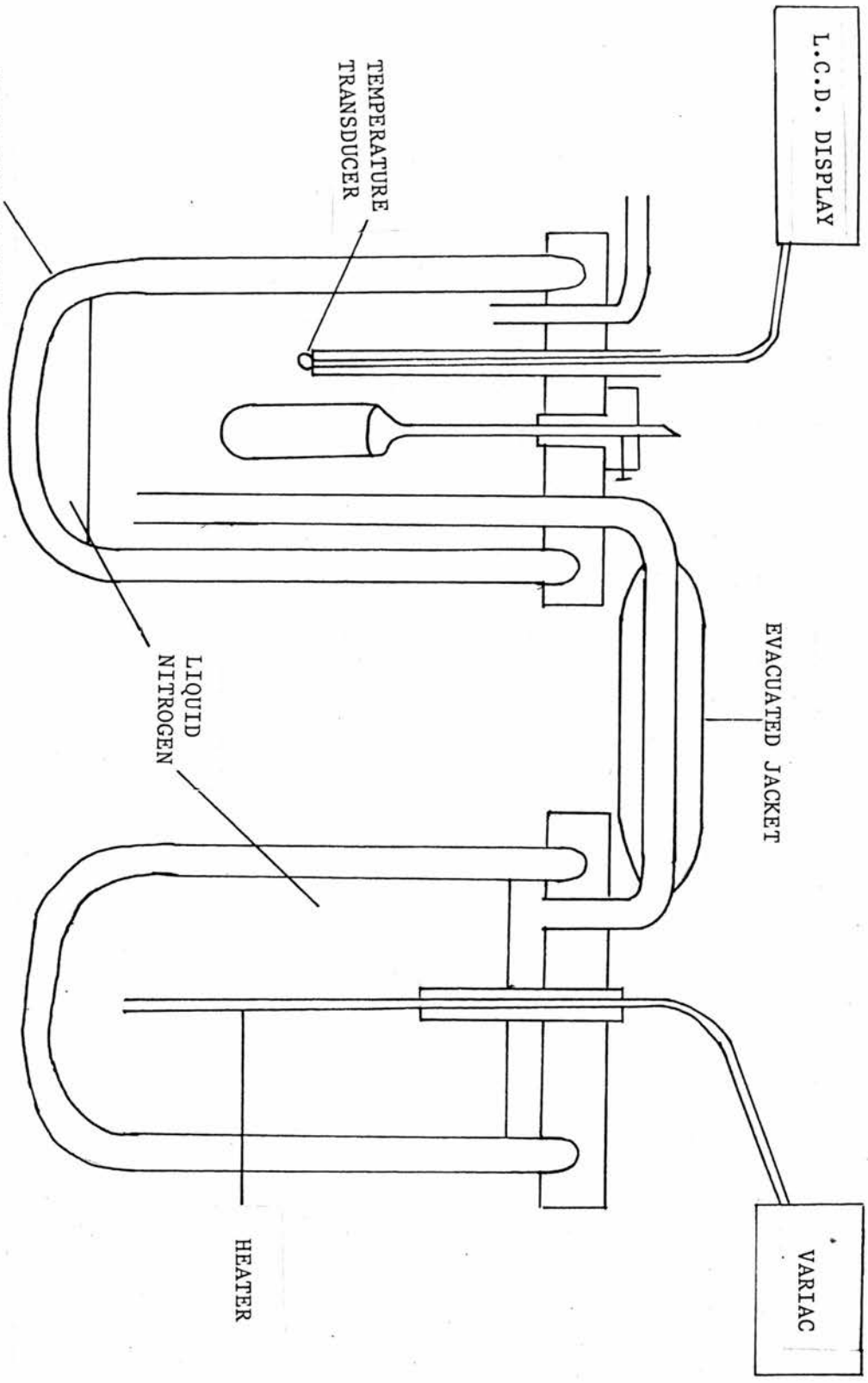

Figure 2.2. Temperature control apparatus for temperatures below room temperature.

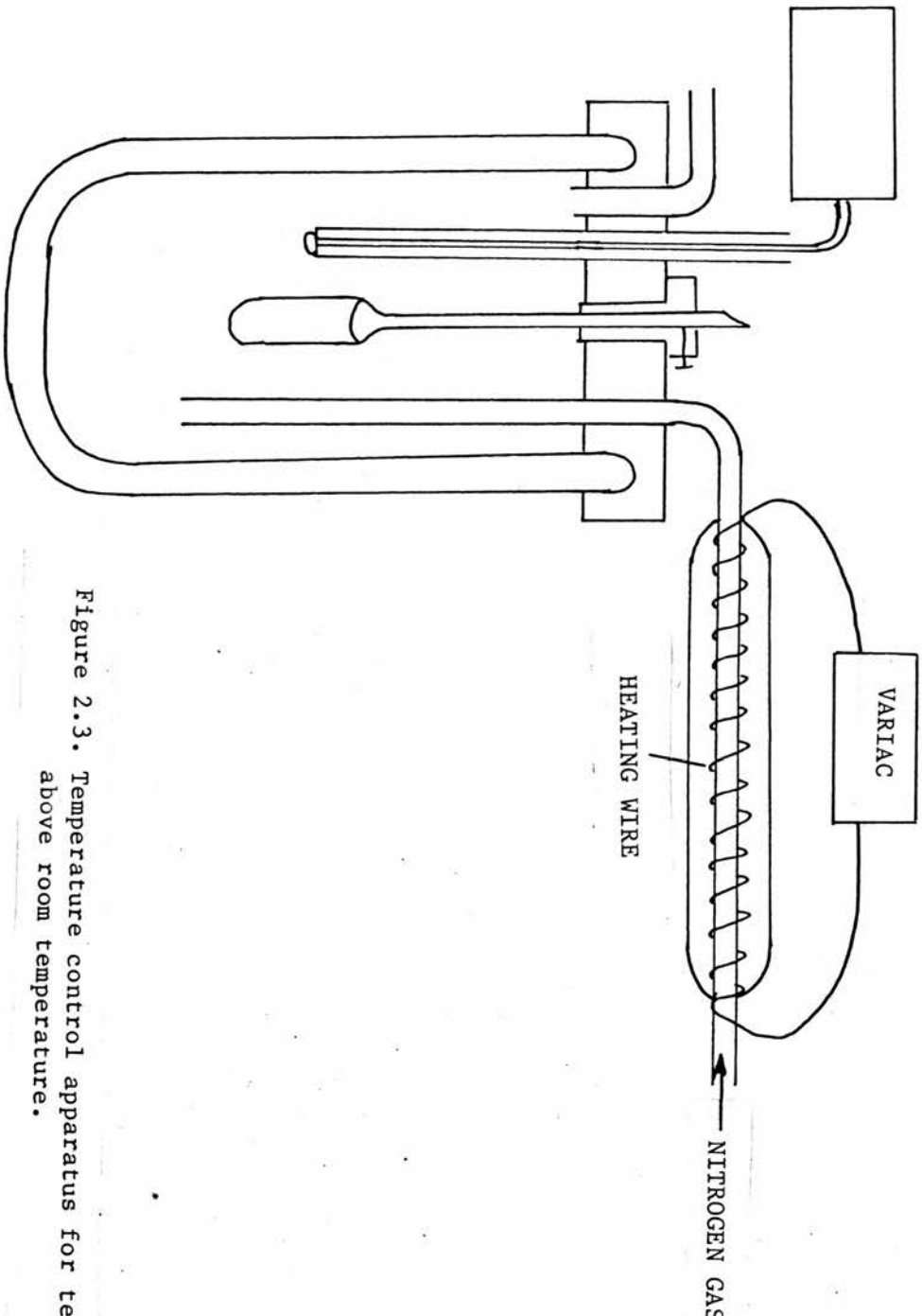

Figure 2.3. Temperature control apparatus for temperatures above room temperature.

be filled with liquid nitrogen or solid carbon dioxide/ solvent slushes to obtain fixed low temperatures. The hot or cold nitrogen gas enters the sample compartment via insulated tubes, as illustrated in Figures 2.2 and 2.3, and the temperature of the sample is determined using an Intersil AD590 two terminal semiconductor temperature transducer. This device produces an output current proportional to absolute temperature passing $1\mu A\ K^{-1}$ for supply voltages between +4V and +30V. This current is appropriately converted to voltage so as to give a direct reading in Kelvins on an Intersil ICL7106 evaluation kit LCD display. The rate of nitrogen flow is metered through a control valve and gave sample temperatures which were reliable to $\pm$1K.

The emission from the sample passes through the monochromator onto an EMI 9526 photomultiplier. The bandwidth and centre wavelength of the emission reaching the photomultiplier is controlled by varying the slit widths and prism setting of the monochromator.

The interfacing of this apparatus to a Data Laboratories DL201 signal averager is shown schematically in Figure 2.4. The measurement cycle is initiated by a trigger pulse generated by the signal averager. This TTL signal is converted using a silicon controlled rectifier based circuit to a 100V pulse which is capable of driving the integral pulse transformed in the FX-31 flash tube base and hence firing the flash tube.

The power supply for the flash tube is of local design and capable of supplying 200-800V at several mA to the $2\mu F$ high voltage storage capacitor (Figure 2.5). This supply was generally operated at 500V giving an electrical input ($1/2CV^2$ Joules) of ca. 0.25 J to the

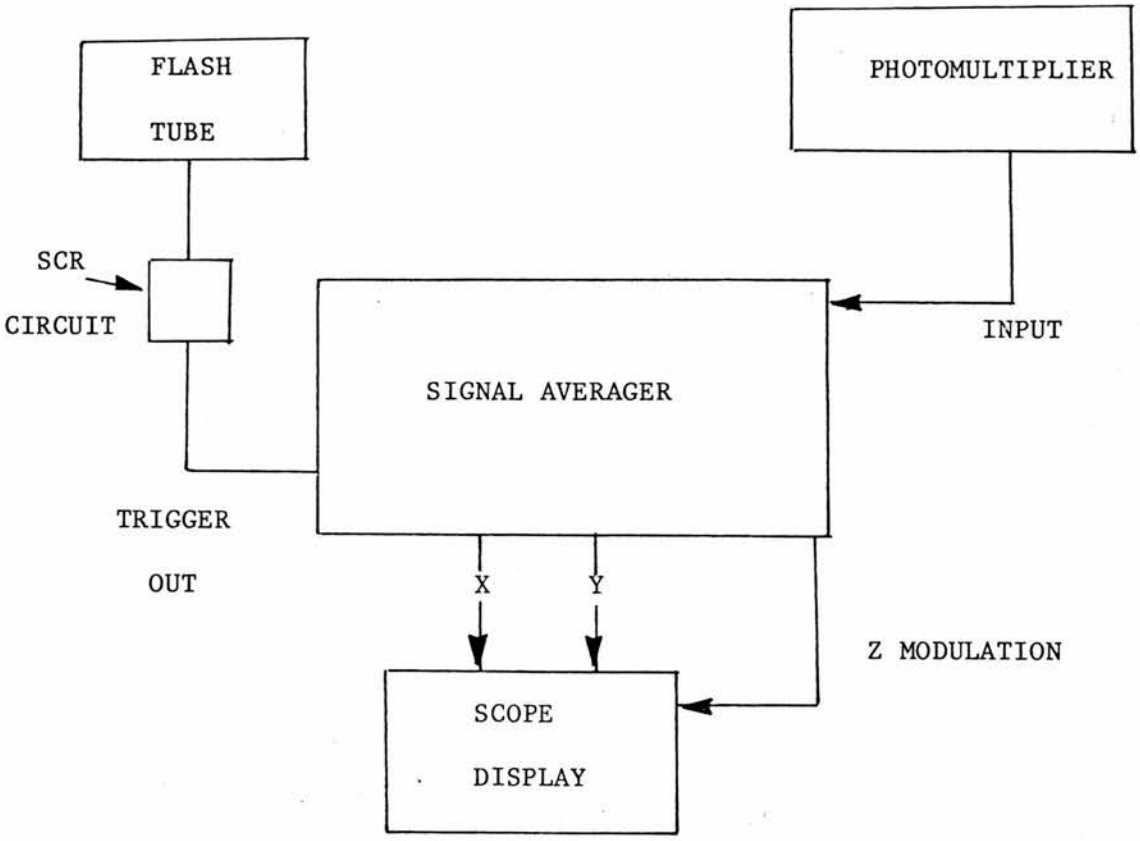

Figure 2.4. Interfacing the signal averager to the sample box.

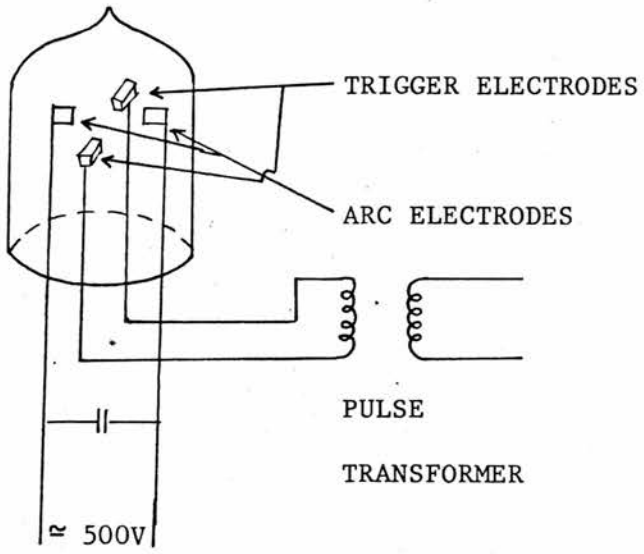

Figure 2.5. The Flash Tube Circuitry.

flash tube. The photomultiplier is operated using a Brandenburg high stability power supply and cathode voltages of -1500V to -2000V were used depending on the quantum efficiency of the sample.

The decay curve can be viewed on an X-Y oscilloscope while the averaging is in progress.

The flash duration and the sampling time of the signal averager limit the lifetimes that can usefully be examined by this apparatus to those greater than ca. 100μs.

The Microcomputer Interface

The DL 201 signal averager uses a 6-bit A-D converter and stores the sum of the averages at each of 200 points as 200 16-bit complementary twos numbers. These may be output from the averager in analysing mode (with 6-bit precision) but are also available in full precision as 16-bit words in digital mode.

Largely due to the work of Mr. A. J. Cairns an interface was built to allow these 16-bit words to be transferred from the averager to the memory of a Nascom 1 microcomputer. This was done via the Z-80 parallel input output (PIO) chip and using a short machine code routine. The necessary handshaking between the averager and the PIO uses one 74123 chip and is shown in Figure 2.6.

The transfer of the entire contents of the averager takes less than one second. The binary numbers in memory are accessed by decimal format and stored as a BASIC array.

The data can now be processed using BASIC and various programs have been written, one of which calculates the lifetime of the phosphorescence decay. The data was transferred to a mainframe computer for further analysis which is described in the following

section.

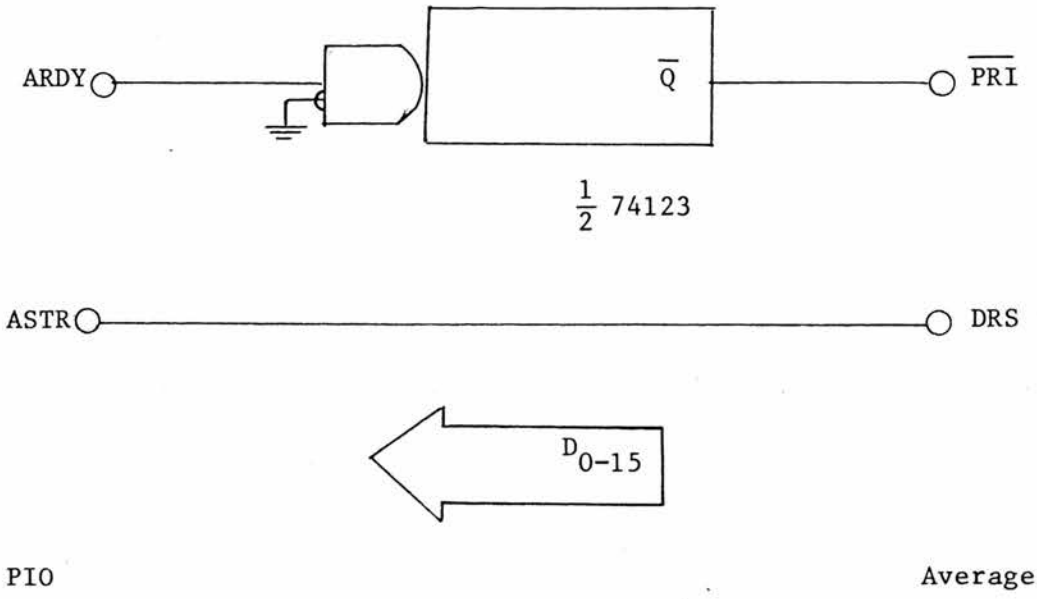

Figure 2.6. Interface hardware.

Typical operation

The flash tube voltage, the photomultiplier voltage and the monochromator were adjusted to give a satisfactory display on the oscilloscope screen. The "Delay before" setting on the signal averager was adjusted to omit from the scan any emission during and immediately following the flash. Sufficient scans were made to minimise photomultiplier noise on the trace.

Two sets of readings were taken in each case (a) with the flash tube operative and (b) with the flash tube inoperative. The latter was used as a background and subtracted from the former before processing the data to eliminate errors due to the A/D converter not being accurately zeroed. Each set of data was sent to the

microcomputer as requested by the contolling program.

Regular checks were carried out using europium chelates which are known to have rigidly exponential phosphorescence decays.

C. Data Analysis

Lifetime determinations

In the absence of additional triplet deactivation processes the decay of phosphorescence is first order and the intensity of the emission at time t is described by:-

$$I(t) = I_o e^{-kt}$$

$$\log I(t) = \log I_o - kt$$

where $I(t)$ is the intensity at time t and I_o is the intensity at some arbitrary zero time. Under these circumstances the rate constant k can be obtained from a graph of log I against time, the gradient is $-k$.

Frequently other energy transfer processes also deactivate the excited triplet state, and if such processes are first order then the overall decay retains its exponential character. Some energy transfer processes do, however, cause non-exponential decay and some of these are considered in more detail below.

(i) Thermal deactivation

Any energy transfer process which is thermally activated has a temperature dependent rate constant and such first order processes include internal conversion, inter-system crossing, and energy

transfer to another species in the system. These possibilities are shown below in Figure 2.7.

Any model for this type of temperature dependence must take into account the intrinsic lifetime of the phosphorescence and may be derived on the assumption that k_o is temperature independent and that variations in k_{nr} are responsible for the observed variations in lifetimes.

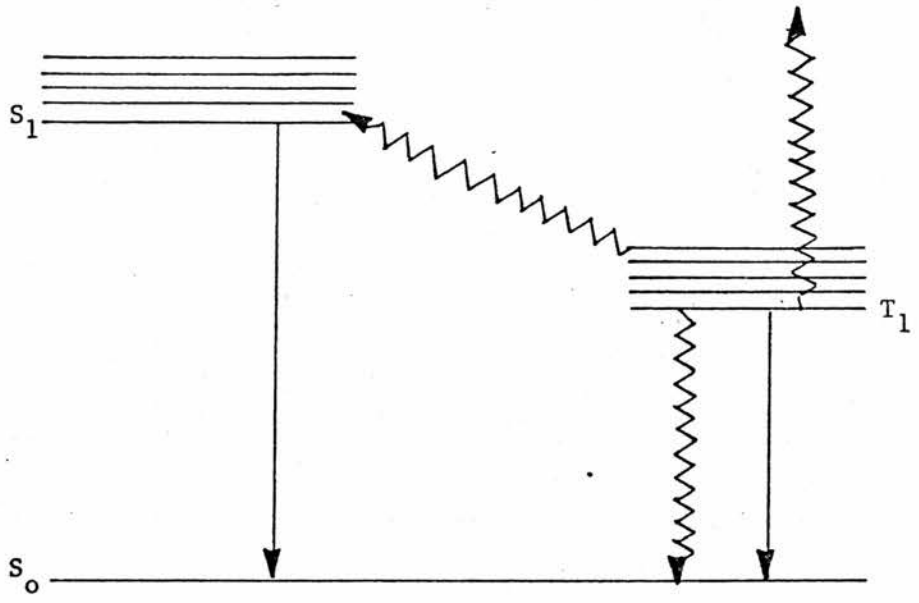

Figure 2.7. Possible triplet state deactivation processes.

Kinetics of this nature may be illustrated by consideration of thermal deactivation to a singlet state by inter-system crossing. The rate of decay of the triplet state can then be expressed by the equation:-

$$\frac{d[T]}{dt} = k_o[T] + k_t[T]$$

Since inter-system crossing is a first order process the decay is exponential and the observed rate constant, k_{obs}, is the sum of the intrinsic and temperature dependent rate constants i.e. $k_{obs} = k_o + k_t$.

The activation energy of the thermally activated process can be determined by substituting for k_t using the Arrhenius relationship:-

$$k_{obs} = k_o + Ae^{-\frac{\triangle E}{RT}}$$

where $\triangle E$ is the activation energy , A is the pre-exponential factor and R is the Gas Constant hence:-

$$\log(k_{obs} - k_o) = \log A - \frac{\triangle E}{RT} \qquad (2.1)$$

Since k_o cannot be determined experimentally the approximation, $\tau_o = \tau_{77}$, was used in the Stern-Volmer plot, $\log (\frac{1}{\tau} - \frac{1}{\tau_o})$ against 1/T, which has a gradient of $-\triangle E/RT$ and an intercept is log A.

The simple model with one thermally activated process, described above, may be extended to include several first order thermal processes described by the rate equation:-

$$\frac{d[T]}{dt} = k_o[T] + k_t' + k_t''[T] + \ldots$$

Consider the case with three processes, the Stern-Volmer plot of log $(k_{obs} - k_o)$ against time, illustrated in Figure 2.8, shows that there are three areas of first order behaviour with breaks at B and C.

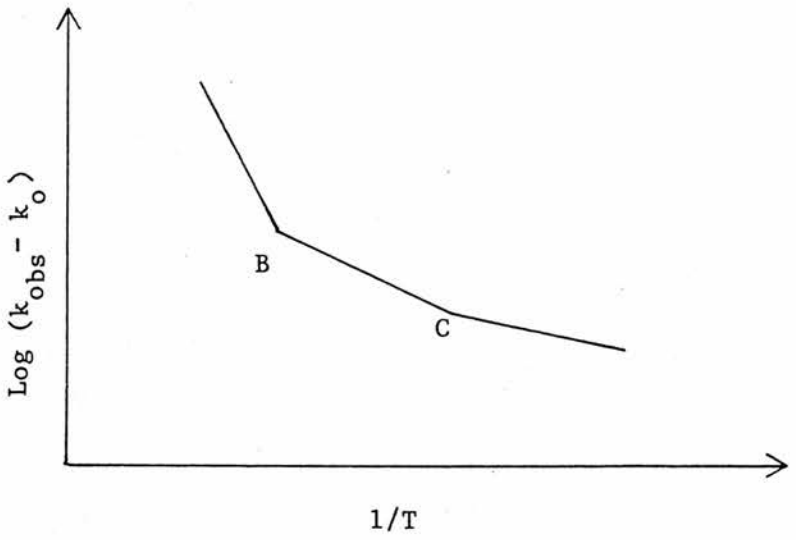

Figure 2.8. Stern-Volmer plot of three thermally activated processes.

At low temperature only the process with the lowest $\triangle E$ is significant and the higher energy processes may be neglected so that equation 2.1 may be used to calculate $\triangle E'$ and A'. These values may then be used to calculate $\triangle E''$ and A'' for the next lowest energy process from the data in the region B ---> C from the equation:-

$$\log(k_{obs} - k_o - (\log A' - \frac{\Delta E'}{RT})) = \log A'' - \frac{\Delta E''}{RT}$$

and in a similar manner $\Delta E''$ and A'' may be calculated from the data in the region C ---> D. The value at 77K was used as an approximation and was varied by a small amount

If the energy transfer is to another triplet of the same type in the system then triplet-triplet annihilation occurs whereby :-

$$T_1 + T_1 \text{ -----> } S_o + S_1$$

In this case the decay is non-exponential and is more fully described in the section below.

(ii) Triplet-triplet annihilation

When triplet-triplet annihilation occurs the decay of the triplet state is a combination of a first order decay

$$T_1 \text{ -----> } S_o$$

and a second order decay

$$T_1 + T_1 \text{ ------> } S_o + S_1$$

and/or $T_1 + T_1 \text{ -----> } 2S_o$

If the repopulation of the triplet state from the newly formed S_1 state is ignored then the rate of decay is :-

$$-\frac{d[T]}{dt} = k_1[T] + k_2[T]^2$$

Integration of the above gives:-

$$\frac{1}{[T]} = \left[\frac{1}{[T]_0} + \frac{k_2}{k_1}\right] \exp(k_1 t) - \frac{k_2}{k_1}$$

where k_1 is the sum of the first order rate constants and k_2 is the second order rate constant. A three variable itterative fitting routine based on the method of differential coefficients[29] was used in the FORTRAN computer pogram TRIP (Appendix I) to calculate the values for k_1 and k_2. The three variables were $[T]_o$, k_1 and k_2.

(iii) Emission from two species

If the emission observed is the combination of emissions from two different types of excited molecule which have different lifetimes then the overall decay will be non-exponential and the sum of two exponential components. If the two processes are:-

$$A^* \xrightarrow{k_1} A$$

$$B^* \xrightarrow{k_2} B$$

the two rates of decay are:-

$$[A^*] = [A^*]_o e^{-k_1 t}$$

$$[B^*] = [B^*]_o e^{-k_2 t}$$

the observed intensity is $[A^*] + [B^*]$ hence

$$[I]_{obs} = [A^*]_o e^{-k_1 t} + [B^*]_o e^{-k_2 t}$$

A three variable fitting routine was used in computer program DEX (Appendix II) to calculate the values of k_1 and k_2. The data was normalized so that $[B^*] = 1 - [A^*]$, the three variables were then $[A^*]$, k_1 and k_2. The second emitting species may be the photoproduct from a photochemical reaction involving the original molecule and the deviation from exponentiality may only occur at higher temperature because there is an activation energy for the photochemical reaction. If a this type of situation occurs then the decay of the phosphorescence at 77K after irradiation should also be non-exponential.

Another possibility is emission from two excited state conformers or an excimer formed on irradiation of the system. In this case the decay at 77K after irradiation should be unchanged .

Activation energies for k_1 and k_2

Values for k_1 and k_2 were calculated from the fitting routines

and were treated in different ways to calculate the corresponding activation energies.

Activation energy from k_2

At temperatures below 300K k_2 is negligible and may be considered as zero for both kinetic schemes so the calculated values of k_2 from the data above 300K is the rate constant of the second order process in the triplet-triplet annihilation scheme and the second emission in the duel emission scheme, hence:-

$$k_2 = Ae^{-\frac{\triangle E}{RT}}$$

an Arrhenius plot of log k_2 against 1/T has a gradient of $-\triangle E/RT$ and an intercept of log A.

Activation energy from k_1

The value of k_1 obtained from the fitting routine is the sum of the rate constants for all the first order processes which deactivate the triplet state, $k_1 = k_o + k_t$, and the activation energies may be calculated as previously described in section (i).

CHAPTER 3

NON-EXPONENTIAL DECAY OF PHOSPHORESCENCE FROM HALOGENATED AROMATIC HYDROCARBONS

The phosphorescence decays of 1-bromonaphthalene, 2-bromonaphthalene, and 9-bromophenanthrene, dispersed in poly-(methylmethacrylate)(PMMA) matrices have been investigated. The phosphorescence decays were determined at various temperatures between 77K and the glass transition temperature of PMMA (ca. 380K). Data was recorded over several first-order lifetimes which were between 1 and 20 milliseconds in all cases.

At temperatures below 300K the decay of the phosphorescence with time was found to be exponential, within experimental error, in each case (Figure 3.1) but above 300K there were significant deviations from exponentiality (Figure 3.2).

Non-exponential behaviour of this nature has been reported previously for the phosphorescence from aromatic hydrocarbons above room temperature[30,31] but it was thought that this type of temperature dependence was probably restricted to molecules with long-lived triplet states with phosphorescence lifetimes of, say, one second.

There have been reports of non-exponential phosphorescence decay at all temperatures for some organic molecules with lifetimes in the millisecond range[32,33,34] but these have been rationalized as the

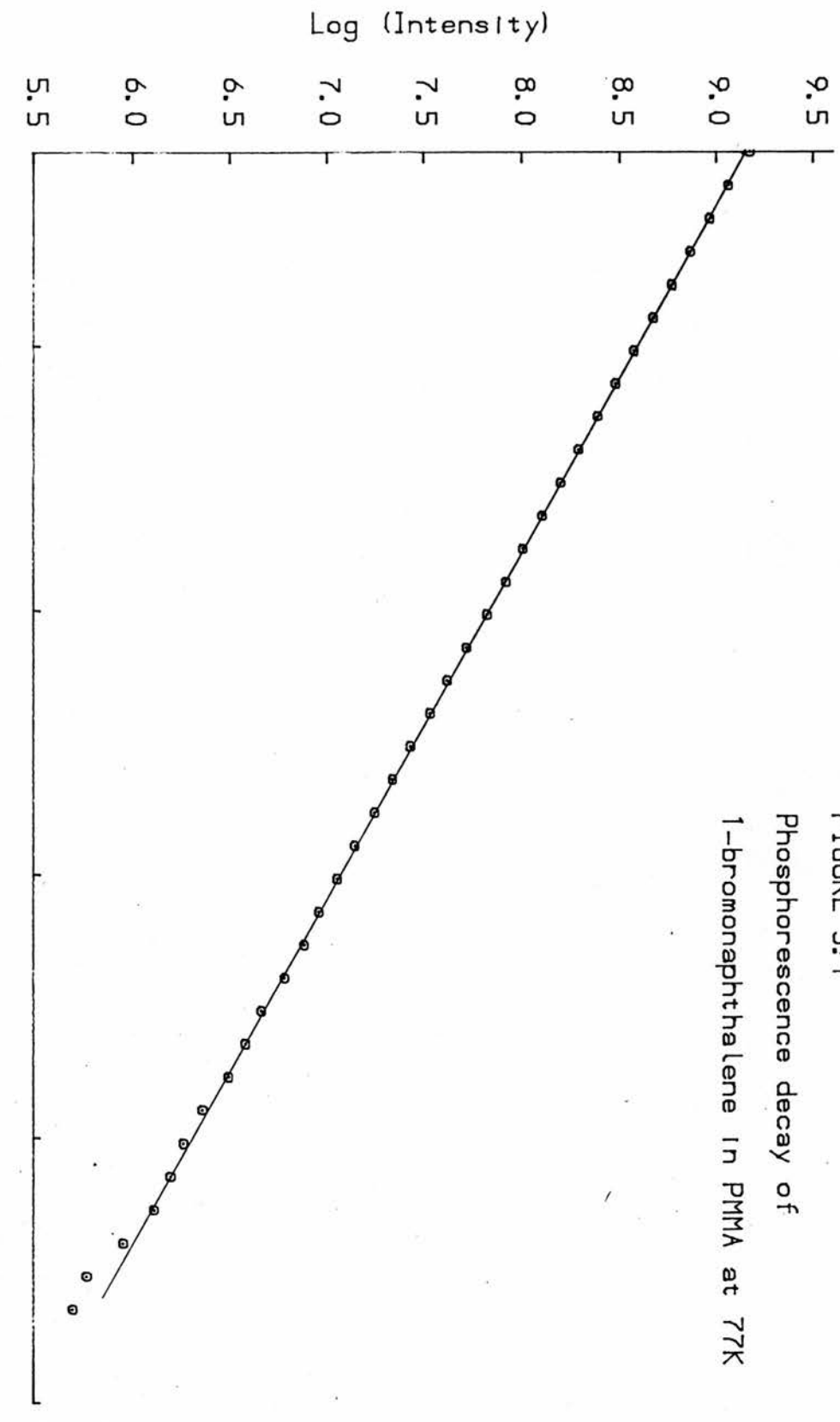

FIGURE 3.1

Phosphorescence decay of

1-bromonaphthalene in PMMA at 77K

FIGURE 3.2

Phosphorescence decay of

1-bromonaphthalene at 352K

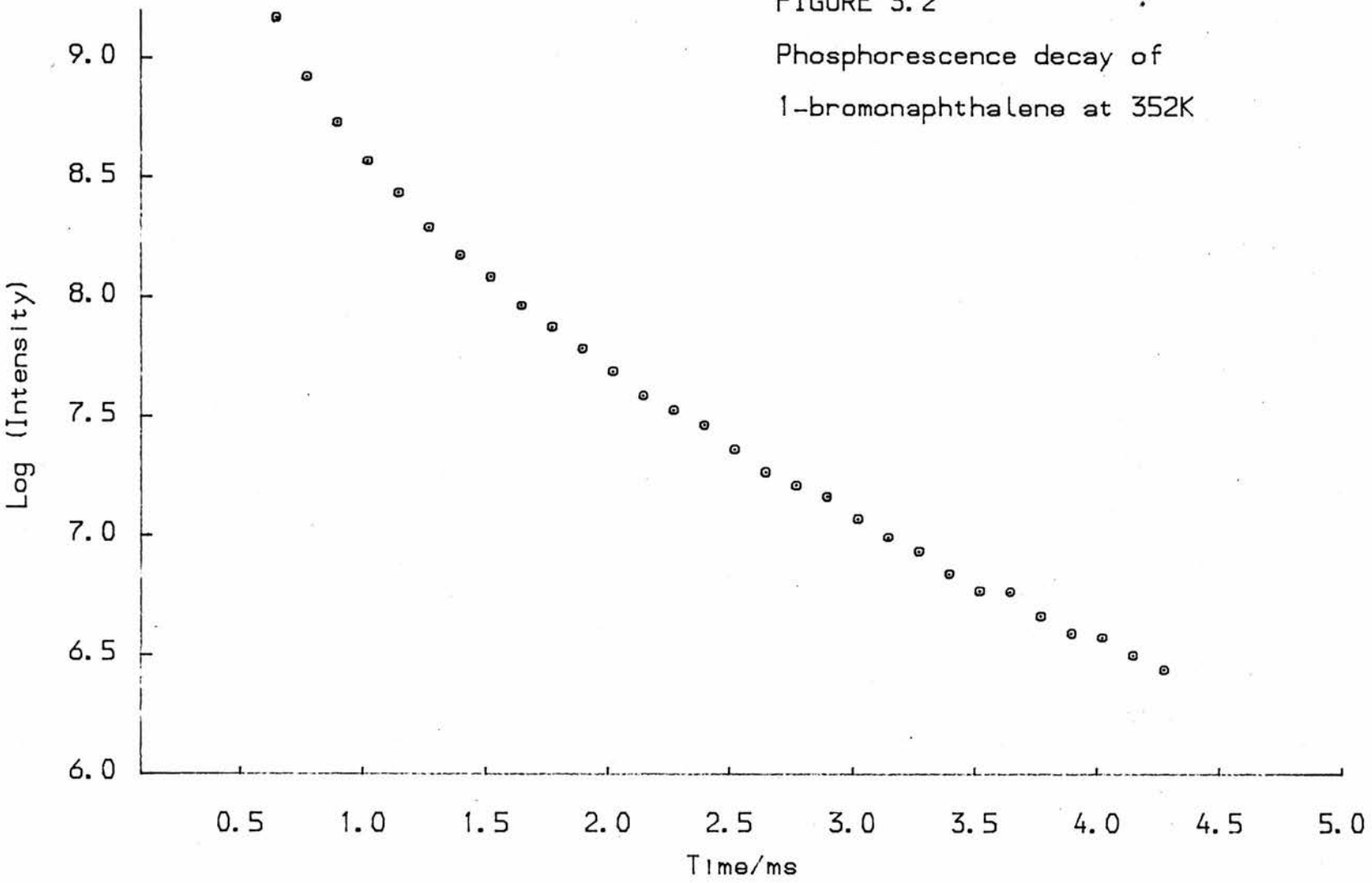

result of fundamental properties of the molecule rather than thermally activated processes.

Causes of non-exponential decay in polymer matrices

Many explanations have been offered to explain the non-exponential decay of the phosphorescence of molecules incorporated in a polymer matrix and they are summarized below:-

a. Direct quenching of the triplet state by impurities[22,35],
b. Quenching by molecular oxygen[36],
c. Free radicals in the PMMA matrix[37],
d. Aggregation of the solute molecules[38],
e. Interaction between the solute and the PMMA[39],
f. Presence of more than one meta-stable state[35],
g. Pseudo first order quenching process occurring in regions of low viscosity in the matrix[30],
h. Photoselection of the substrate[40] and
i. Inhomogeneous medium[41].

Failure to consider these possibilities has lead to confusion in the past and hypotheses such as "Multiple meta-stable states"[42,43] have been found to be explained by the presence of impurities.

Careful preparation of the samples can prevent many of the above effects and in this work precautions were taken to exclude oxygen. Free molecular oxygen is known to be consumed during the polymerization process but to ensure the total exclusion of oxygen the samples were degassed before polymerization by the vacuum freeze-thaw method and the sample tubes containing the polymerized samples were pumped out for two hours before being sealed.

Thin polymer films were prepared and the phosphorescence decays

were compared to those of the bulk samples prepared by polymerization of the monomer solution as described in Chapter 2. Purified, uniform molecular weight PMMA was dissolved in redistilled, dried CH_2Cl_2 with some of the recrystallized solute and thin films were cast by evaporating the CH_2Cl_2. The resulting films were ca. 50 microns thick and had a solute concentration of ca.10^{-3}M. The lifetimes and the profile of the phosphorescence decay were identical in both samples indicating that impurities, low-viscosity regions in the polymer, different solute-solvent environments and aggregation of the solute molecules make no significant contribution to the decay of the triplet state. Any effect from these would be minimized in the thin films and this would be reflected by differences in the phosphorescence decay between the two samples.

Jones and Siegel[37] observed non-exponential decay at room temperature in samples of several aromatic hydrocarbons in PMMA when they irradiated the sample with intense broad-band radiation, the decays were exponential if the exciting radiation was monochromatic and of low intensity. This was attributed to diffusion controlled quenching of the triplet state by photochemically produced free radicals.

Persistent free radicals are known to be present in PMMA and have been characterized by their e.s.r. spectra[44]; the spectrum remains unchanged over several months. The e.s.r. spectrum of a sample of pure PMMA in a quartz tube which had been irradiated with a medium pressure mercury lamp for 20 minutes indicated that the concentration of radicals remained at about 10^{-6}M. In the phosphorescence lifetime measurements, the exciting radiation was restricted to wavelengths above 350nm which is well above the absorption band in PMMA and should

preclude further radical formation. It is unlikely that photoinitiated free radicals ever reach a high enough concentration to affect the decay to a significant degree.

Photoselection of the substrate molecules during excitation was proposed as another reason for non-exponential decay[40]. If the first order lifetimes of the excited molecules and their isotropic rotational relaxation times are of the same order then both positive and negative deviations from linearity in the plots of log I against time are possible[45] and there is a calculable upper limit for the deviation from exponentiality in this model. Only positive deviations from linearity were observed in this work and at higher temperatures the calculated limit of the deviation from exponentiality due to photoselection was exceeded. These results indicate that photoselection is not an important factor.

There was no evidence to suggest that there was any chemical interaction between the solute molecules and the polymer. An irradiated sample was dissolved in CH_2Cl_2 and the PMMA was precipitated with ethanol. The fluorescence characteristic of the substrate was found in the CH_2Cl_2 solution and was undetectable in the precipitated PMMA.

The phosphorescence decay of acetone has been shown to have a non-exponential decay at all temperatures[32] and this has been attributed to emission from both the $n-\pi^*$ and the $\pi-\pi^*$ triplet levels. Mixing of the excited states is a fundamental property of the molecule and is independent of temperature and excitation light[33], and cannot satisfactorily describe the non-exponential decay observed in these experiments. Two other possibe causes of the non-exponential behaviour are examined in more detail below.

Triplet-triplet annihilation

Triplet-triplet annihilation occurs when the energy from two triplet molecules interact to form two singlet states. These may consist of either one excited and one ground state singlet or two ground state singlets,

$$T_1 + T_1 \text{ -----> } S_o + S_1$$

and/or $$T_1 + T_1 \text{ -----> } 2S_o.$$

If one of the resulting singlet states is an excited state then p-type delayed fluorescence may also occur. It has been well documented in fluid solution, by Parker[25], where it is diffusion controlled.

Triplet-triplet annihilation is not, however, restricted to fluid solutions and may occur in solid solutions even at low temperatures where material diffusion is negligible.

The delayed fluorescence observed by McGlynn and Azumi[46,47] from EPA glasses containing aromatic molecules at 77K was interpreted as the result of direct resonance transfer between triplet states.

Polymer matrices have also been shown[17] to support triplet-triplet annihilation and in such systems it may occur over relatively long distances. Triplet energy can migrate along the polymer chain until it comes close enough to another triplet (ca. 1.5nm) to undergo triplet-triplet annihilation with the formation of S_o and S_1 which initiates delayed fluorescence.

The kinetics for triplet-triplet annihilation, which are more fully described in Chapter 2, are based on the equation:-

$$-\frac{d[T^*]}{dt} = k_1[T^*] + k_2[T^*]^2$$

where [T] = triplet state concentration, t = time and k_1 and k_2 are first and second order rate constants respectively. The computer program used for the fitting procedure (TRIP) is listed in Appendix I .

Emission from two excited species (Dual Emission)

If two emitting species are present in the system and their emission bands overlap then apparently non-exponential decay will be observed if the emission lifetimes and intensities are similar. If the latter condition is not fulfilled then the emission from one of the species will predominate and the effect from the other component will be undetectable. The second emitting species could, for example, be an excited state conformer as in benzil[48], a photoproduct formed on irradiation of the sample or an excimer.

The kinetics for emission from two species are described in Chapter 2 and obey the following equation:-

$$I(t) = Ae^{-k_1 t} + Be^{-k_2 t}$$

where I(t) = the intensity at time t, k_1 and k_2 are rate constants and A and B are constants. The computer program used for the fitting procedure (DEX) is listed in Appendix II.

Temperature Dependence of Phosphorescence in PMMA Matrices

Aromatic molecules containing the heavy atom, bromine, were

particularly chosen for this study because they have phosphorescence lifetimes of a few milliseconds. The heavy atom lowers the lifetime compared to the corresponding hydrocarbon. e.g. τ_p of naphthalene is 2.3s[49] and τ_p of 1-bromonaphthalene is 16ms.

All three molecules have exponential lifetimes over at least three lifetimes at 77K (see Table 3.1).

SAMPLE	τ_p /ms	R
1-bromonaphthalene	13.88	0.999
2-bromonaphthalene	16.50	0.999
9-bromophenanthrene	9.80	0.999

Table 3.1. Lifetimes and correlation coefficients from least squares regression.

The phosphorescence decay was measured at 77K and at various temperatures up to 380K, and where the decay was exponential lifetimes were calculated.

Results

Below 300K the decays were exponential over at least three lifetimes but there was significant deviation from exponentiality at temperatures above 300K. The rate of decay of the phosphorescence was found to be temperature dependent over the entire temperature range.

Figures 3.3 - 3.5

Comparison of the experimental phosphorescence decay data with the curves generated in the fitting routines for triplet-triplet annihilation and dual emission

⊙ Experimental data

x Triplet-triplet annihilation data

\+ Dual emission data

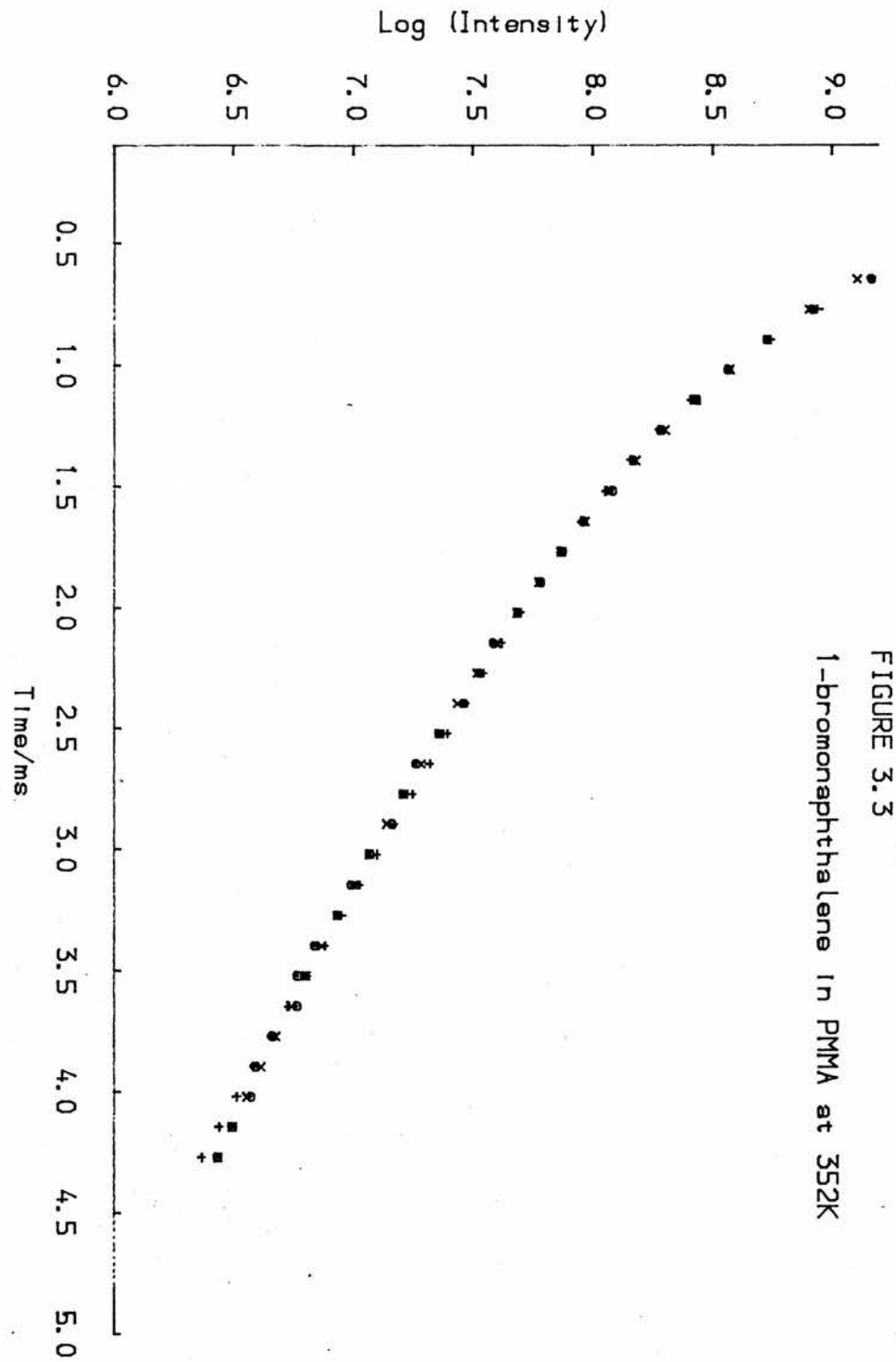

FIGURE 3.3

1-bromonaphthalene in PMMA at 352K

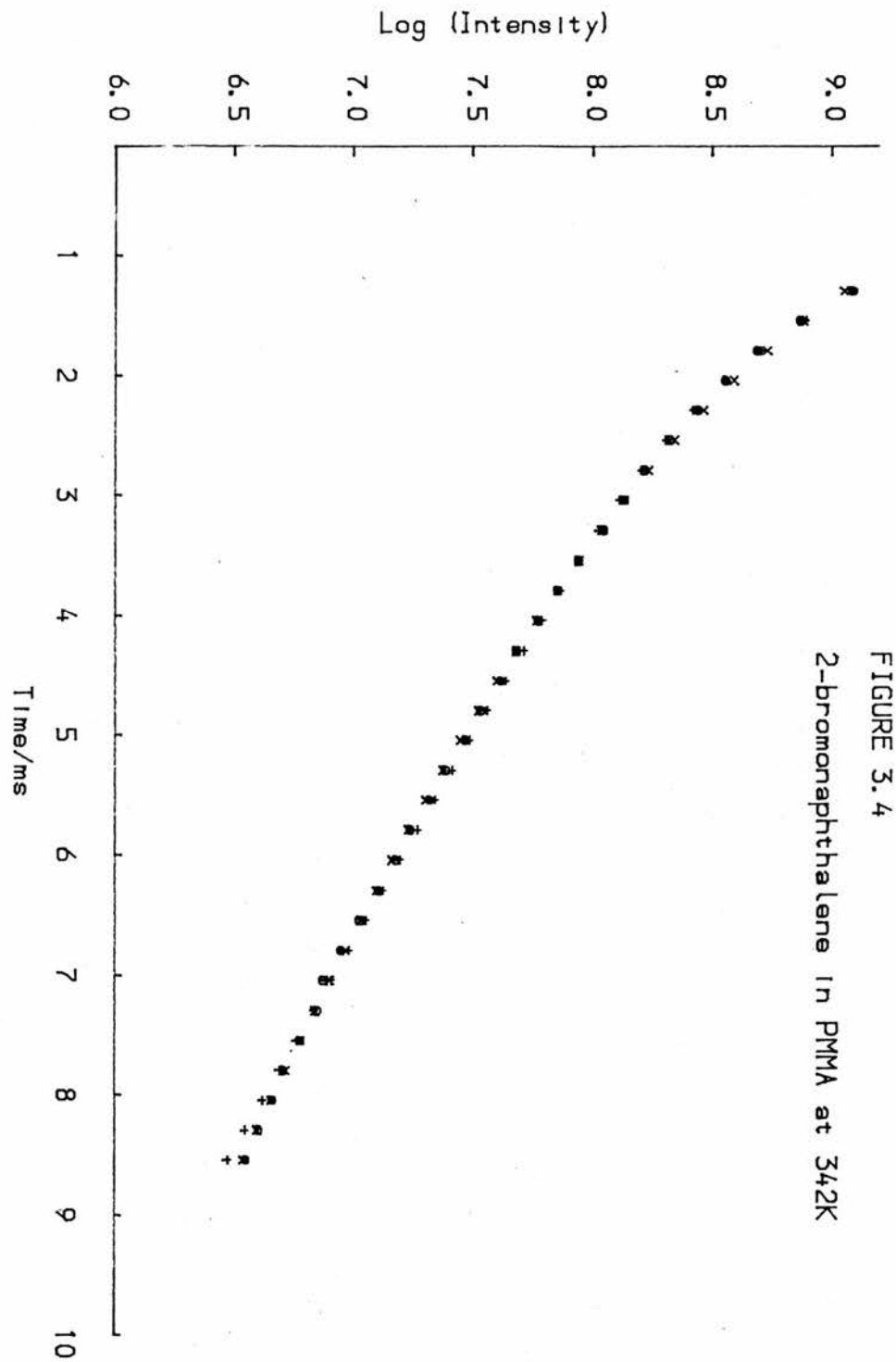

FIGURE 3.4
2-bromonaphthalene in PMMA at 342K

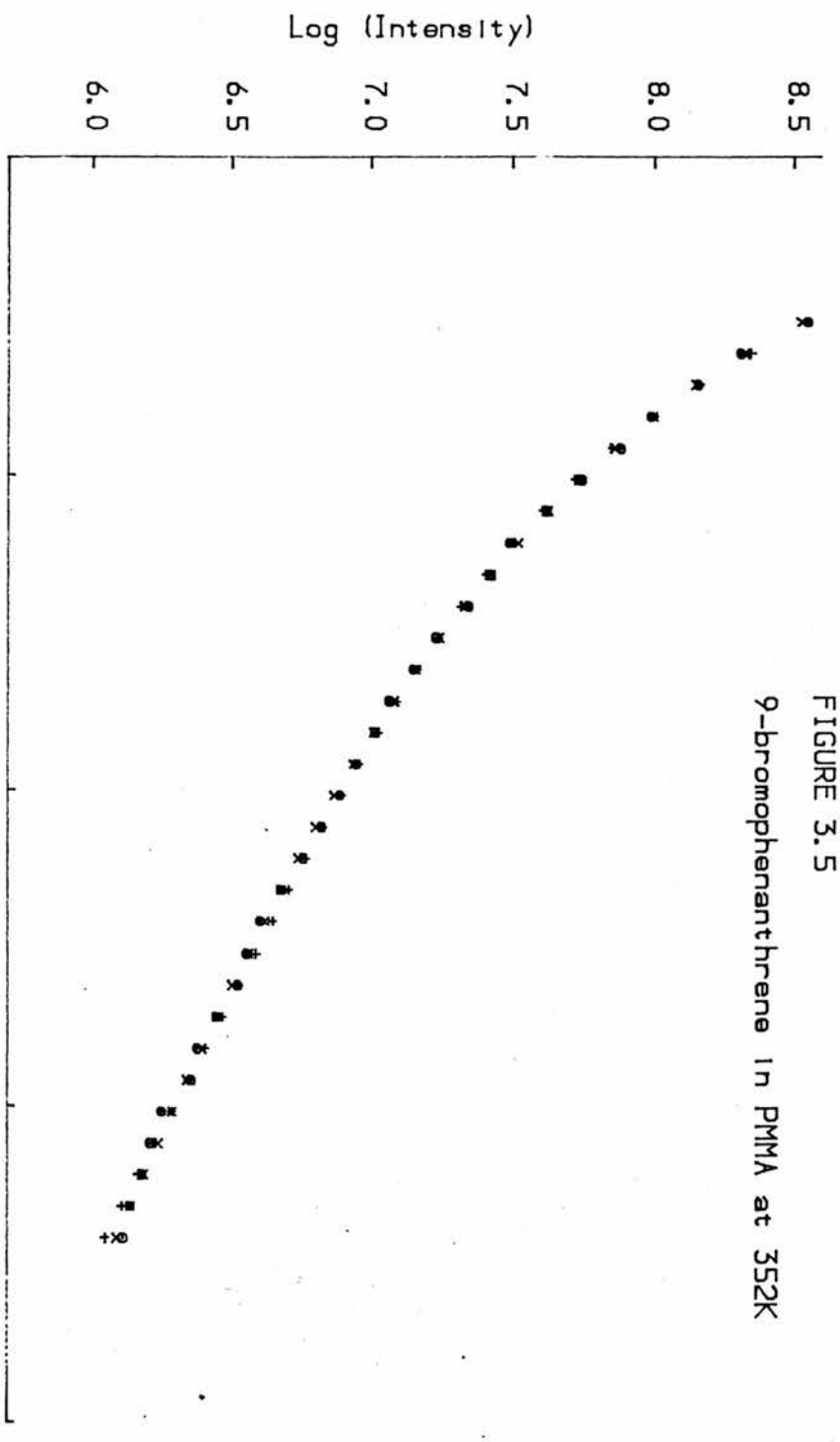

FIGURE 3.5
9-bromophenanthrene in PMMA at 352K

TEMPERATURE /K	TRIPLET-TRIPLET ANNIHILAION		DUAL EMISSION	
	k_1	k_2	k_1	k_2
311	129.54	.0112	180.08	1602.11
312	154.27	.007	164.85	680.94
313	141.80	.0106	159.43	672.13
318	152.3	.015	207.69	1576.32
318	141.43	.0061	154.79	679.99
318	154.36	.0144	171.23	733.28
320	165.2	.0126	208.69	1411.08
322	180.40	.0053	188.94	743.01
325	167.34	.0284	236.94	1727.80
327	196.37	.0096	198.03	840.54
328	185.00	.0257	245.52	1546.44
333	211.82	.0404	291.91	2007.21
334	214.56	.036	241.07	949.86
335	208.94	.0480	290.98	1706.05
339	215.16	.0389	249.63	881.85
342	248.86	.0481	320.75	1491.66
345	267.91	.0626	355.09	1651.05
347	268.04	.0992	488.02	2945.50
350	338.33	.1283	534.32	3101.61
352	341.18	.083	417.21	1913.50
352	372.36	.1526	580.00	3282.55
357	381.90	.1517	600.58	3230.80
361	382.59	.2474	645.9	3412.40
365	464.47	.3731	797.04	4263.06

Table 3.2. Rate constants from fitting procedures for triplet-triplet annihilation and DUAL emission kinetics for 1-bromonaphthalene

TEMPERATURE /K	TRIPLET-TRIPLET ANNIHILATION		DUAL EMISSION	
	k_1	k_2	k_1	k_2
299	108.87	.0041	119.34	637.22
308	113.71	.0081	131.59	657.05
308	86.55	.0139	150.63	1691.3
316	120.20	.0143	147.22	726.00
319	105.95	.0173	175.47	1612.18
320	122.00	.0205	184.89	1669.54
323	116.61	.0222	187.14	1599.08
329	154.22	.0357	224.84	1689.80
332	133.68	.0417	255.10	1801.72
337	149.80	.0658	261.00	2039.31
341	157.06	.0474	252.34	1443.49
342	190.99	.0626	289.41	1761.97
345	173.14	.0635	282.04	1668.32
345	230.01	.0612	381.70	2487.17
350	244.09	.0575	281.75	1574.66
350	239.35	.0816	435.00	2682.75
354	233.46	.1411	467.98	3068.32
356	289.98	.1519	530.39	3319.59
360	189.27	.1676	469.75	2674.00
362	327.58	.3109	623.63	3965.35
364	232.33	.1916	513.56	3384.03

Table 3.3. Rate constants from fitting procedures for triplet-triplet annihilation and DUAL emission kinetics for 2-bromonaphthalene.

TEMPERATURE /K	TRIPLET-TRIPLET ANNIHILATION		DUAL EMISSION	
	k_1	k_2	k_1	k_2
290	182.09	.0176	222.74	895.48
300	206.01	.0304	253.70	1046.01
302	196.30	.0354	252.01	1025.73
303	214.75	.0444	268.55	1161.63
308	227.33	.0441	289.27	1289.50
310	245.97	.0460	293.50	1245.25
312	275.28	.0337	300.85	1286.10
315	250.25	.1103	326.17	1325.58
319	304.74	.0472	333.99	1375.15
322	179.94	.1591	654.10	4372.34
326	282.65	.1425	480.71	2717.34
327	292.37	.2092	771.03	5018.09
330	313.72	.2490	817.94	5616.27
332	355.41	.2502	562.64	3003.53
334	381.21	.3104	878.53	5241.15
338	454.86	.3654	943.31	5896.60
340	486.16	.4600	1052.29	6470.19
345	815.57	.5615	1217.80	6793.66
346	539.14	.6401	1143.65	6857.60
348	922.67	.06552	1262.83	645.71
350	615.59	.7598	1181.51	6838.14

Table 3.4. Rate constants from fitting procedures for triplet-triplet annihilation and DUAL emission kinetics for 9-bromophenanthrene

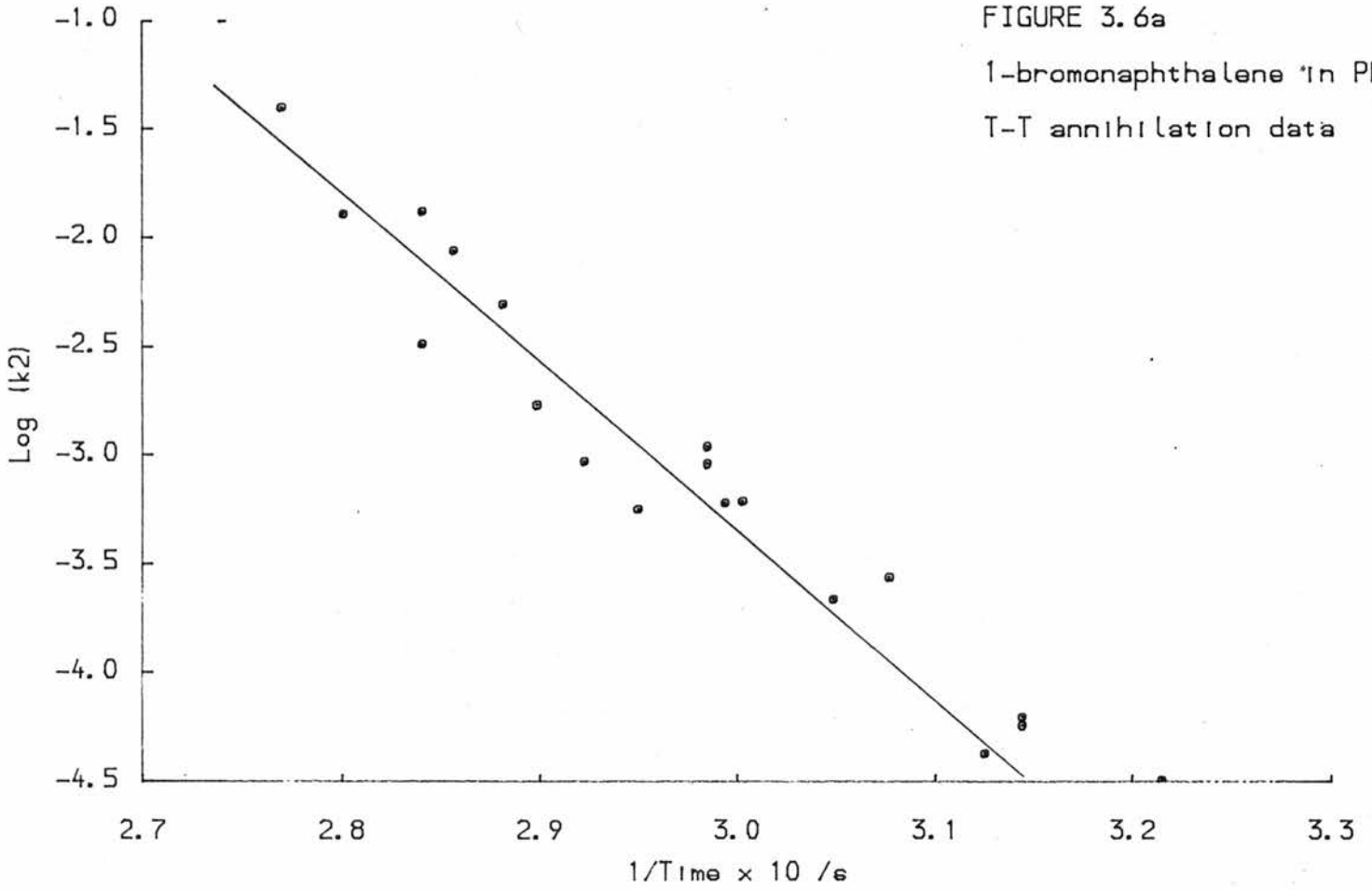

FIGURE 3.6a

1-bromonaphthalene in PMMA

T-T annihilation data

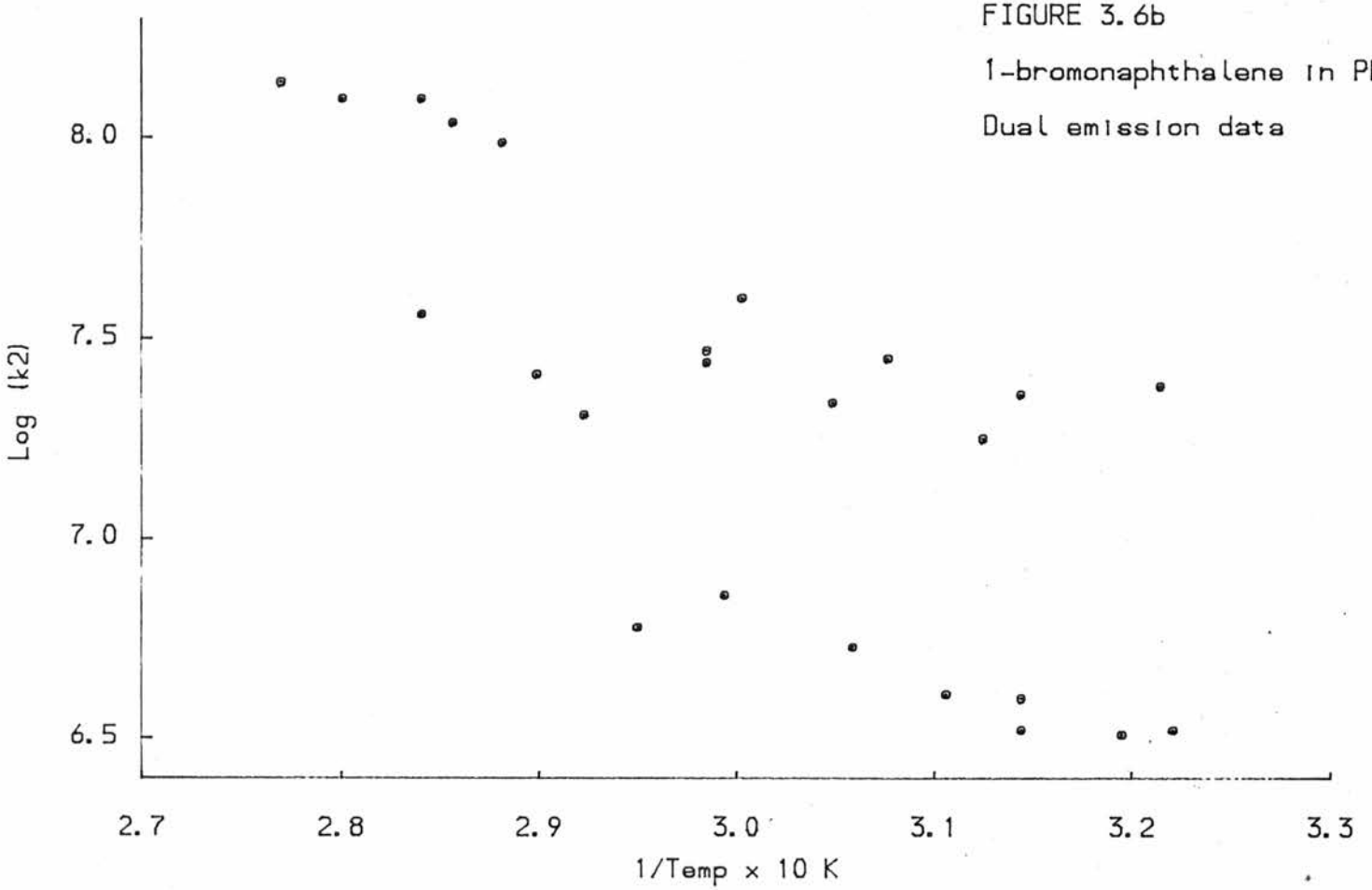

FIGURE 3.6b

1-bromonaphthalene in PMMA

Dual emission data

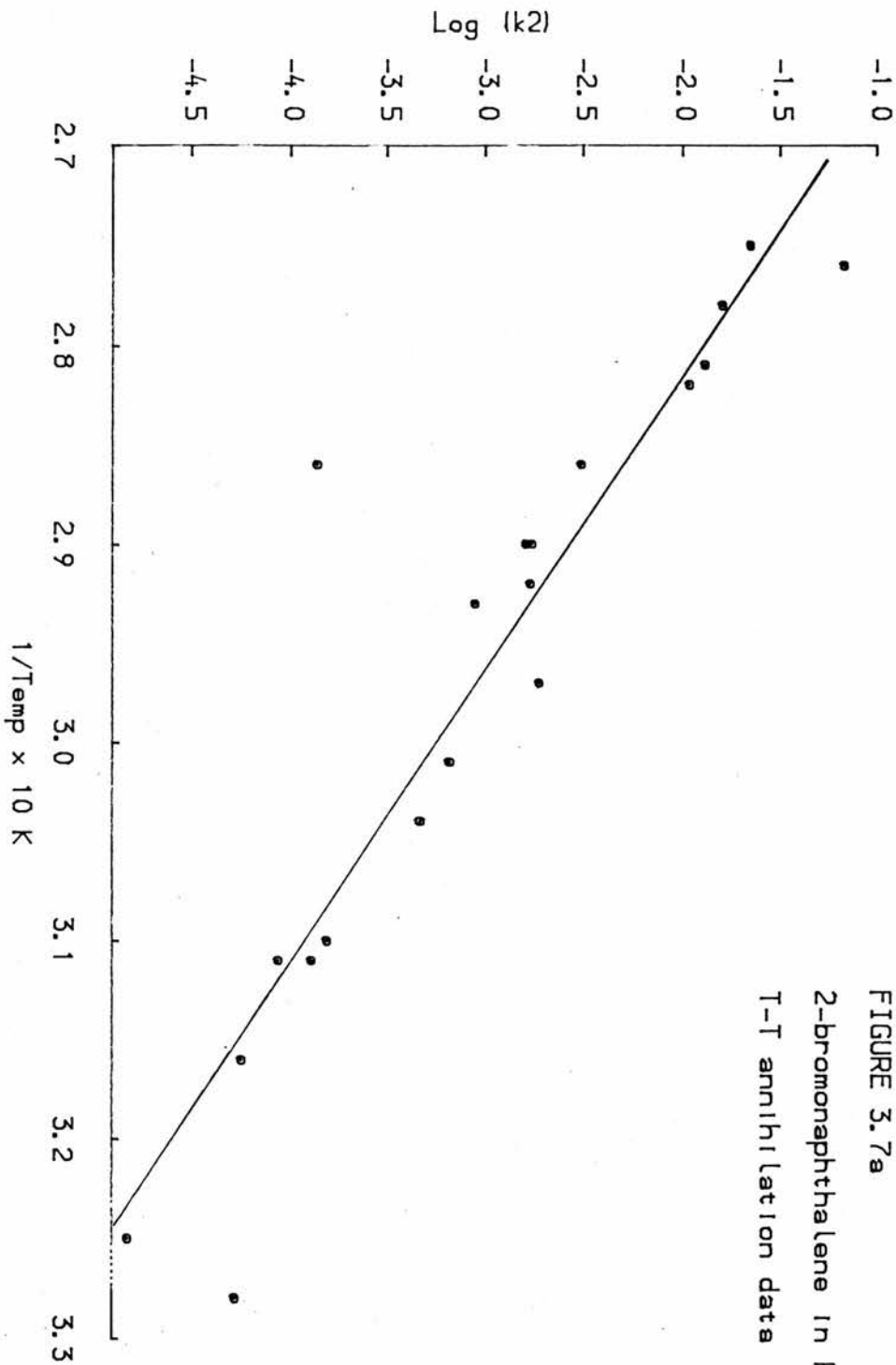

FIGURE 3.7a

2-bromonaphthalene in PMMA

T-T annihilation data

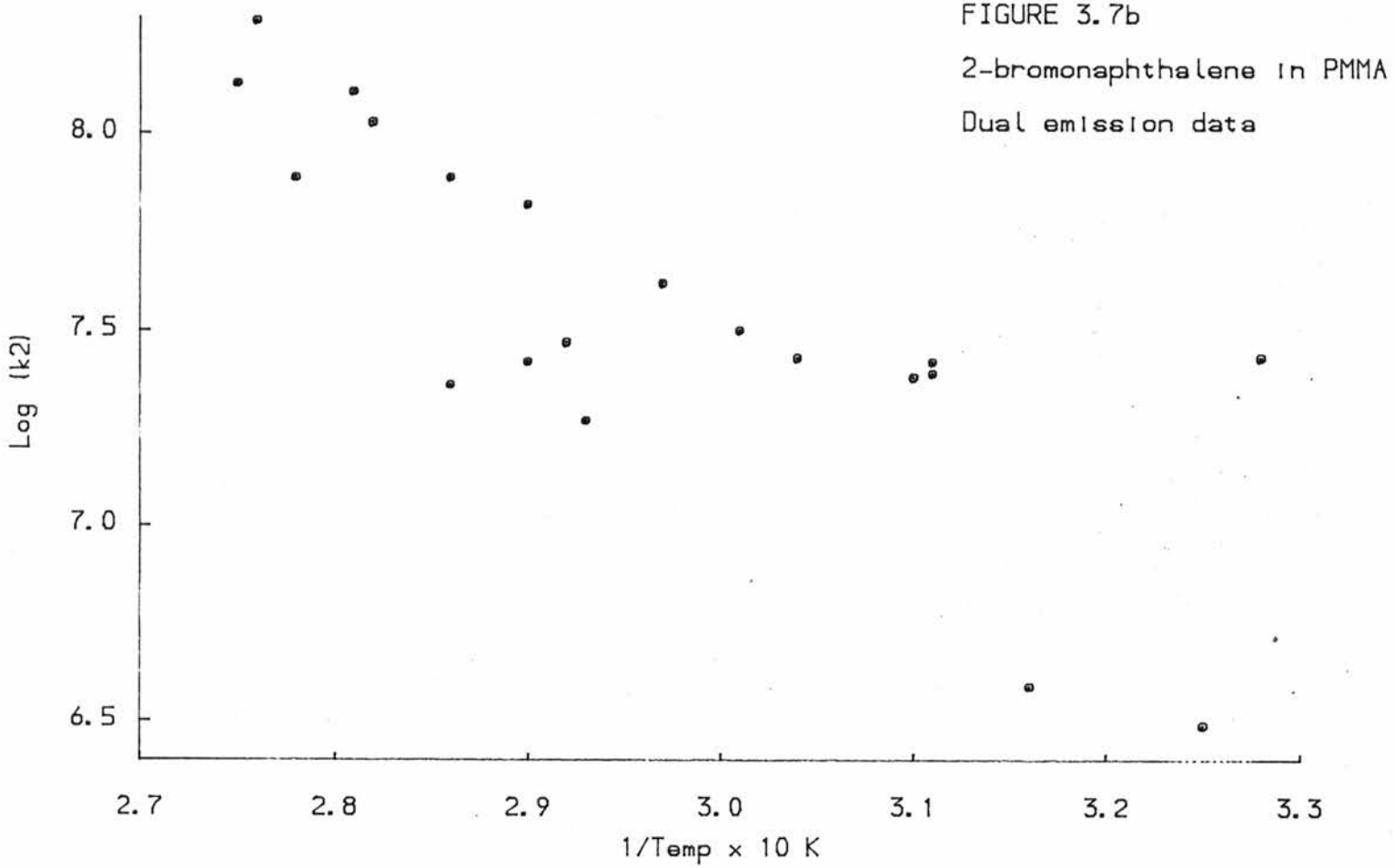

FIGURE 3.7b

2-bromonaphthalene in PMMA

Dual emission data

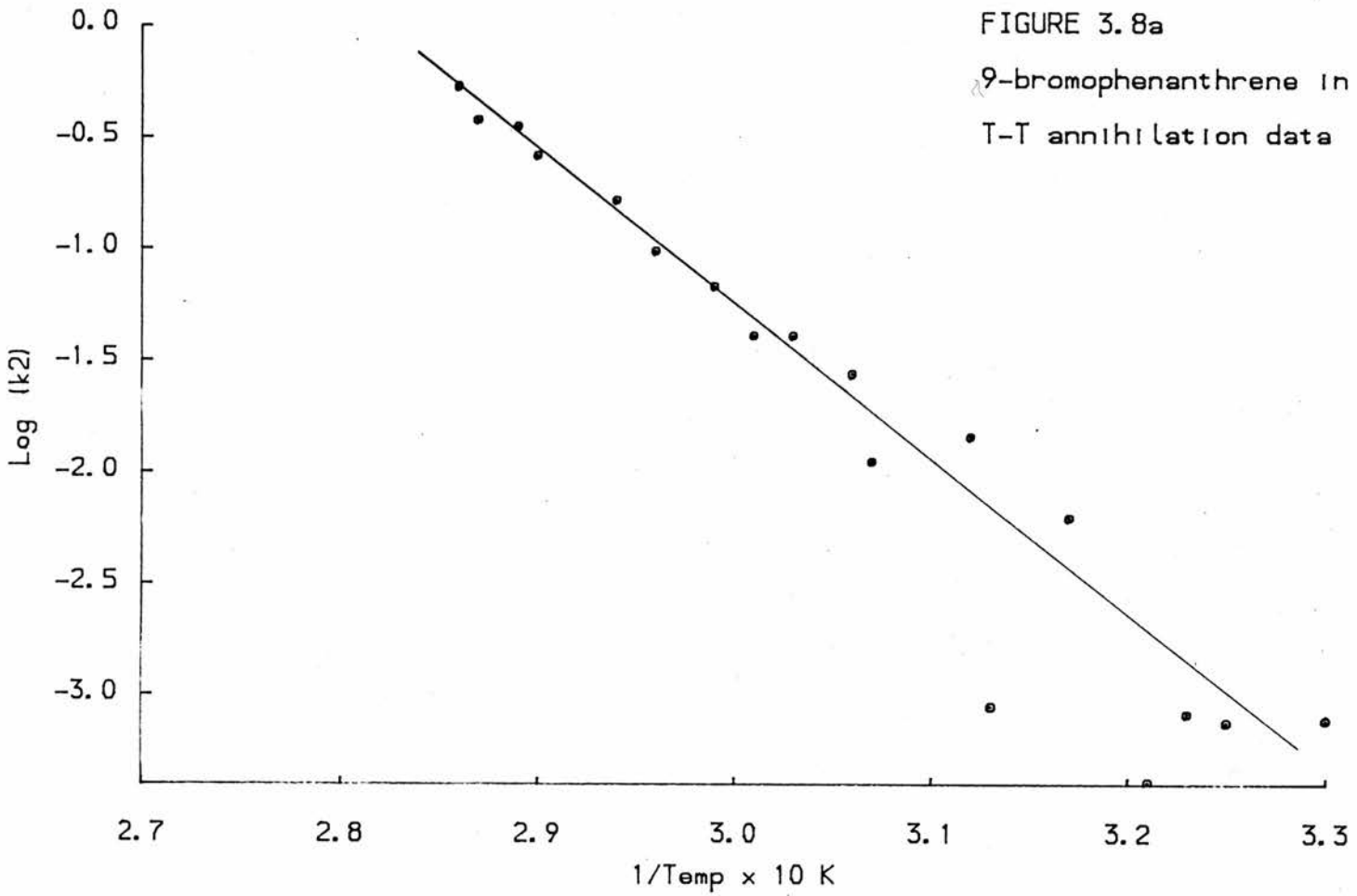

FIGURE 3.8a

9-bromophenanthrene in PMMA

T-T annihilation data

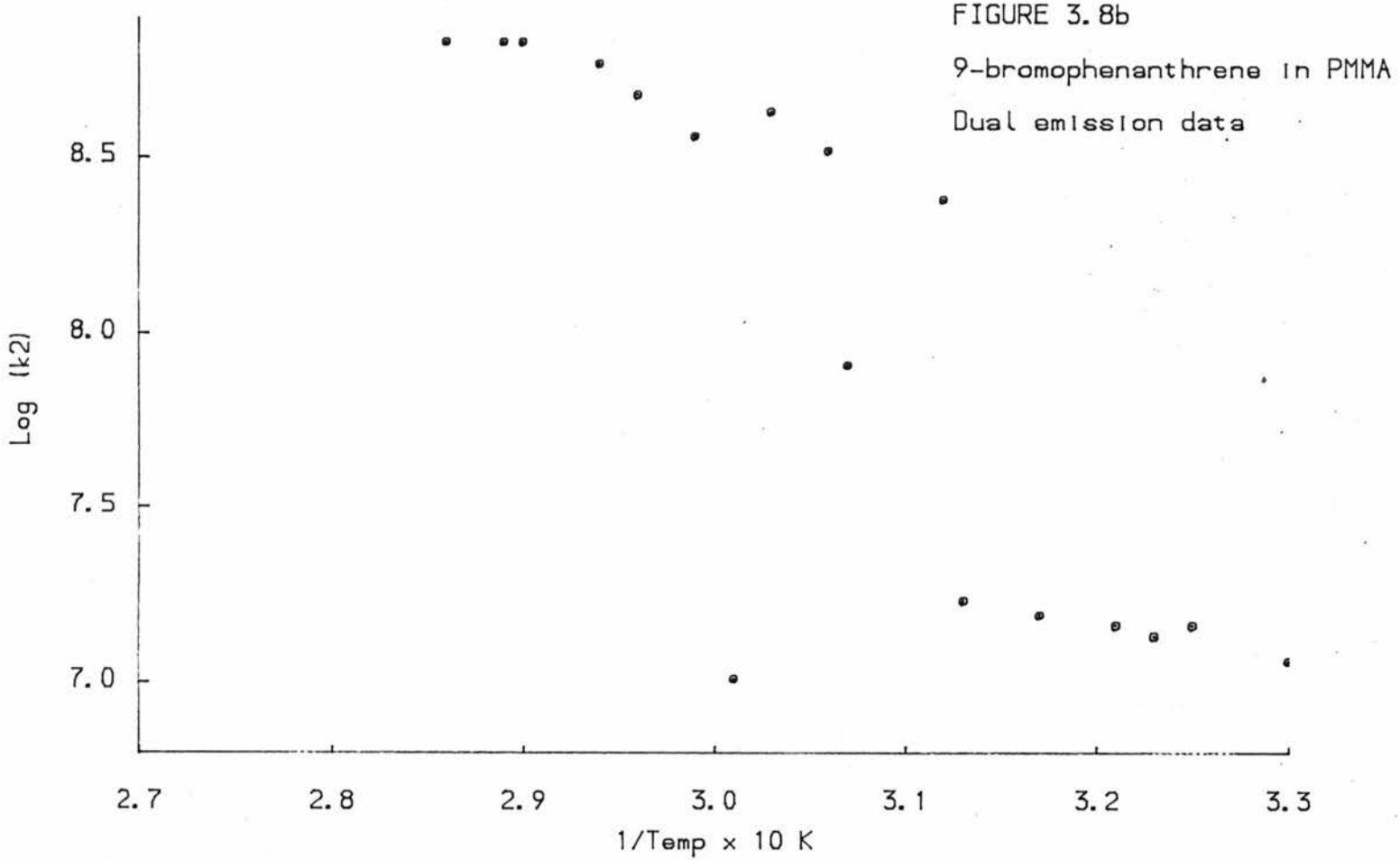

FIGURE 3.8b

9-bromophenanthrene in PMMA

Dual emission data

High Temperature

As previously described, care was taken during the sample preparation to preclude the many possible causes of non-exponential decay suggested in the literature. Two possible kinetic schemes were examined, triplet-triplet annihilation and dual emission, to determine which gave the closest agreement with experimental data. This involved analysing the the intensity against time decay profiles using the iterative fitting routine described in Chapter 2 and the calculated values of k_1 and k_2 are given in Tables 3.2-3.4.

Initially this fitting procedure proved to be inconclusive because both kinetic schemes fitted the data with an error of less than 5% over all the points.

On closer inspection it can be seen that the best fit and the experimental data (shown in Figures 3.3 - 3.5) favours the triplet-triplet annihilation kinetics as a more accurate description of the decay as the error is evenly distributed whereas in the dual emission model the error is concentrated in the last 10% of the data.

Both the first and second order rate constants exhibited temperature dependence and further evidence favouring the triplet-triplet annihilation scheme came from the activation energies calculated for these processes From Figures 3.6 - 3.8 it is clear that the Arrhenius relationship, log k_2 against 1/T is closer to linearity for the computed data from the triplet-triplet annihilation model than the dual emission model.

Emission of delayed fluorescence is often used as evidence for the occurrence of triplet-triplet annihilation but it was not possible to observe this with our experimental apparatus as the apparatus recorded a weak emission at the wavelength where delayed fluorescence would be expected. The emission was present whether or not there was a

sample in the sample chamber and the lifetime of the emission was ca. 1.2ms at room temperature which is of the order expected for the delayed fluorescence.

It was concluded that the triplet-triplet annihilation kinetics gave the most satisfactory description of the experimental phosphorescence decay above 300K.

Temperature Dependence of Second Order Rate Constants

Temperature dependence of the second order rate constants, calculated from triplet-triplet annihilation kinetics, were investigated and the activation energies and pre-exponential factors were calculated using the appropriate method from Chapter 2. At temperatures below 300K k_2 was negligible and if it is assumed that $k_2 = 0$ then the activation energy can be calculated from the Arrhenius plot of log k_2 against 1/T, the results are summarized in Table 3.5.

SAMPLE	ΔE_2 /kJmol^{-1}	A	R
1-bromonaphthalene	68.06	2.7×10^9	0.901
2-bromonaphthalene	50.04	3.1×10^8	0.915
9-bromophenanthrene	46.42	4.6×10^6	0.956

Table 3.5. ΔE_2 and A factors with correlation coefficients from least squares regression

Discussion

Similar studies, carried out on aromatic hydrocarbons with

longer-lived triplet states[31,50,51], gave conflicting results and two possible mechanisms for the depopulation of the triplet state have been proposed to explain the temperature dependence of the phosphorescence.

McGlynn et.al.[50] and Kropp[51] suggested that the temperature dependence was due to thermal deactivation of the triplet state of the solute to the triplet state of the PMMA, however, they did not report any deviation from exponentiality in the decay even at 390K.

El-Sayed et al.,[31] did observe non-exponential decay above room temperature and they fitted their data to triplet-triplet annihilation kinetics; the activation energies they calculated for [$^2H_8$]naphthalene, fluorene, perfluorobiphenylene, triphenylene and coronene are summarized in Table 3.6.

SAMPLE	ΔE_2 /kJmol^{-1}	T_1 /kJmol^{-1}	$T_1 + \Delta E_2$ /kJmol^{-1}
[$^2H_8$]naphthalene	53	245	308
triphenylene	102	279	381
fluorene	48	284	332
coronene	92	235	327

Table 3.6. PMMA tripet $+\Delta E_2$ for El-Sayed's results[31].

The kinetics and activation energies were rationalized by proposing that a diffusion controlled process was responsible for the deactivation of the state. Comparison of their results with those for the diffusion of benzene through a PMMA matrix[13] indicated that the

results were consistent with a diffussion controlled process.

Using the value for the Diffusion Coefficient of the aromatics estimated by El-Sayed of 10^{-12} and a molecular radius of 0.5nm the rate constant for diffusion is:-

$$k_D = 16 \times 10^{-10} \quad r\ N\ D$$

where N = Avogadro's number, r = the atomic radius and D = the Diffusion Coefficient.

$$k_D = 1.5 \times 10^{3} \quad l mol^{-1}\ s^{-1}$$

$$k_D = \frac{k_1}{[T]_o}$$

In 1-bromonaphthalene at 293K $k_1 = 117s^{-1}$ so in order for the relationship to hold the initial concentration of the triplet state would have to be 0.078 mol dm^{-3} which is clearly impossible since the concentration of the solute is only ca. 0.001 mol dm^{-3}. Diffusion through the polymer is therefore discounted as an explanation for the non-exponential decay with the brominated compounds.

The activation energies calculated by El-Sayed et al.,[31] differed from those reported by Kropp[51] and McGlynn[50] for the same compounds and the methods of measuring the lifetimes may have been responsible for this.

El-Sayed's apparatus permitted the output voltage of a spectrofluorimeter to be sequentially sampled at intervals of 0.33s at a precision of $\pm$ 1 V on an initial voltage of 15mV and the decay was measured over several lifetimes.

McGlynn and Kropp's method was less precise, they took a photograph from an oscilloscope trace of the decay profile of a single emission and the results quoted do not mention over how many lifetimes the decay was measured. If only one or two lifetimes were used then the rate constant they calculated at a particular temperature would be a combination of the first and second order rate constants and would be anomalously high.

Bearing this in mind further consideration was given to the possibility of thermal depopulation to the triplet of the polymer which has been estimated to have an energy of $299 kJmol^{-1}$.

It is obvious that the second order component of the triplet-triplet annihilation kinetics is responsible for the non-exponential decay of the triplet state and Table 3.7 shows that, within experimental error, the sum of the triplet energy of the solute and ΔE_2 is a constant - the triplet energy of PMMA, i.e. $\Delta E_2 + T_1 = 299 kJmol^{-1}$.

SAMPLE	T_1 /kJMOL^{-1}	$T_1 + \Delta E_2$ /kJMOL^{-1}
1-bromonaphthalene	248	316
2-bromonaphthalene	253	303
9-bromophenanthrene	253	299

Table 3.7. PMMA triplet $+ \Delta E_2$.

These experimental results are consistent with a model in which triplet-triplet annihilation occurs with energy transfer from the

solute to the lowest triplet level in the PMMA as the first step. The results obtained by El-Sayed et al.,[31] also fit this model, as shown in Table 3.6.

It must be noted that $\Delta E + T_1$ for triphenylene is rather high for the PMMA triplet at 318kJmol^{-1}, this discrepancy may be accounted for if the values for ΔE_2 are considered in conjunction with the correlation coefficients, R, from the least squares regression. The lower value, R = 0.92 in the triphenylene calculation compared to 0.97-0.99 in the others, suggests that the triphenylene data is less reliable.

Triplet-triplet annihilation initiated by energy transfer to the PMMA triplet requires subsequent transfer of energy along the PMMA chain until the energy from the two triplets come close enough together to allow mutual annihilation.

Triplet energy migration through polmers giving rise to triplet-triplet annihilation have been observed on many occasions[19,17,52] and it has been shown that the efficiency of such energy transfer is dependent upon the constituents of the matrix. This dependence is exemplified by observations, made by Fox and Cozzens[19], on energy transfer in terpolymers containing styrene (S), vinylnaphthalene (VN) and methylmethacrylate (MMA) units. Their experiments were carried out at 77K and 293K on a random terpolymers of P(S-co-2VN-co-MMA) which had the same composition as the alternating system and from their results they concluded that triplet energy migration is greatly reduced by a sequence of MMA units in the polmer chain at these temperatures.

Nakahira et al.,[53] came to similar conclusions i.e. energy migration is inefficient in PMMA and markedly so below 297K.

Although energy migration in PMMA is inefficient it has been shown to occur[52] even at 77K.

Suggestions that polymer matrices containing aromatic molecules are indistinguishable in their photophysical properties from copolymers of analogous molecules[18] endorses the argument for the mechanism whereby energy is transferred to the triplet state of the PMMA then migrated along the chain until it encounters another solute triplet.

Conclusions

Triplet-triplet annihilation can satisfactorily describe the kinetics of the observed non-exponential decay of the phosphorescence of several halogenated aromatic molecules above 300K.

Initiation of the triplet-triplet annihilation and the temperature dependence of the second order component of the decay have been accounted for by energy transfer from the solute triplet to the PMMA triplet and subsequent energy migration through the polymer matrix until another solute triplet is encountered.

The relatively high temperatures required to observe this phenomenon has been rationalized by the inefficient nature of energy migration in PMMA.

Temperature Dependence of First Order Rate Constants

It was noted in the previous section that the decay of the phosphorescence in each halogenated aromatic hydrocarbon was, within experimental error, exponential over at least three lifetimes below 300K and that non-exponential decay above 300K could satisfactorily be

accounted for by triplet-triplet annihilation kinetics.

In both temperature regions the rate constants for the deactivation of the triplet state were readily obtainable, as $1/\tau_p$ below 300K and from the fitting procedure (TRIP) above 300K. Figure 3.9 illustrates the temperature dependence of k_1 between 77 and 400K for 1-bromonaphthalene which was found to be representative of the behaviour in all the samples, namely the rate constant increased with temperature.

The kinetics of a simple model to describe this type of behaviour are derived in Chapter 2 and may be expressed as:-

$$k_1 = k_o + k_{nr}$$

where k_o is the temperature independent intrinsic rate constant and k_{nr} is the temperature dependent, non-radiative first order rate constant. It is clearly impossible to evaluate k_o experimentally and it is often assumed that at 77K k_{nr} is zero which allows k_o to be approximated to $1/\tau_{77}$. From Figure 3.10 it can be seen that this assumption may not be valid for these molecules as the rate constants were still increasing as the temperature was decreased towards 77K.

Preliminary investigations, however, were made using this approximation in order to establish the general picture of the temperature dependence and this revealed that three distinct first order processes were responsible for the observed variations, with breaks occurring at ca. 240 and 300K (Figure 3.11).

The non-radiative part of the rate constant, k_{obs}, is then the sum of these three rate constants

FIGURE 3.9

1-bromonaphthalene in PMMA

First order rate constants

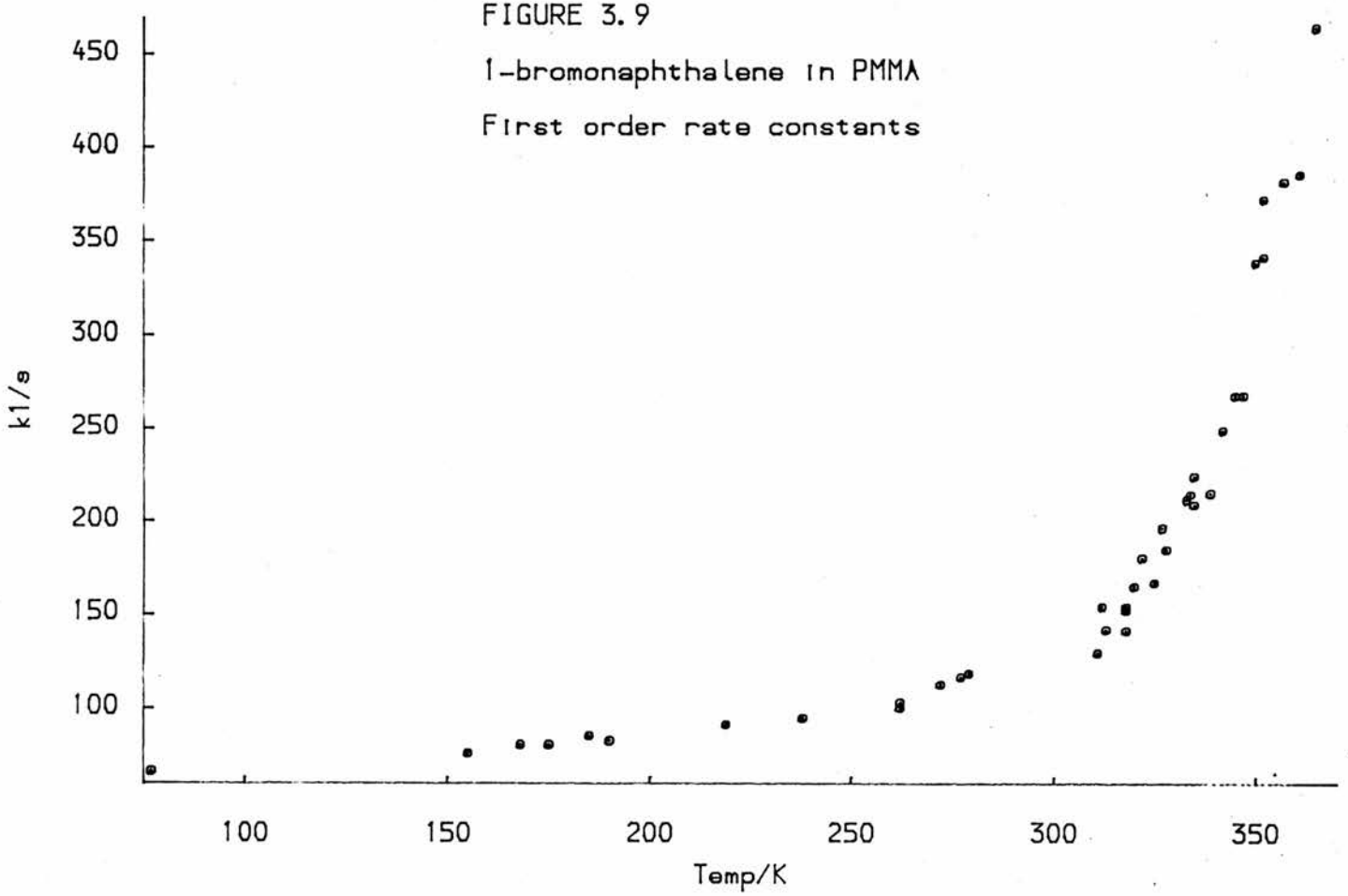

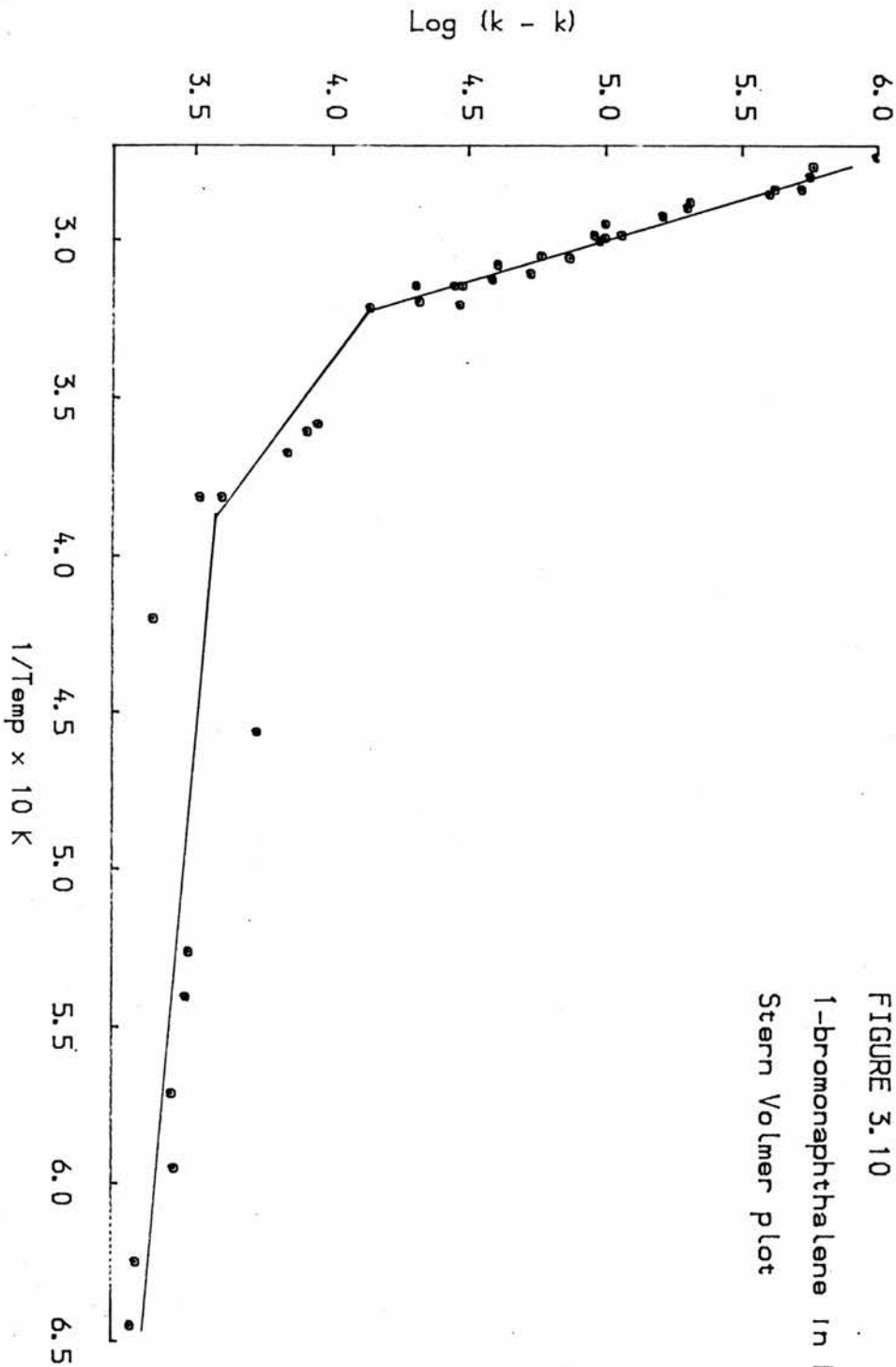

FIGURE 3.10

1-bromonaphthalene in PMMA

Stern Volmer plot

$$K_{obs} = k_o + k_{lt} + k_{mt} + k_{ht}$$

where the subscripts lt,mt and ht refer to the temperature ranges 77-240K, 240-290K and 300-400K respectively. At temperatures below 240K k_{mt} and k_{ht} are negligible and activation energies in this range were calculated from the equation:-

$$\log (k_{obs} - k_o) = \log A - \frac{\Delta E}{RT}$$

k_o was initially taken as $1/\tau_{77}$ and was decreased until the best straight line was achieved in the plot of $\log (k_{obs} - k_o)$ against time (indicated by the highest correlation coefficient from the least squares regression).

Between 240 and 290K activation energies were calculated, taking the lower temperature process into account by the inclusion of k_{lt} in the following equation:-

$$\log (k_{obs} - k_o - k_{lt}) = \log A - \frac{\Delta E}{RT}$$

and in a similar fashion the high temperature activation energy from:-

$$\log (k_{obs} - k_o - k_{lt} - k_{mt}) = \log A - \frac{\Delta E}{RT}$$

The values for k_{lt} and k_{mt} being calculated from the appropriate values of ΔE and A in the Arrhenius equation

$$k = Ae^{-\frac{\Delta E}{RT}}$$

SAMPLE	ΔE_1 /kJmol^{-1}	A	R
1-bromonaphthalene	8.62	2.0×10^3	0.935
2-bromonaphthalene	8.90	3.1×10^3	0.940
9-bromophenanthrene	9.80	6.2×10^3	0.989

Table 3.8. ΔE_1 and A factors with correlation coefficients from least squares regression 77- 240K.

SAMPLE	ΔE_1 /kJmol^{-1}	A	R
1-bromonaphthalene	8.62	2.0×10^3	0.935
2-bromonaphthalene	8.90	3.1×10^3	0.940
9-bromophenanthrene	9.80	6.2×10^3	0.989

Table 3.9. ΔE_1 and A factors with correlation coefficients from least squares regression 240-300K.

SAMPLE	ΔE_1 /kJmol^{-1}	A S^{-1}	R
1-bromonaphthalene	27.21	2.7×10^6	0.958
2-bromonaphthalene	28.15	2.3×10^6	0.912
9-bromophenanthrene	29.36	1.2×10^7	0.884

Table 3.10. ΔE_1 and A factors with correlation coefficients from least squares regression 300-360K.

Discussion

Consistent with the behavior described above previous studies [37,51,50] of the temperature dependence of the phosphorescence of aromatic hydrocarbons below 300K have also reported two regions of temperature dependence of the lifetimes with the break occurring at ca. 240K.

The low temperature activation energies, below 240K, have been estimated at ca. 5.9kJmol^{-1} for PMMA solutions of [$^2H_8$] naphthalene and [$^2D_{10}$] pyrene[37] and at ca. 5.5kJmol^{-1} for coronene[51], and have been attributed to some kind of intramolecular energy transfer. Jones and Siegel[37] suggested that a low frequency vibration of the triplet state was a suitable acceptor level and the results presented here are also consistent with their interpretation.

At higher temperatures, however, these workers reported exponential decay of the phosphorescence even up to 380K, and as previously pointed out, rate constants and activation energies above 300K must be interpreted with extreme caution.

The non-exponential decay observed by El-Sayed et al.,[31] became exponential if the measurements were taken at low light intensities and from the decays recorded under these conditions they calculated activation energies and pre-exponential factors for several aromatic hydrocarbons in PMMA. The main conclusions from their work were that a single deactivation process was predominant with an activation energy which was independent of the nature of the solute (18-20kJmol^{-1}), and a pre-exponential factor which varied by an order of magnitude; the results are summarized in Table 3.11.

SAMPLE	ΔE_1 /kJmol^{-1}	A
[$^2H_8$]naphthalene	19.3	58
triphenylene	19.6	170
fluorene	20.5	473
coronene	19.9	137

Table 3.11. ΔE_1 and A El-Sayed's results[54].

Experimental techniques used by El-Sayed did not permit measurements between 77 and 273K but the observed decrease in lifetime, which was ca. 10% over this range was assigned to a second process with an activation energy of a few kJmol^{-1}. Consideration of this second process indicated that the values in Table 3.11. were likely to be underestimated by ca.10% and should in fact have been be about 20-22kJmol^{-1}. The work here indicated that there were two first order processes with activation energies of ca. 4 and 9kJmol^{-1} and

consideration of these indicate that El-Sayed's values should be in the region 25-30kJmol^{-1}.

In essence the conclusions derived from the present work concur with these, in that the activation energies appear to be independent of the nature of the solute molecule and the pre-exponential factors vary by an order of magnitude. There is some discrepancy over the actual value of the activation energy of some 25% but this could be due to the choice of k_o and the error in the estimation of the low temperature process; El-Sayed et al., only allowed for one low temperature process whereas the present results indicate that there are two.

An activation energy which is independent of the nature of the solute is indicative of a process which is related to the nature of the matrix.

CHAPTER 4

TEMPERATURE DEPENDENCE OF THE PHOSPHORESCENCE OF BENZIL AND BENZOPHENONE

The phosphorescence lifetimes of benzil[48,55] and benzophenone[56-58] have been shown to be temperature dependent. The nature of the dependence has been investigated in this work to find if the kinetic scheme proposed for aromatic hydrocarbons in Chapter 3 can be extended to aromatics containing a carbonyl group. Benzophenone and benzil were chosen because they both have phosphorescence decays at 77K which are exponential over at least three lifetimes.

Analysis of the results was more complicated than for the hydrocarbons because, in addition to the possibility of energy transfer the carbonyl group is susceptible to photolysis via hydrogen abstraction from the PMMA. The photophysics and photochemistry of benzil and benzophenone are discussed in more detail below.

Where the decay of the phosphorescence was non-exponential the data were analysed using the procedures (DEX and TRIP) described in the previous chapter to find which model best fitted the observed kinetics. The models examined were triplet-triplet annihilation and dual emission i.e. emission by two separate species, and the activation energies and pre-exponential factors for k_1 and k_2 were calculated using the appropriate method given in Chapter 2.

Benzophenone

Extensive studies of the photochemistry of benzophenone have been carried out in the past and from these certain aspects of its behaviour have been well characterised. In a hydrogen donating medium, for example, an excited benzophenone molecule may abstract a hydrogen atom and form a diphenyl radical; this has been observed both in solution[59] and in a PMMA matrix[12].

Absorption by benzophenone occurs to an excited singlet state and this is usually followed by very efficient intersystem crossing to the triplet manifold. In some solvents the quantum efficiency of intersystem crossing is very close to unity[27,60], consequently the majority of emission occurs as phosphorescence. This has a maximum at 450nm.

In addition to phosphorescence, E-type delayed fluorescence has been observed in both solution and PMMA matrices;[57,58,61] it has been shown to have the same lifetime as the phosphorescence over a range of temperature and is the result of thermally activated intersystem crossing back to the excited singlet manifold.

The majority of benzophenone photochemistry takes place when there is a hydrogen donor in the system. The initial step of the reaction is hydrogen abstraction by an excited state benzophenone molecule to produce a diketyl radical, $Ph_2\dot{C}OH$. Triplet lifetimes in hydrogen donating media are generally lower than in systems where no hydrogen atoms are available for abstraction and if a hydrogen donor is added to such a system, e.g. tetrachloromethane solution, then a decrease in lifetime is observed[62]. Photochemically initiated hydrogen abstraction has also been observed in polymers.[57,58]

The intermediates and products of the photoreduction of benzophenone have been investigated, using a variety of techniques including n.m.r.,[62] emission and absorption spectroscopy,[63] to try to establish the mechanism of the reaction.

It has now been generally accepted that the triplet state must participate as photochemistry is greatly reduced when naphthalene is present and naphthalene is a well known triplet energy acceptor.[59,64,65] It has been suggested, however, that the singlet and triplet excited states are in equilibrium and the reaction may involve either or both excited state species.[57]

The major product of photoreduction in a hydrogen donating medium, benzpinacol,[66-69] is formed by dimerization of two diphenylketyl radicals. The benzpinacol decomposes to regenerate benzophenone if free molecular oxygen is present in the system. Other photoproducts depend upon the actual system. For example in isopropanol the following reactions occur:-

$$Ph_2CO \longrightarrow Ph_2CO\ (s) \longrightarrow Ph_2CO\ (T) \quad (1)$$

$$Ph_2CO\ (T) + Me_2CHOH \longrightarrow Ph_2C\dot{O}H + Me_2C\dot{O}H \quad (2)$$

$$2Ph_2C\dot{O}H \longrightarrow (Ph_2COH)_2 \quad (3)$$

$$Me_2C\dot{O}H + Ph_2CO \longrightarrow Me_2CO + Ph_2C\dot{O} \quad (4)$$

Step (4) was proposed rather than dimerization of $Me_2\dot{C}OH$ because the quantum yield of benzpinacol was approximately unity.[64]

Porter and Windsor[70,71] noted a transient formed in liquid paraffin solution which had two band progressions in the absorption spectrum and they suggested that it was the the diphenylketyl radical.[72] A similar transient was observed in an E.P.A. glass at liquid oxygen temperature by McClure and Hanst.[73]

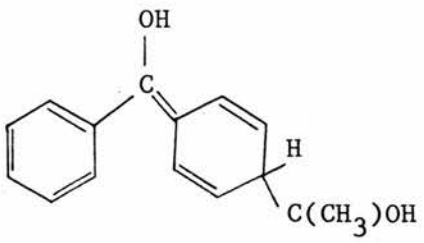

I

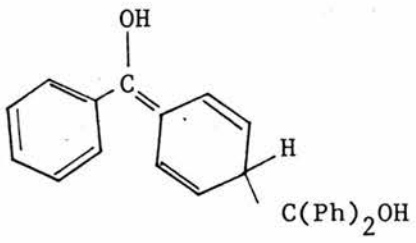

II

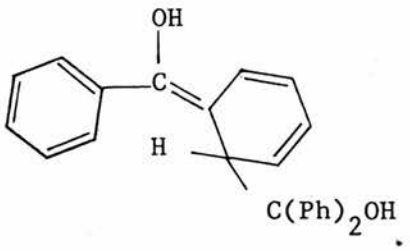

III

Figure 4.1. Possible intermediates in the photoreduction of benzophenone.

Filipescu and Minn[74] suggested that the benzpinacol is actually

formed via a slow dark reaction of an intermediate which in isopropanol has the structure I, shown above.

Schenk[75] suggested that some intermediates (with structures II and III) can act as diffusion controlled quenchers[76,77] because of their low triplet energies.

Several other transient intermediates have been observed in solution and there is evidence to show that some of these can exist for several days.[62]

The phosphorescence of benzophenone is longer-lived in a polymer matrix than in solution and the rate of photoreduction is decreased[11,12] which suggests that the steric requirements for hydrogen abstraction are hindered in the polymer.

Recent work by Burland et al.,[78] using holographic photochemistry has provided more detailed information about the photochemistry of benzophenone in a PMMA matrix and has clarified some of the earlier observations. These studies produced evidence to show that in a PMMA matrix hydrogen abstraction is a two photon process and that at 293K no irreversible hydrogen abstraction can occur via the lowest triplet level of benzophenone.

Results

Between 190 and 250K the results from the fitting routines (TRIP and DEX see Chapter 2) showed that both dual emission and triplet-triplet annihilation kinetics could satisfactorily describe the decays of the phosphorescence of the benzophenone samples.

Higher temperature measurements were not possible because at temperatures above 250K the emission was too short-lived to be

FIGURE 4.2

Benzophenone in PMMA

Stern Volmer plot

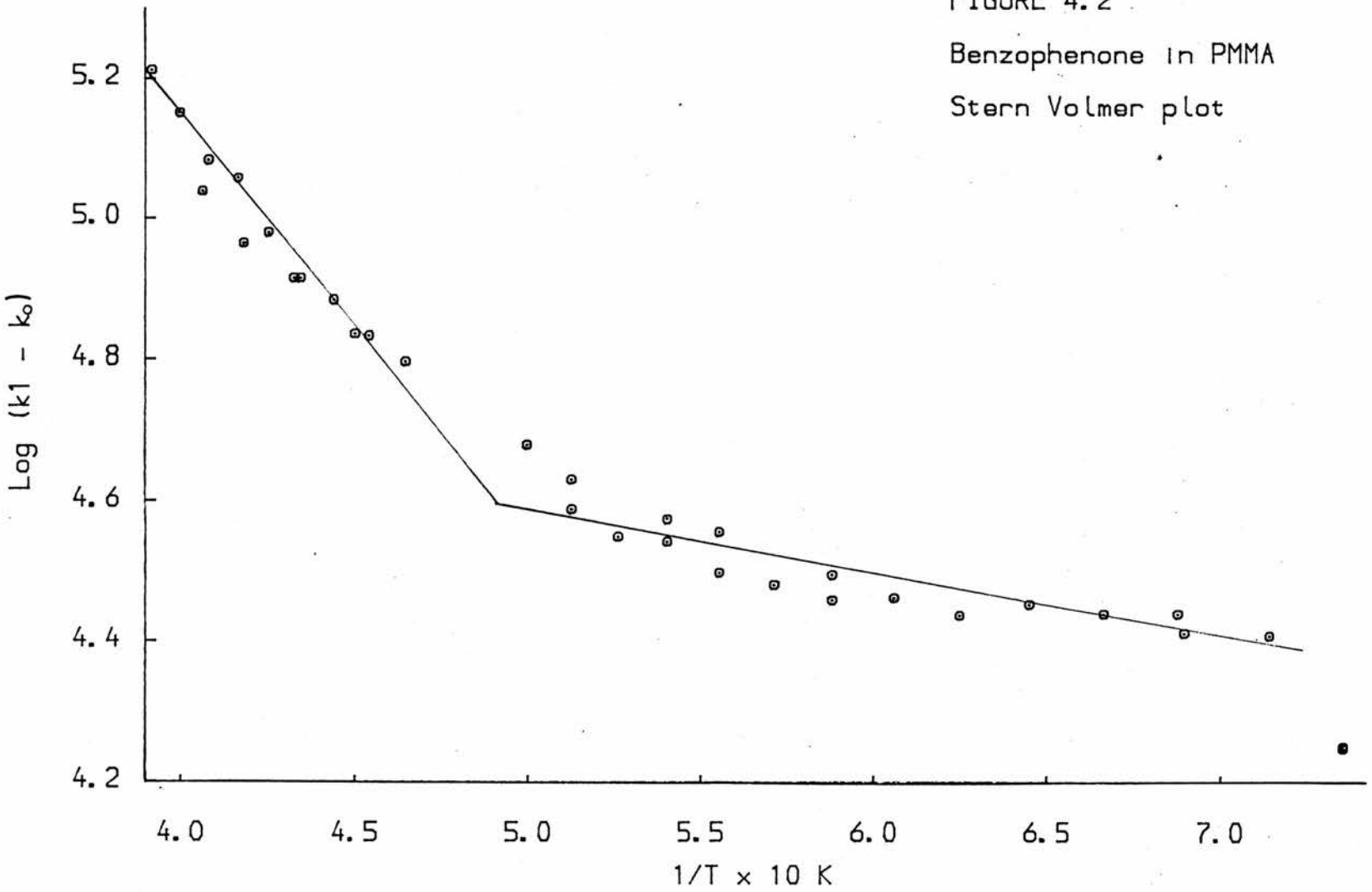

measured with the present experimental apparatus.

TEMPERATURE /K	TRIPLET-TRIPLET ANNIHILATION		DUAL EMISSION		
	k_1	k_2	k_1	k_2	
215	242.51	.0093	268.10	1831.94	a
220	250.61	.0081	272.76	1599.75	a
222	253.41	.0069	273.03	1165.09	b
225	250.13	.0113	279.26	1662.39	a
230	259.43	.0104	283.44	1597.17	a
231	263.81	.0087	283.33	1205.41	b
235	257.49	.0146	292.60	1614.19	a
239	267.83	.0104	290.41	1188.74	b
240	263.99	.0162	304.34	1626.09	a
245	271.27	.0168	308.51	1581.95	a
246	277.83	.0114	301.33	1215.97	b
250	273.10	.0245	319.69	1580.89	a
255	290.53	.0247	330.49	1633.83	a

Table 4.1. Rate constants from fitting procedure for triplet-triplet annihilation and dual emission kinetics for benzophenone.

Values of k_1 and k_2 from both fitting routines are presented in Table 4.1 and from these it can be seen that, within experimental error, the dual emission model calculated k_2 to be constant for a given sample, a or b.

$k_2(a) = 1600 s^{-1}$ or $(b) = 1200 s^{-1}$

In contrast to these results no simple rationalization of the k_2 values from the triplet-triplet annihilation model could be found as they were neither constant nor did they produce a straight line in an Arrhenius plot.

The other rate constant from the dual emission model, k_1, increased with increasing temperature between 77 and 250K. A plot of log k_1 against 1/T (Figure 4.2) indicated that two processes were necessary to describe the the type of temperature dependence observed with the break occurring around 190K. Activation energies for both processes were calculated using the Stern-Volmer method described in Chapter 2.

$\triangle E = 1.1 kJmol^{-1}$ $A = 2.0 \times 10^2 s^{-1}$ 77-190K

$\triangle E = 4.7 kJmol^{-1}$ $A = 1.6 \times 10^3 s^{-1}$ 190-250K

Discussion

The above results indicate that the decay of the phosphorescence of benzophenone in a PMMA matrix can be rationalized by a dual emission kinetic model. Benzophenone is known to be photoreduced in a PMMA matrix and overlap of emissions from benzophenone and a photoproduct of benzophenone are consistent with kinetics of this type. The constant nature of k_2 for a given sample indicates that the photoproduct emission is temperature independent below 250K.

The second component of the decay was only observable above 190K

and if the sample was only irradiated below room temperature the decay regained its exponential characteristics when the temperature was lowered again. Extended irradiation above room temperature, however, caused a permanent change; the subsequent decay at 77K after irradiation was significantly faster and was non-exponential.

The rate of photoreduction of benzophenone is known to be reduced in PMMA because the matrix hinders the steric requirements for hydrogen abstraction and restricts diffusion.[12] Bearing this in mind it seems unlikely that, in the time scale of these experiments, the photochemical reaction could go as far as producing benzpinacol. The species responsible for the second emission, above 190K, is more likely to be some intermediate which is formed reversibly below room temperature but reacts further at higher temperatures. Comparison of the the emission spectra before and after irradiation at 300K suggest that the final product is indeed benzpinacol.

As previously mentioned, holographic photochemistry[78] has been used to provide evidence to support the hypothesis that only reversible hydrogen abstraction occurs from the lowest triplet level of benzophenone and absorption of another photon is required to produce irreversible hydrogen abstraction.

If hydrogen abstraction is, indeed, reversible below 293K then the species responsible for the second emission could be a transient in which the benzophenone is attached to the polymer chain via the hydrogen atom as illustrated below.

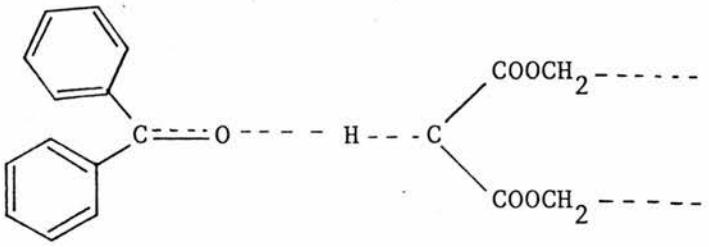

Further investigations are, however, necessary to unambiguously determine the nature of the intermediate and final photoproducts.

Benzil

Studies of the photophysics of benzil[79,80,48,55] in solution and in rigid matrices have established that a single ground state conformer gives rise to two excited state conformers.

In the ground state the two carbonyl groups are perpendicular to each other, the skewed conformation, and excitation produces two emissions, at 525nm and 565nm, which have different lifetimes but a common excitation spectrum. Rapid geometric partitioning into two emitting states, which are kinetically independent, is thought to occur from the excited singlet skewed state at a rate which is faster than inter-system crossing (I.S.C. has a rate constant of ca. $10^9 s^{-1}$.) as fluorescence is observed from both excited conformers.[48]

Work by Morantz and Wright[81] indicated that the most likely excited configuration has a transplanar carbonyl system with one phenyl ring out of the plane of the carbonyl group; the cis (near-skewed) conformer also exists but at lower concentration. The phosphorescence spectra presented by Singer et al.,[48] supported this

suggestion showing the emission from the transplanar conformer at 525nm to be stronger than that from the near-skewed isomer at 565nm.

The excited singlet state conformers may undergo the common deactivation processes, fluorescence or inter-system crossing to the triplet state and these transitions occur with retention of conformation. Transitions to the transplanar or near-skewed lowest singlet state is rapidly followed by relaxation to the ground state skewed conformation, see Figure 4.3.

Triplet energies have been estimated[80] for the transplanar and near-skewed conformers at 243kJmol^{-1} and 218kJmol^{-1} respectively,[48] but the exact positions of the excited states of the conformers are uncertain and are indicated by broken lines in Figure 4.3.

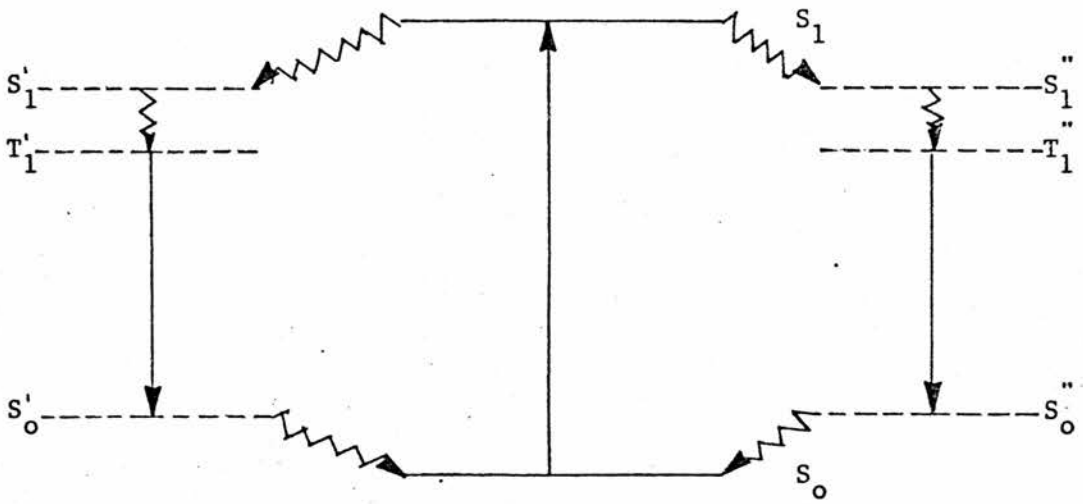

Figure 4.3. Energy level diagram of the excited conformers of benzil

Singer et al.,[48] examined the phosphorescence of both conformers in PMMA and concluded that between 77 and 240K the decay was exponential but above 240K deviations from exponentiality were observed over the first 10μs. From Arrhenius plots two activation

energies were estimated for the two regions, at $4.2kJmol^{-1}$ between 77 and 240K and $33kJmol^{-1}$ between 240K and room temperature. Discontinuity in the plot at 240K was related to the onset of rotation of the carbomethoxy groups in the PMMA[82] and it was suggested that the non-exponentiality was caused by the formation of an exiplex between the excited conformers and a specific subgroup of the PMMA possibly the carbomethoxy group. Energy transfer to the PMMA triplet, as suggested by McGlynn[50], was discounted because the energy required for this process was ca. $50kJmol^{-1}$.

Avdeenko et al.,[55] also discounted energy transfer to the PMMA triplet as an explanation of the temperature dependence of the phosphorescence lifetimes they observed. They found that two processes were responsible for the fall in the lifetimes and the activation energies, estimated from data below 293K and shown below, were too low to be consistent with energy transfer to the matrix.

$\triangle E_1 = 9.9kJ\ mol^{-1}$ $\quad A_1 = 30s^{-1}$

$\triangle E_2 = 16.7kJ\ mol^{-1}$ $\quad A_2 = 1500s^{-1}$

This type of temperature dependence had been observed previously for several other aromatics and they concluded that their results were consistent with a stable distortion in the excited state benzil caused by carbonyl interactions.

Results

Non-exponential decay[83] of benzil phosphorescence has been reported in a cyclohexane/isopentane glass at 77K and the decay was

successfully fitted to triplet-triplet annihilation kinetics.

In the present work phosphorescence lifetimes of benzil in PMMA matrices were measured at 515nm and 565nm at 77K and at various temperatures up to 293K. Previous studies have indicated that emission occurs from the near-skewed and transplanar excited state conformers at 525 and 565nm respectively and the measurements were taken at 515 and 565nm to minimize the overlap of the two emissions. Indeed at these wavelengths the decays were found to be exponential, within experimental error, over three to four lifetimes although the values differed with that at 565nm being the shorter.

Variation in the emission intensities permitted measurements at 515nm to be taken using a considerably lower voltage across the photomultiplier and hence to be less affected by the background voltage, for this reason the data recorded at 515nm was used in the following analysis.

Below 190K the decay of the phosphorescence was found to be exponential over three to four lifetimes (Figure 4.4) but at higher temperatures deviation from exponential behaviour was observed at both wavelengths.

Measurements could only be taken up to 340K because at higher temperatures the decay became too fast to be measured on this apparatus.

As with benzophenone, benzil exhibited exponential phosphorescence decays over at least three lifetimes between 77 and 190K.

Between 190 and 240K the results from the fitting routines indicated that both the kinetic models could describe the non-exponential decay of the benzil phosphorescence with the error, in

TEMPERATURE /K	TRIPLET-TRIPLET ANNIHILATION		DUAL EMISSION	
	k_1	k_2	k_1	k_2
199	234.42	.0108	237.55	617.04
200	241.75	.00527	234.56	581.96
210	253.84	.0180	272.11	840.94
210	246.28	.0139	254.91	692.16
220	244.02	.0368	275.78	924.38
225	260.36	.0413	301.24	849.73
230	290.72	.0487	325.01	1027.32
235	282.15	.0508	320.87	1081.67
235	302.98	.0335	334.30	1017.29
240	302.84	.062	352.31	1239.72
300	397.10	9.23		
304	1154.90	12.45		
309	509.10	17.15		
312	2104.00	18.80		
313	4108.00	18.43		
315	2396.00	30.26		
317	6201.40	29.20		
319	4840.00	28.70		
320	8280.00	30.93		
327	1478.40	38.61		
327	15057.00	14.39		
332	3582.40	16.66		
332	17654.00	21.97		

Table 4.2. Rate constants from fitting procedure for triplet-triplet annihilation and dual emission kinetics for benzil.

both cases, evenly spread over all the data. Comparison of the values of k_1 and k_2 (Table 4.2) with those for benzophenone (Table 4.1) indicated that the kinetics of the two systems differed.

Above 300K the phosphorescence decay could be satisfactorily described by the triplet-triplet annihilation model (Table 4.2) but no values of k_1 and k_2 could be found to describe the data using the dual emission model.

Using the values of k_1 and k_2 from the triplet-triplet annihilation fitting routine a plot of log k_2 against 1/T between 190 and 340K (Figure 4.4) indicated that two processes were responsible for the non-exponential decay and that the break occurred between 240 and 300K. A more precise estimation of the break temperature was difficult because there was a large scatter on the data.

Activation energies and pre-exponential factors were calculated for the lower temperature process using the values of k_2 from both kinetic models, as described in Chapter 2, and they are given in Table 4.3.

ΔE_2 /kJmol^{-1}	A	R	
17.4	3.99×10^2	0.960	triplet-triplet
6.3	2.71×10^4	0.960	dual emission

Table 4.3. Activation energies, pre-exponential factors and correlation coefficients for the low temperature second order process.

At higher temperatures the observed rate constants were a combination of the rate constants for the two processes. To calculate the rate constant for the higher temperature process the contribution to the decay from the lower temperature component must be considered. Since the activation energies from the two kinetic models differed both cases were considered.

(i) Triplet-triplet annihilation kinetics.

If the lower temperature process was triplet-triplet annihilation then the decay may be represented as:-

$$A^* \xrightarrow{k_1} A$$

$$A^* + A^* \xrightarrow{k_2} 2A$$

$$A^* + A^* \xrightarrow{k_3} 2A$$

and can be described by the equation:-

$$-\frac{d[T]}{dt} = k_1[T] + k_2[T]^2 + k_3[T]^2$$

which simplifies to:-

$$-\frac{d[T]}{dt} = k_1[T] + k_{obs}[T]^2$$

where $k_{obs} = k_2 + k_3$ and k_2 and k_3 are rate constants for the low and high temperature components respectively.

Under these conditions the equations in the triplet-triplet annihilation fitting routine may be used without modification and the

second order rate constant calculated correspond to k_{obs} in the above equation. Using values of ΔE and A calculated between 190 and 240K the activation energy of the higher temperature process was calculated from a plot of log $(k_{obs} - k_2)$ against 1/T (see Chapter 2 for details) and these values are shown below.

$$\Delta E = 49 kJmol^{-1} \qquad A = 3.5 \times 10^{9} s^{-1}$$

(ii) Dual emission.

If the low temperature process is due to a second emission then the observed emission may be represented as:-

$$A^* \xrightarrow{k_1} A$$

$$B^* \xrightarrow{k_3} B$$

$$A^* + A^* \xrightarrow{k_2} A + A$$

The observed intensity in these circumstances is proportional to the sum of the concentration of the two triplets and hence is a can be described by a combination of the triplet-triplet annihilation and dual emission equations:-

$$I(t) = Ce^{k_2 t} + \left[\left(\frac{1}{I_o} - \frac{k_3}{k_1}\right) e^{k_1} + \frac{k_3}{k_1}\right]^{-1}$$

The dual emission fitting procedure showed C to be approximately constant at 5940 and k_2 can be found for any temperature from $k_2 = Ae^{\frac{-\Delta E}{RT}}$. If I(t) is replaced by $I(t) - Ce^{k_2 t}$ then k_3 and k_1 may be

calculated from the fitting routine (TRIP) as before.

In the case of benzil it was impossible to find values of k_1 and k_3 which gave a satisfactory fit with the experimental data. This does not necessarily mean, however, that the dual emission model should be discounted because there was a large error associated with the estimation of C and the fitting procedure is very sensitive to the quality of the data used.

The activation energy and pre-exponential factor calculated using Stern-Volmer plot of log $(k_{obs} - k_2)$ against 1/T, were compared to those estimated from plots of log (k_{obs}) against 1/T with no correction for the lower temperature process. As can be seen in Table 4.4, the two values were within experimental error which implies that the lower temperature process did not have a significant effect on the kinetics above 300K.

$\triangle E_2$ kJmol^{-1}	A	R	
48.6	2.6×10^9	0.957	corrected
49.3	3.5×10^9	0.956	uncorrected

Table 4.4. Activation energies, pre-exponential factors and correlation coefficients for the higher temperature second order process.

The other rate constant, k_1, was evaluated between 77 and 340K and, as can be seen from Figure 4.5 the plot of log k_1 against 1/T has three regions with breaks occurring at 190K and ca. 250K

FIGURE 4.4a

Benzil in PMMA

190 - 240K

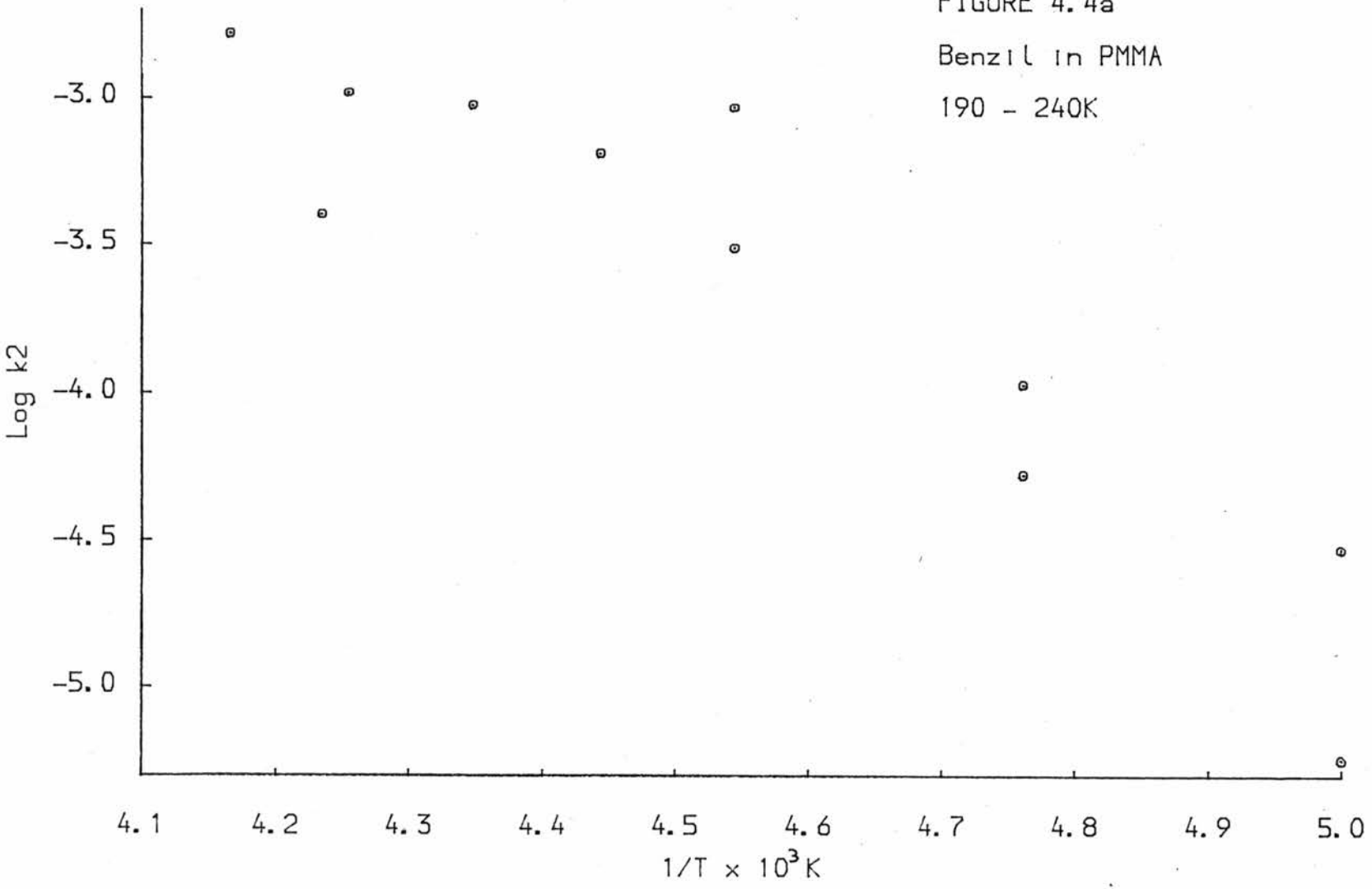

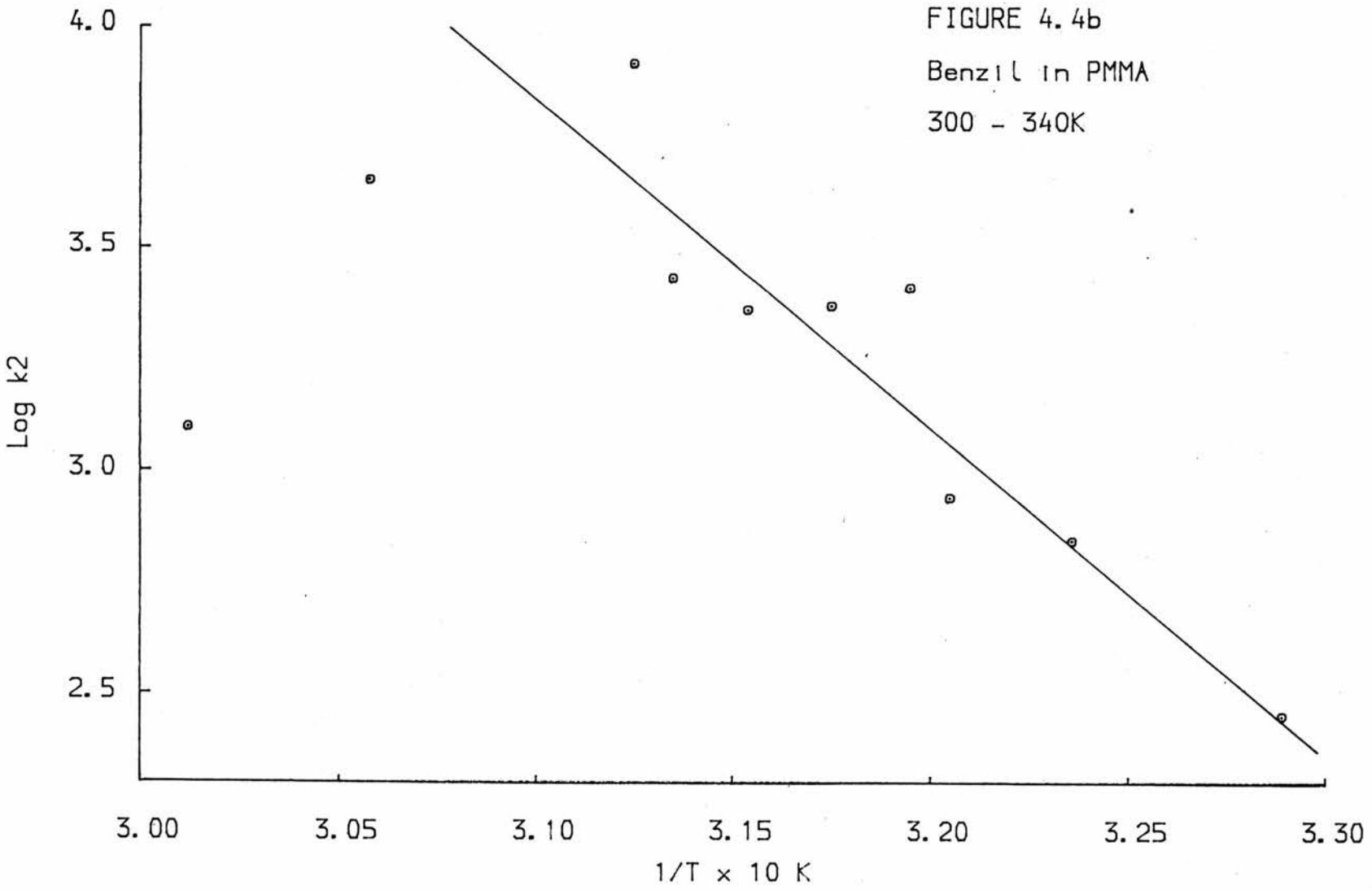
FIGURE 4.4b
Benzil in PMMA
300 - 340K
4.0
3.5
3.0
2.5
Log k2
3.00
3.05
3.10
3.15
3.20
3.25
3.30
1/T x 10 K

FIGURE 4.5

Benzil in PMMA

Stern Volmer plot

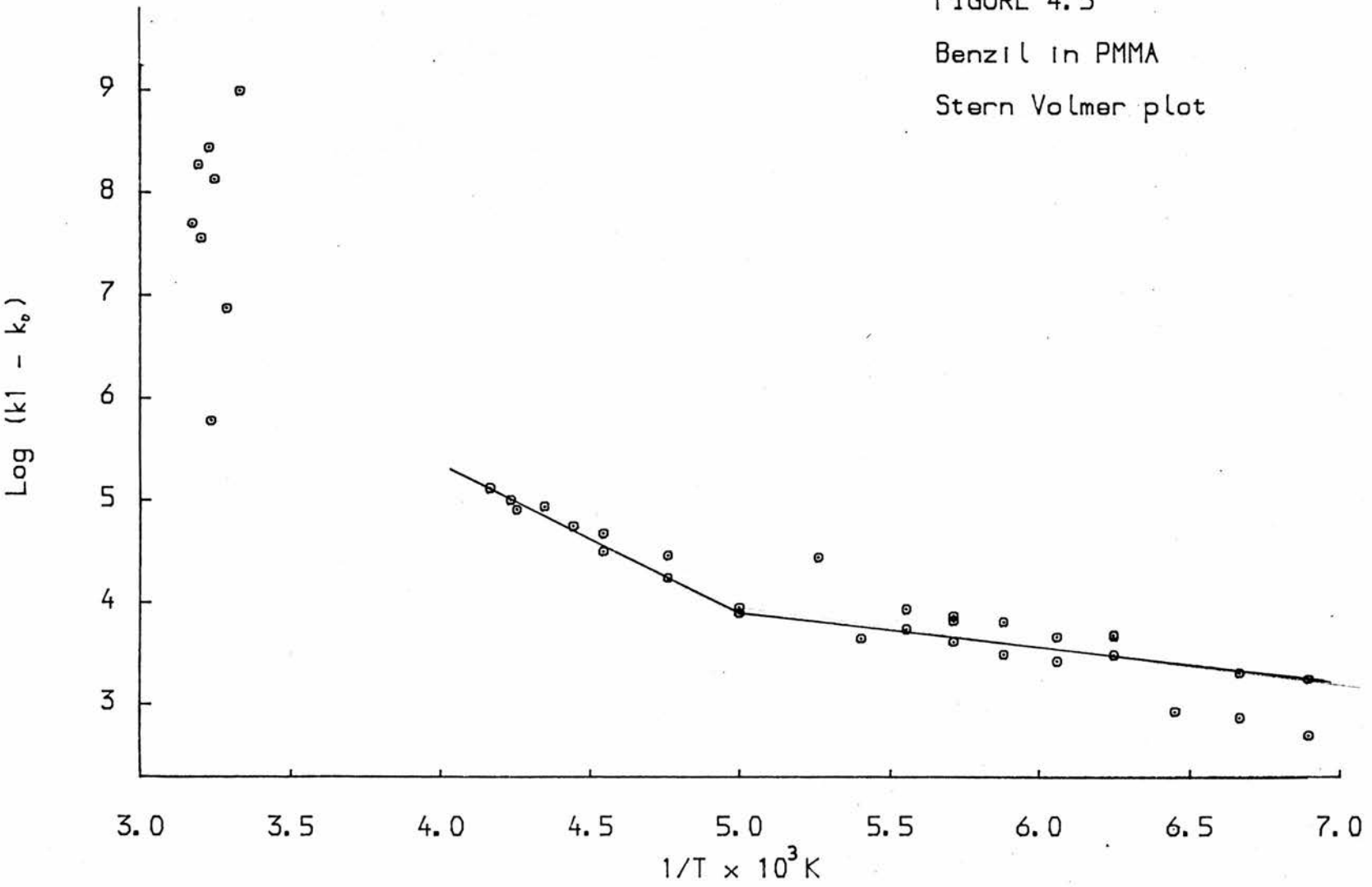

Below 190K the data is very scattered but it is clear that the process responsible for the rise in lifetime has a small activation energy of a few $kJmol^{-1}$. A least squares regression on the data below 190K gave an activation energy of $4.5kJmol^{-1}$ and this value was used in the ensuing calculations.

k_1 values from both the kinetic models between 190 and 250K gave activation energies and pre-exponential factors within 4% of each other which is less than the experimental error on the data.

ΔE_1 /$kJmol^{-1}$	A /s^{-1}	R	
4.5	1×10^3	0.83	77-190K
12.7	9.8×10^4	0.98	190-240K
92.9	8.9×10^{18}	0.96	240-340K

Table 4.5. Activation energies, pre-exponential factors and correlation coefficients for the first order processes.

Discussion

Variation of k_2 with temperature

Previous studies of the temperature dependence of the phosphorescence decay of benzil in PMMA matrices have not, in general, revealed any non-exponentiality and consequently the conclusions drawn are of little value in rationalizing the above results.

Non-exponential decay which lasted for *ca.* 10μs was observed by Singer et al.,[48] but they could offer no explanation to account for it

and made their calculations on the data after 10μs.

In the present study it was found that the non-exponential decay of the phosphorescence of benzil between 300 and 340K could be described by triplet-triplet annihilation kinetics and from the rate constants, calculated by the fitting procedure, the activation energy for the second order component of the decay was found to be $48.6 kJmol^{-1}$.

The triplet energy of the transplanar conformer of benzil has been estimated[48] at $243 kJmol^{-1}$. Using this value the sum of the activation energy and the triplet energy are, within experimental error, equal to the lowest triplet level of PMMA ($299 kJmol^{-1}$).

In Chapter 3 a mechanism was proposed to account for the triplet-triplet annihilation kinetics and activation energies of this kind, whereby energy was transferred from one triplet to another via the lowest triplet level of the PMMA.

Investigations leading to this mechanism were carried out on brominated aromatic hydrocarbons but it was demonstrated that it could also account for the temperature dependence of the phosphorescence of several aromatic hydrocarbons.

The temperature dependence of the second order component of the phosphorescence decay of benzil above 300K showed that this energy transfer mechanism could also describe the kinetics observed in benzil.

The second component of the emission between 190 and 250K made no significant contribution to the overall decay above 300K but, as with benzophenone, prolonged irradiation above 300K caused a permanent change in the sample which was reflected by a decrease in the lifetime at 77K.

Several features of the temperature dependence of the phosphorescence below 250K were common to both benzil and benzophenone and, since they are both aromatic carbonyl compounds, similarities in their photochemistries are not unexpected.

The phosphorescence of both molecules had exponential decays below 190K and the non-exponential decays above 190K could be described by dual emission kinetics.

Earlier in the Chapter these kinetics were rationalized for benzophenone by proposing that below 250K the second emitting species was an intermediate in the photoreduction of benzophenone. It is conceivable that an analogous species was responsible for the non-exponential decay of the benzil phosphorescence below 250K. Unlike benzophenone, however, the second emission was temperature dependent and probably became too short-lived above 300K to be observable with the present apparatus.

Temperature dependence of k_1

All the molecules investigated in Chapter 3 had kinetics which were consistent with two first order processes which were responsible for the observed temperature dependence below 300K; activation energies were ca. 4 and 9kJmol^{-1} with the break occurring at 240K. The conclusions from this work, which were supported by various reports in the literature, were that the processes were related to the structure of the polymer and essentially independent of the nature of the solute.

The temperature dependence of k_1 in benzophenone and benzil also showed that two first order processes were operative below 293K but

the break occurred at a lower temperature (190K) in both cases. In benzophenone the activation energies were also considerably lower.

In view of the photochemical possibilities of the carbonyl systems it is not surprising that their kinetics differ from the hydrocarbon systems.

Benzil above 300K

It was demonstrated that both benzil and benzophenone required irradiation at or above room temperature to cause any irreversible reaction which produced a permanent change in the samples.

Consideration of the conclusions drawn by Burland et al.,[78] for the benzophenone system provided a possible explanation for the temperature dependence of k_1 above 300K in the benzil samples. Their results indicated that no irreversible hydrogen abstraction could occur from the lowest benzophenone triplet state at 293K because there was insufficient energy for the diketyl radical to diffuse or reorientate itself to form a stable species. At this temperature they found that absorption of a second photon was required to provide the extra energy. In the present investigations it was unlikely that the excited triplet could absorb another photon because the duration of the flash was too short and the time between flashes too long.

Above 293K absorption of a second photon may not be necessary to achieve irreversible hydrogen abstraction as the diketyl radical may be able to obtain sufficient thermal energy to escape the polymer radical.

In studies carried out by El-Sayed et al.,[31] calculations were made to estimate the activation energies of diffusion of various

molecules through a PMMA matrix. They concluded that activation energies of 50-100kJmol^{-1} were consistent with diffusion controlled processes for naphthalene, coronene, and fluorene in this matrix.

CHAPTER 5

PHOTOLYSIS OF ANTHRAQUINONE IN PMMA

The mechanism of the photolysis of anthraquinone in alcohol and hexane solutions has been previously investigated.[84-87] All these investigators have agreed that the initial step in the reaction is likely to be the formation of the anthrasemiquinone radical, AQH$^{\bullet}$, which is the product of hydrogen abstraction from solvent by the anthraquinone triplet state.

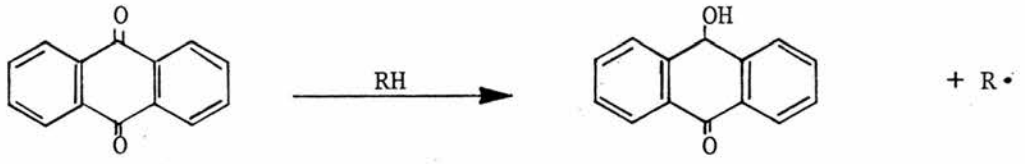

Formation of AQH$^{\bullet}$ by hydrogen abstraction.

Once formed the radical disproportionates into anthraquinone and 9,10 dihydroanthraquinone, 9,10 DHA.[84]

$$2\ AQH^{\bullet} \longrightarrow AQ + 9,10\ DHA$$

In ethanol the AQH$^{\bullet}$ radical absorbs at 575,631 and 678nm;[84] lower wavelength absorptions of the radical are usually difficult to observe because they are masked by absorption of 9,10 DHA which occurs in the 300-500nm region.

The e.s.r. spectrum of the AQH$^{\bullet}$ radical has been reported in

E.P.A. glass[88] at 77K, and in methanol solution below 120K.[89] Both spectra shows 13 resolved lines spread over approximately 6.0 Gauss. Deffner and Brunner[90] observed an identical e.s.r. spectrum in an alkaline methanol solution of anthraquinone with added PtO_2 and this solution had a red/brown colour.

The 9,10 DHA can be identified by its blue/green emission. Emission maxima are at 460nm in hexane and 480 and 495nm in ethanol[84] (Figure 5.1). This shift in the emission with change of solvent was attributed to a charge transfer effect; it was not reflected in the absorption spectrum and was too large to be explained entirely by solvent effect.

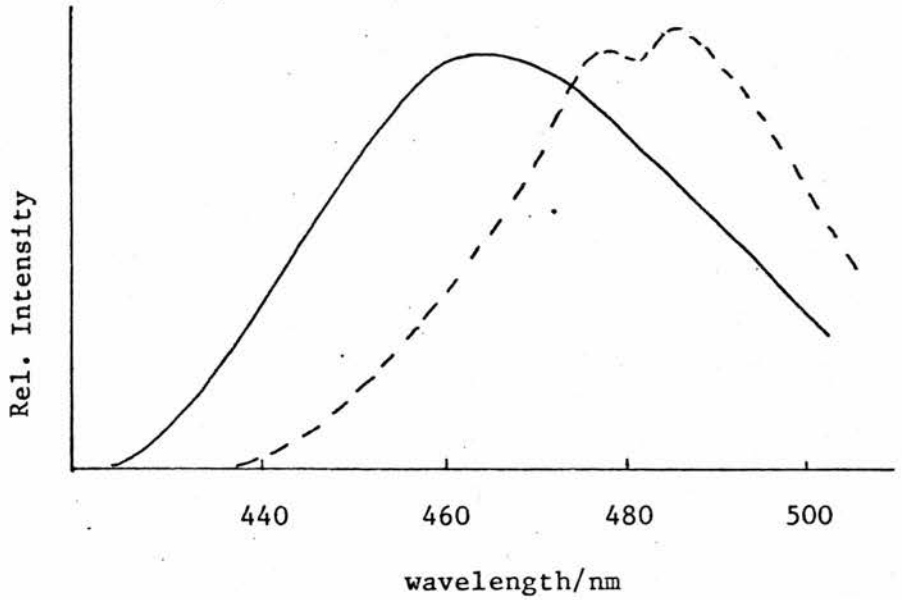

Figure 5.1. Emission spectra of anthraquinone in ethanol (---) and hexane (——).

Anthraquinone is rapidly regenerated from 9,10 DHA in the presence of oxygen. In the absence of oxygen tautomerism to oxanthrone occurs; oxanthrone emits phosphorescence with a maximum

at 408nm which has a lifetime of 2.2ms.[85]

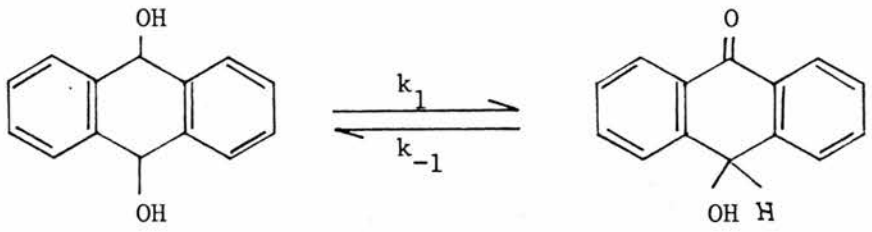

Figure 5.2. Equilibrium between 9,10 DHA and oxanthrone.

In solution at room temperature the tautomerism is slow and at equilibrium 9,10 DHA is the major product, only 11% is in the keto form[85] and $k_{-1} = 3.6 \times 10^6 s^{-1}$. In the excited state tautomerism is thought to occur more rapidly.

Prolonged irradiation has been shown to photolyse both 9,10 DHA and oxanthrone to produce a variety of products.[85,86] Some of these have been positively identified (e.g. 9-anthrol, anthrone and anthrapinacol the structures are illustrated below). One of the products in ethanol solution has an emission maximum at 410nm and an isomer of oxanthrone, the precise structure of which has not been determined, has been proposed as the source.

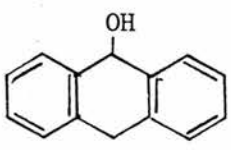

9-anthrol

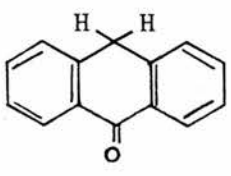

anthrone

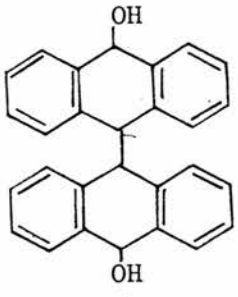

anthrapinacol

Solutions of anthraquinone at a concentration of 10^{-3}M in ethanol, carbon tetrachloride, methylmethacrylate ,dichloroethylene and PMMA were irradiated by a medium pressure mercury lamp at room temperature. Dissolved gasses were removed from the solutions by the vacuum freeze-thaw method and the behaviour of these solutions was compared to that of oxygen saturated solutions. The results are described below.

Results

The degassed ethanol and dichloroethylene solutions rapidly turned blue/green with emission peaks at 480-500nm. This colour faded over 12 hours leaving a green solution with the same emission spectrum.

The same blue/green colour and emission peaks appeared on irradiation of the oxygen saturated ethanol solution but only after about 15 minutes irradiation and the colour faded within 10 minutes of removal of the irradiation. The oxygen saturated dichloroethylene solution went yellow after about 15 minutes irradiation but the emission was identical to that of the other solutions and also faded within about 10 minutes.

Degassed solutions of carbon tetrachloride at room temperature, in which there is no hydrogen available for abstraction, showed no observable reaction after 30 minutes irradiation. Similarly there was no observable reaction in an ethanol solution at 77K where the rate of hydrogen abstraction is extremely slow.

Methylmethacrylate solutions turned yellow on irradiation, after 10 minutes in the degassed solution and after 30 minutes in the oxygen

saturated sample, both solutions exhibited a broad emission peak over 450-510nm which faded when the irradiation ceased. The fading was more rapid if oxygen was present.

The PMMA solution turned red/brown on irradiation, irrespective of whether the sample had been degassed before polymerization, with an absorption band at 485 and 395nm and emission at 462 and 540 nm. Maximum absorption and emission intensities were achieved after about 30 minutes irradiation whereupon further irradiation decreased the intensities of both emission bands but had no significant effect on the absorption intensity.

Excitation of the sample at 485nm gave further evidence to suggest that absorption in this region was not responsible for the emission at 462 and 540nm.

The red/brown colour faded completely when the sample was left in the dark at room temperature for several months. At 378K the colour and the 485nm absorption band became undetectable after 17 hours, the absorption is shown in Figure 5.3. Below about 350nm the spectrum was complicated by PMMA absorption and this region was not considered in the following discussion.

Heating the sample until the red/brown colour and the 485nm absorption were undetectable left one emission peak (at 462nm), which was more intense by a factor of 10 than the emission from the newly irradiated sample, and an absorption spectrum which was significantly different from the original spectrum of anthraquinone.

Polymer samples, where the monomer solution had been irradiated before polymerisation, produced the red/brown colour only if the solution was oxygen saturated and produced it at a slower rate than the non-irradiated sample. PMMA samples prepared from a degassed

monomer solution which was irradiated before polymerization produced no red/brown colour but turned yellow then to a blue/green which did not fade over several weeks.

The e.s.r. spectra of a 10^{-3}M anthraquinone solution in PMMA and of a sample of pure PMMA which had been irradiated for 20 minutes were identical. They consisted of a quintet with a quartet interspersed and were identical with the spectrum of characteristic radicals found in all PMMA matrices, as described by Abraham et al..[44] The concentration of the radical was estimated to be between 10^{-5} and 10^{-6}M.

The decay of the 485nm absorption peak was monitored at three temperatures, 378K, 368K and 358K. Figure 5.3 shows the decay at 378K. The latter stages of the reaction appeared to be first order and the rate constants were determined from the gradient of the plot of log O.D. against time over the last half of the reaction (Figures 5.4-5.6). Activation energies of the first order reaction were calculated from these rate constants using Arrhenius plots (Figure 5.7 and Table 5.1). The first order contribution to the decay was calculated using these values and was subtracted from the experimental optical densities then the remaining change in optical density with time was analysed for the possibility of a second order reaction. Once the first order reaction has been accounted for the change in optical density is very small and therefore any errors are amplified; Figures 5.8-5.10 show second order plots of $1/O.D.-1/O.D._o$ against time and although the scatter on the points on the graph is high it does suggest that the reaction is second order.

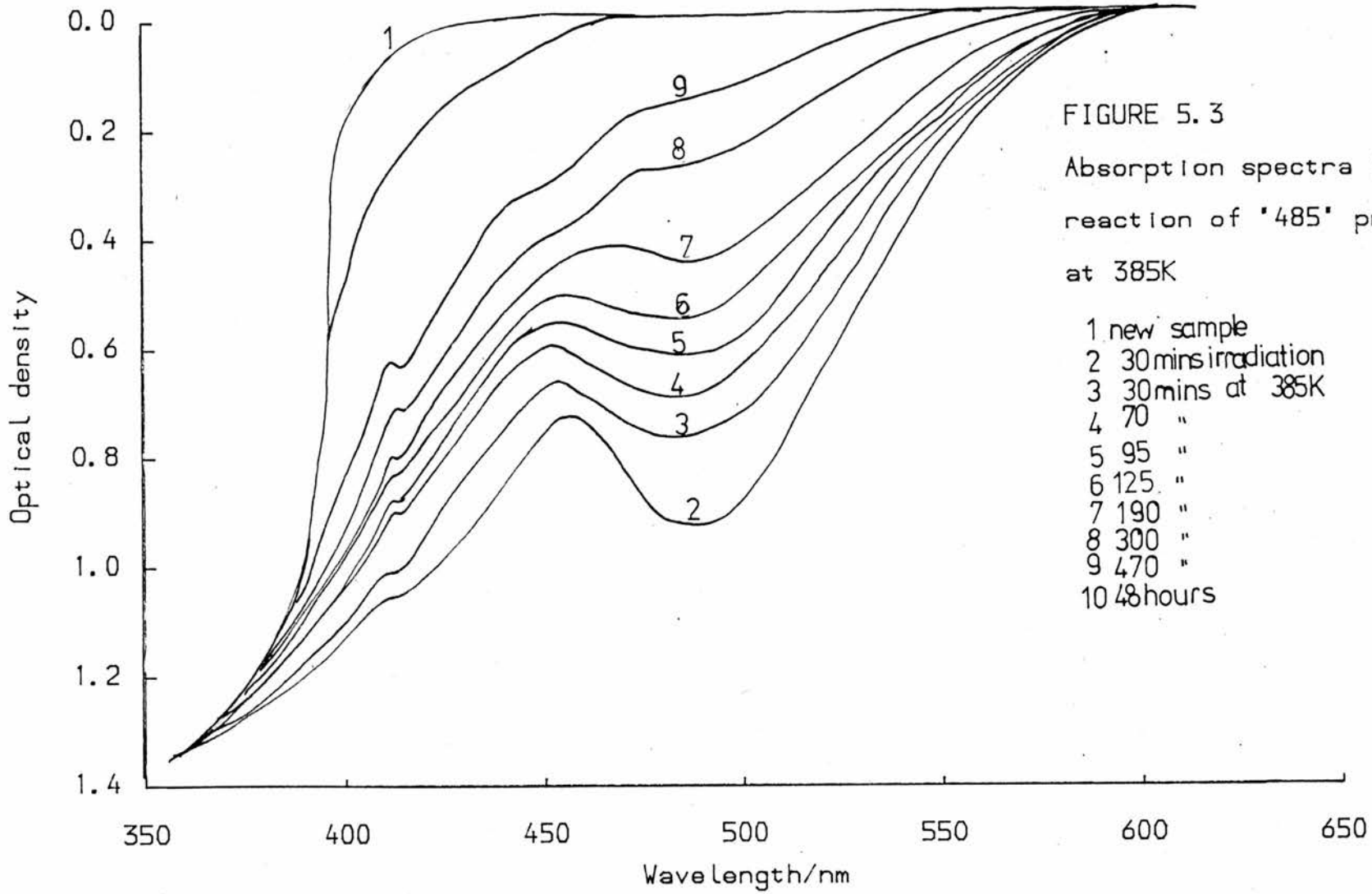

FIGURE 5.3

Absorption spectra following reaction of '485' product at 385K

1 new sample
2 30 mins irradiation
3 30 mins at 385K
4 70 "
5 95 "
6 125 "
7 190 "
8 300 "
9 470 "
10 48 hours

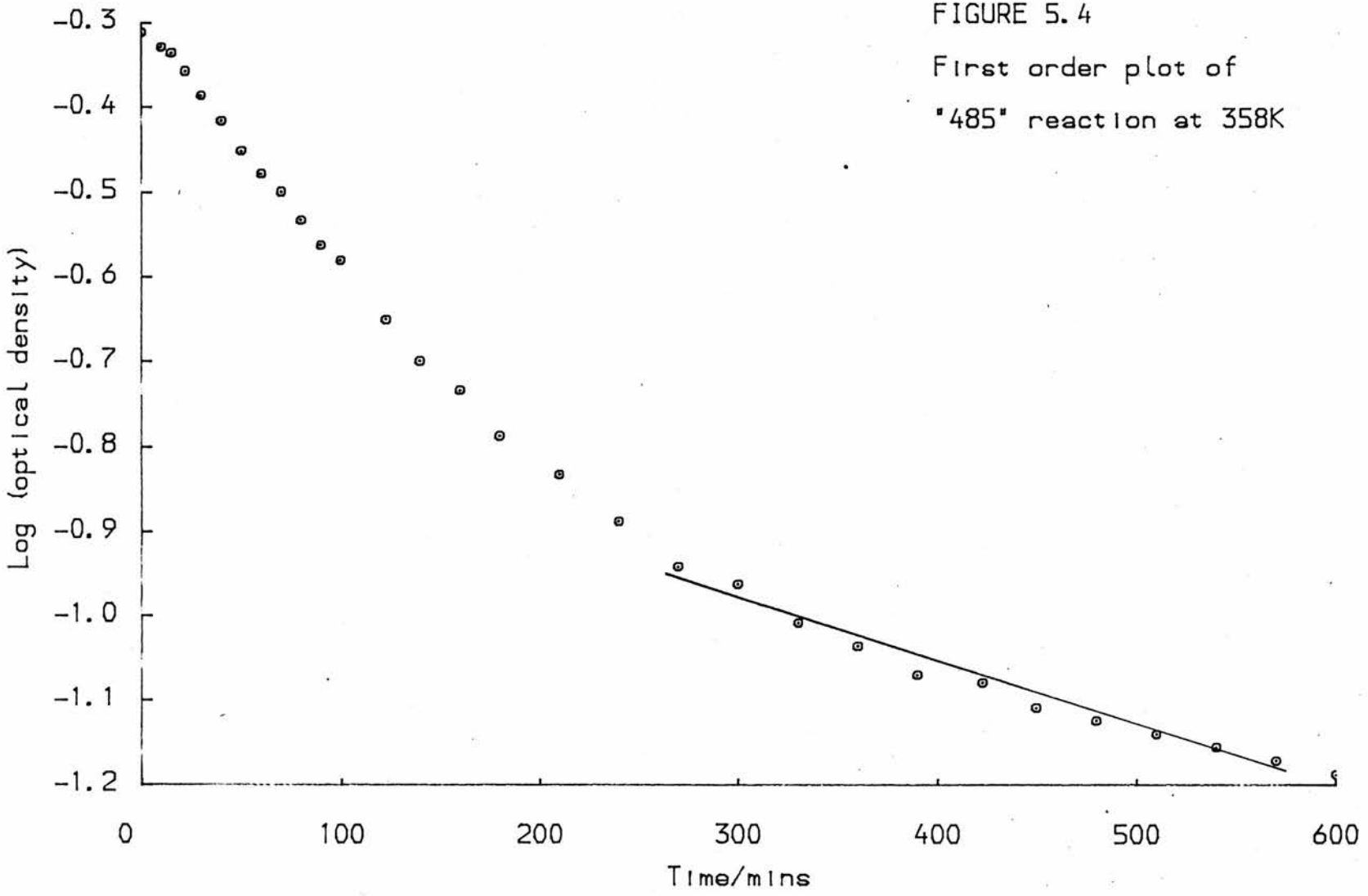

FIGURE 5.4

First order plot of

"485" reaction at 358K

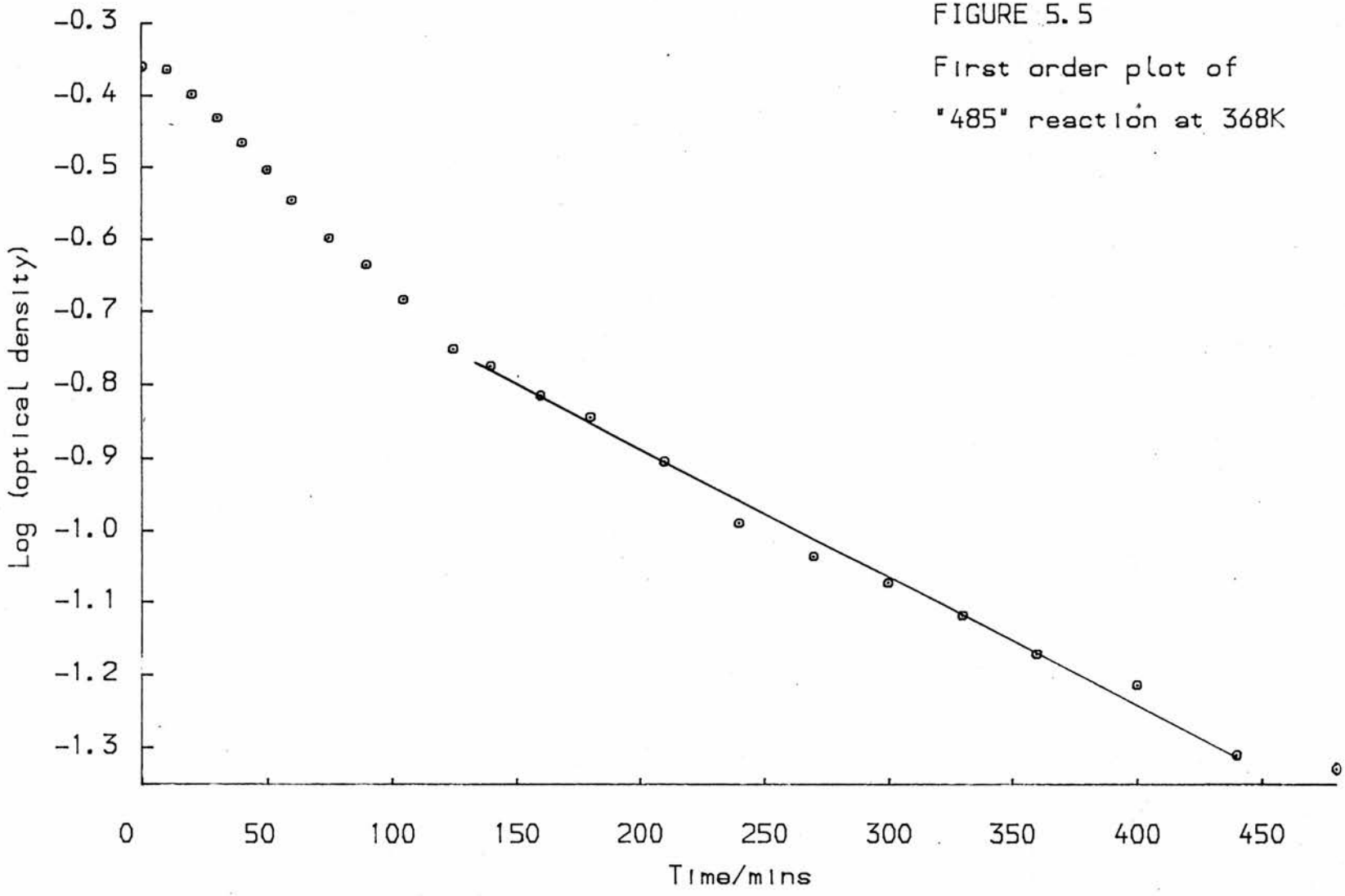

FIGURE 5.5

First order plot of

"485" reaction at 368K

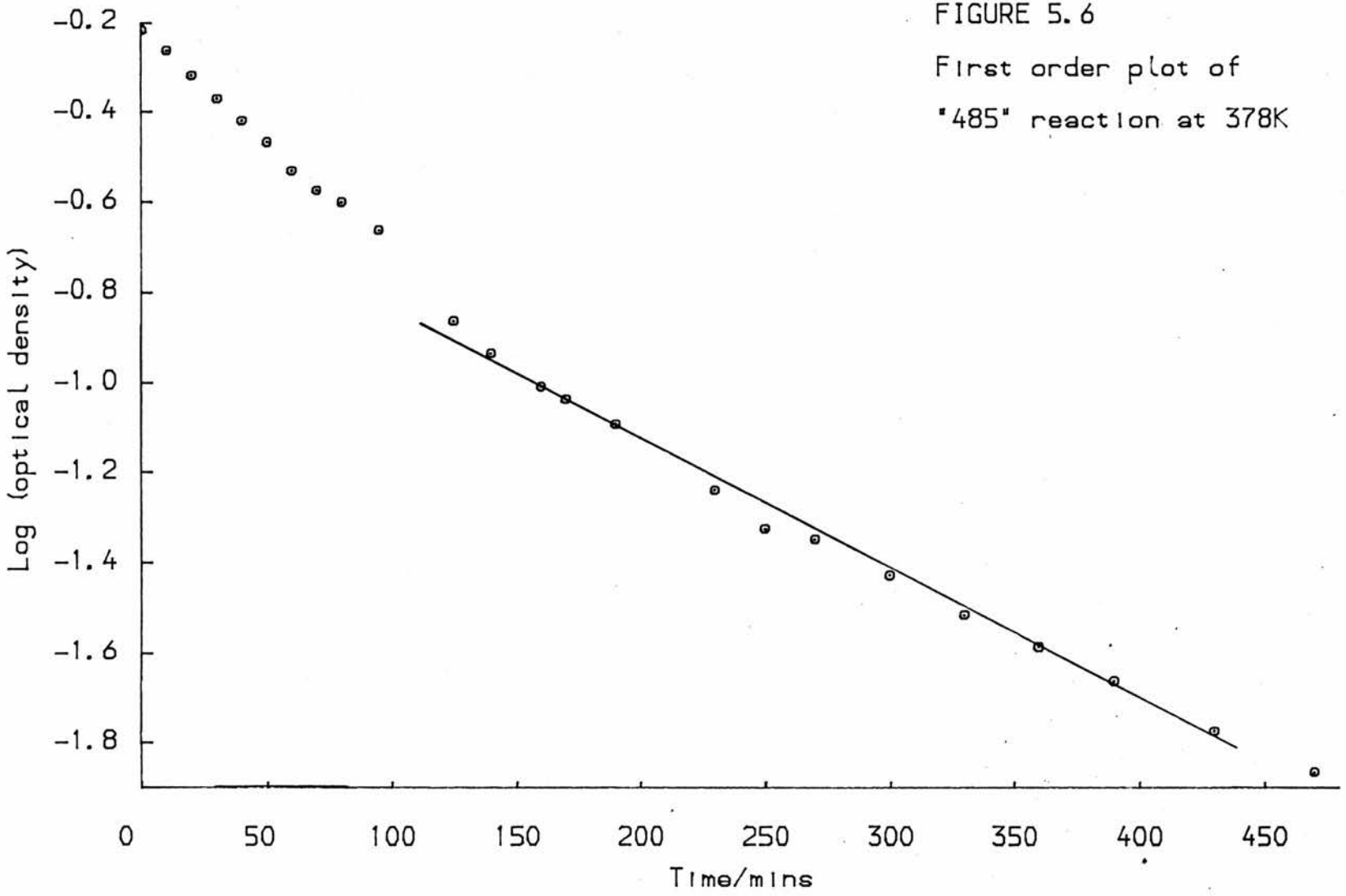

FIGURE 5.6

First order plot of

"485" reaction at 378K

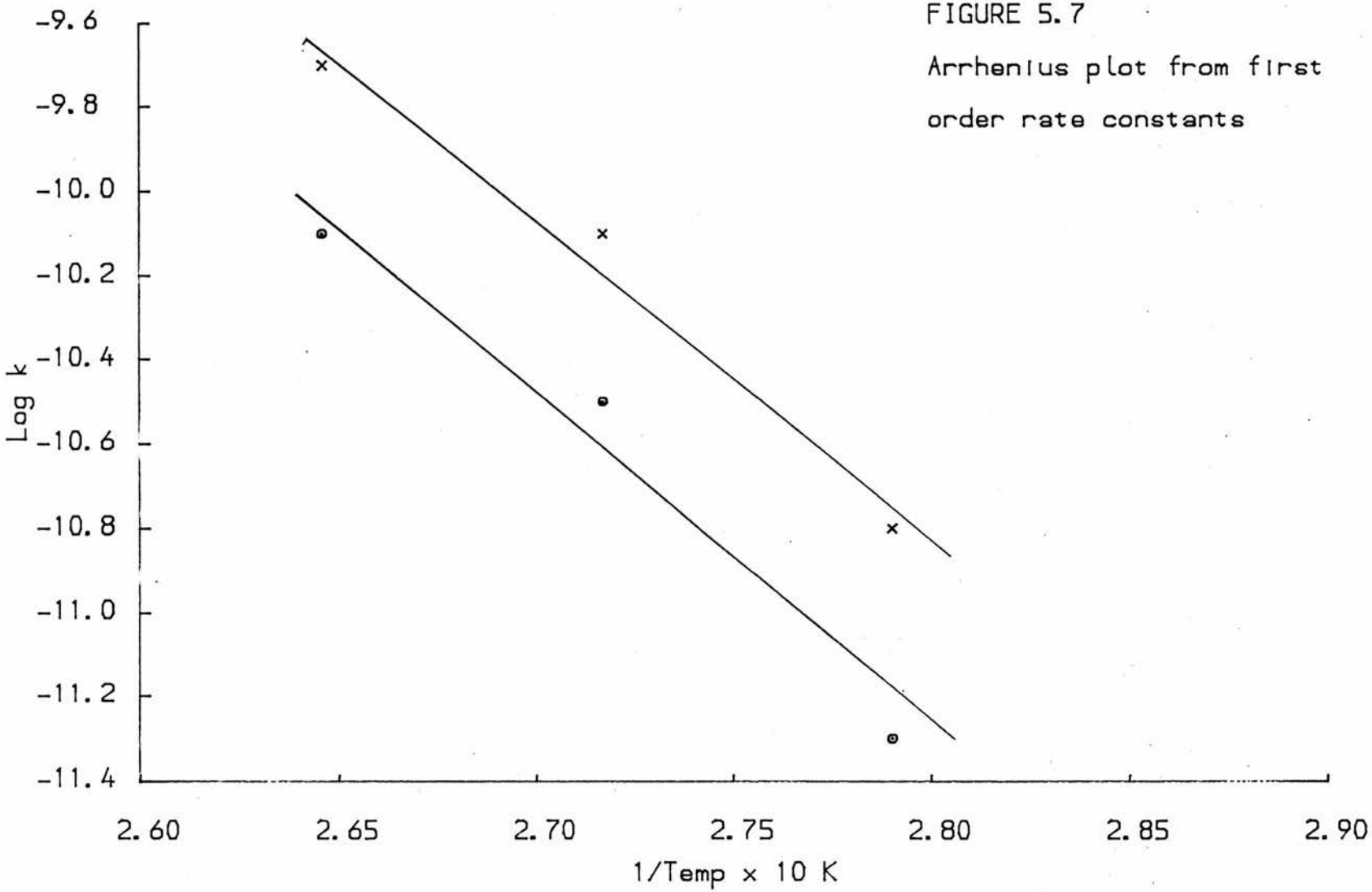

FIGURE 5.7

Arrhenius plot from first order rate constants

FIGURE 5.8

Second order plot of

'485' reaction at 358K

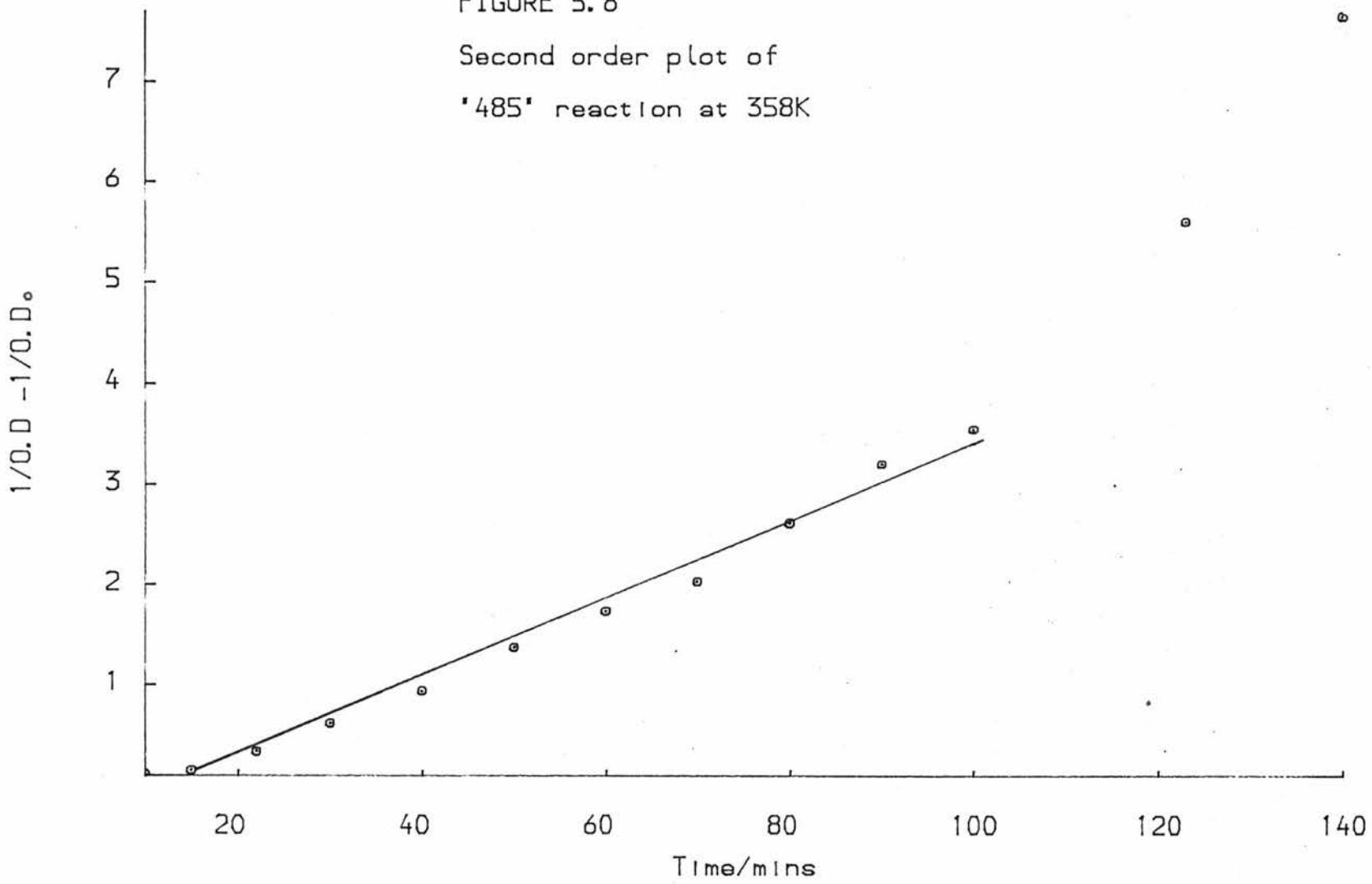

FIGURE 5.9

Second order plot of

'485' reaction at 368K

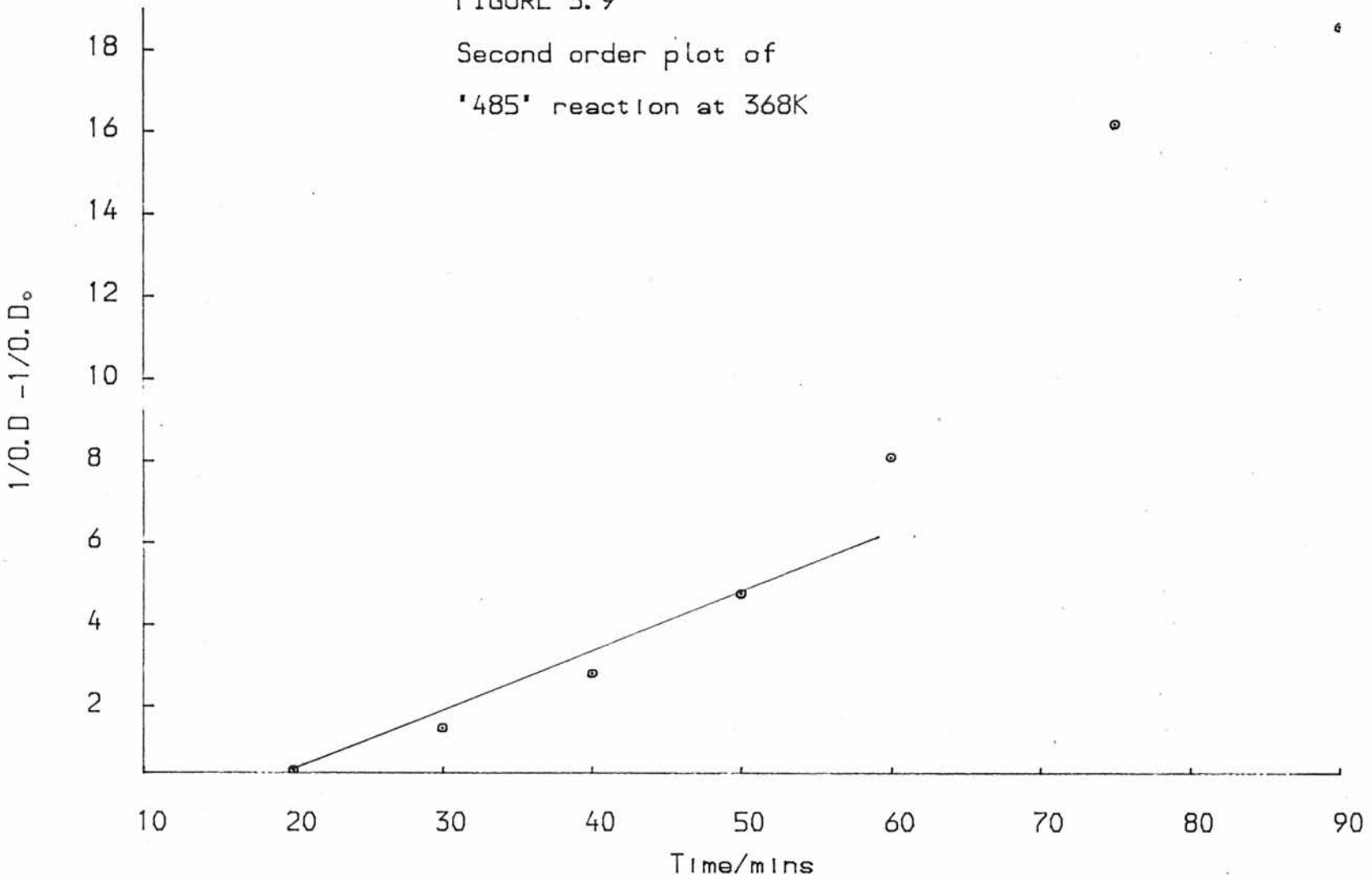

FIGURE 5.10

Second order plot of

"485" reaction at 378K

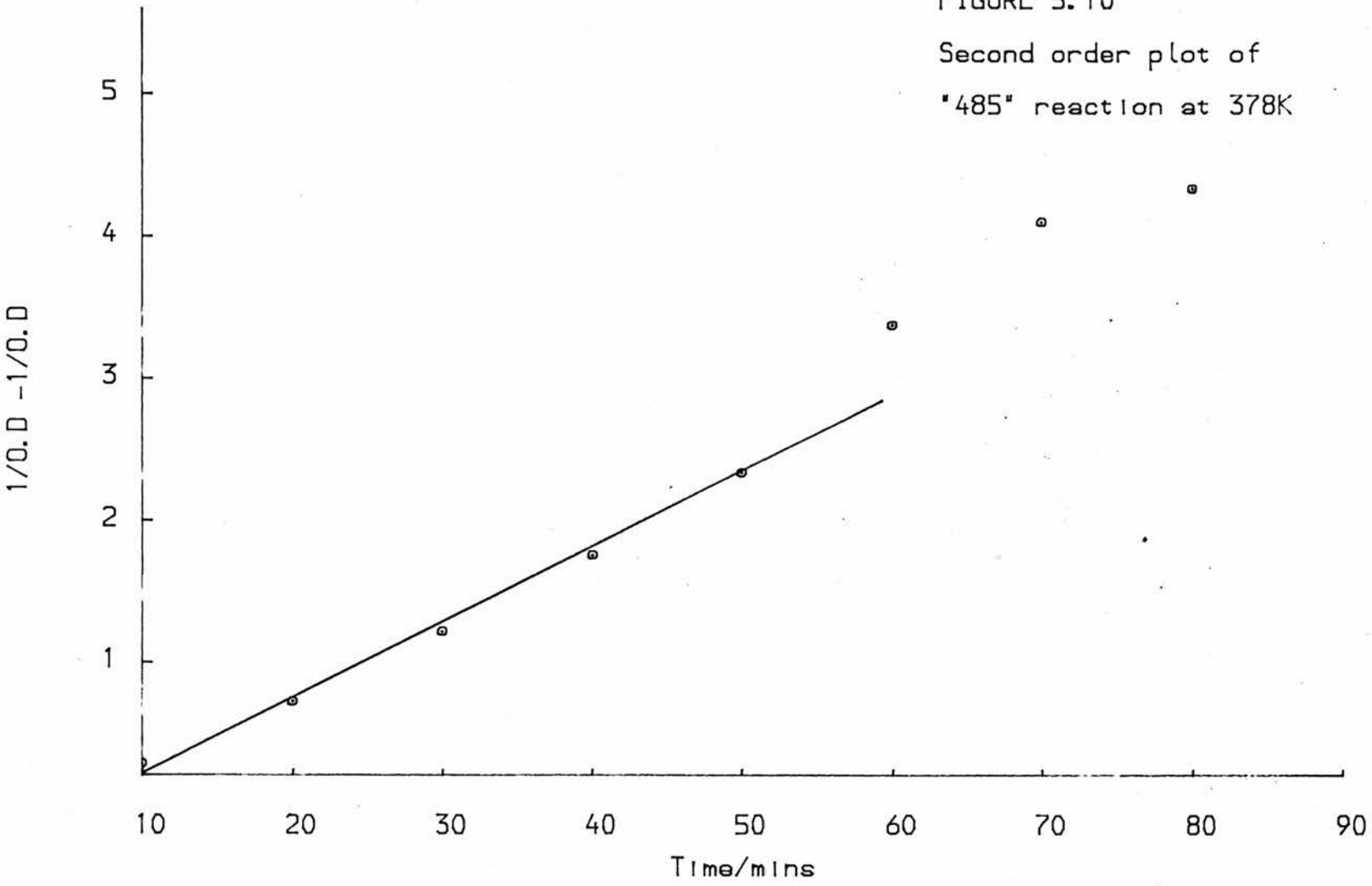

temperature /K	sample 1 k/s^{-1}	sample 2 k/s^{-1}
378	4.3×10^{-5}	6.2×10^{-5}
378	———	8.8×10^{-5}
368	2.8×10^{-5}	4.3×10^{-5}
358	1.0×10^{-5}	2.0×10^{-5}
358	1.3×10^{-5}	———
$\Delta E/kJmol^{-1}$	69.0	71.0

Table 5.1. Rate constants and activation energies for the reaction of the "485nm" product.

Lifetime Measurements

The emission spectra of the 10^{-3}M degassed ethanol and PMMA solutions of anthraquinone consisted of a broad emission over ca. 50nm with the maximum at 500nm.

The phosphorescence lifetimes at 400 and 500nm were determined at 77K after different periods of irradiation and heating. The lifetimes were measured at 77K to prevent any further photochemical reaction being initiated by the excitation source and they are given in Table 5.2.

Initially the lifetimes at 400 and 500nm were the same in both solutions and the decays were exponential (Figure 5.11). There was a small difference (ca. 4%) between the lifetimes in the two solutions

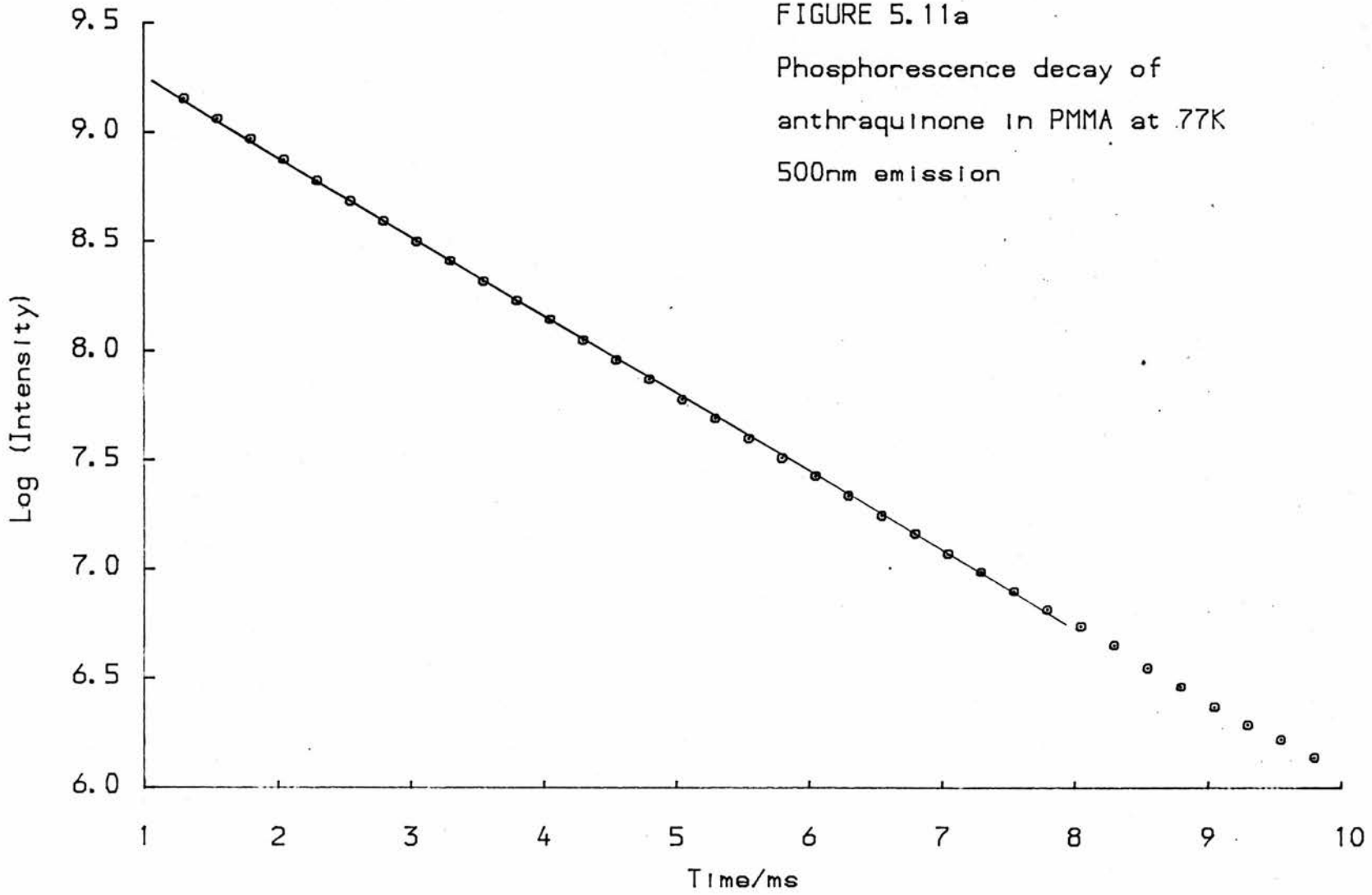

FIGURE 5.11a

Phosphorescence decay of anthraquinone in PMMA at 77K

500nm emission

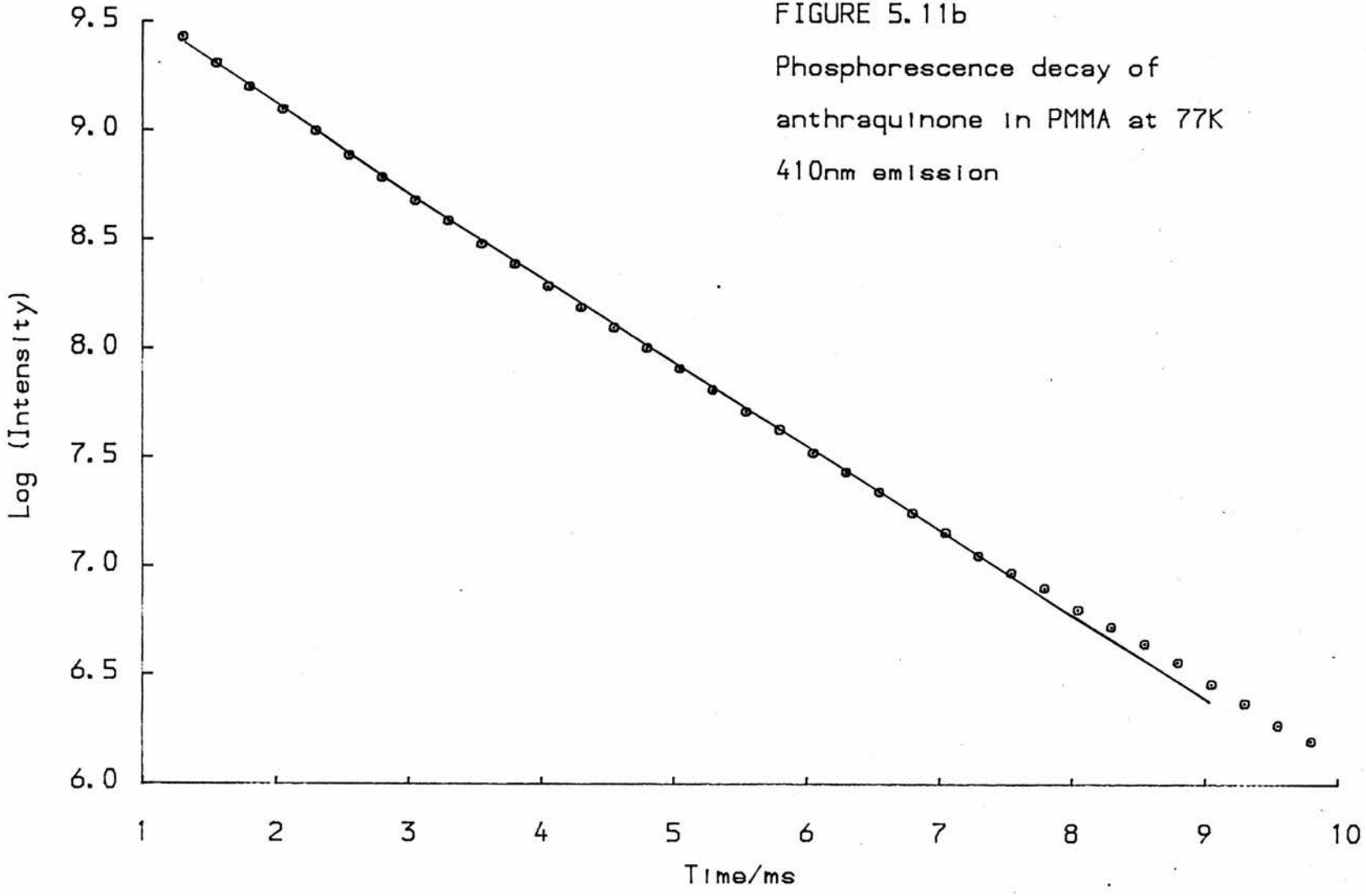

FIGURE 5.11b

Phosphorescence decay of anthraquinone in PMMA at 77K

410nm emission

but this was within the variation expected due to solvent effects and experimental error.

λ/nm	STATE OF SAMPLE	τ_p/ms PMMA	exp?	τ_p/ms ETHANOL	exp?
500	New sample	2.72	✓	2.88	✓
	20 mins irradiation	2.57	x	2.85	✓
	18 hrs heating	2.67	x	2.85	✓
410	New sample	2.71	✓	2.86	✓
	20 mins irradiation	2.33	x	2.54	x
	18 hrs heating	2.45	x	2.54	x

Table 5.2. Lifetimes of emission at 500 and 410nm in PMMA and ethanol solutions of anthraquinone.

Irradiation produced different behaviour in the two solutions. In ethanol the 500nm lifetime remained unchanged while the 400nm lifetime decreased. These lifetimes were unchanged after heating the sample to 378K for 18 hours. In contrast to the above behaviour, both the lifetimes decreased in on irradiation of the PMMA solution and on heating the 500nm lifetime returned to its original value. Non-exponential decay was observed in both solutions at 400nm after heating.

Discussion

9,10 DHA, characterized by emission at 460nm, was produced only

in solvents which had hydrogen available for abstraction and was rapidly destroyed if oxygen was present in the solution.

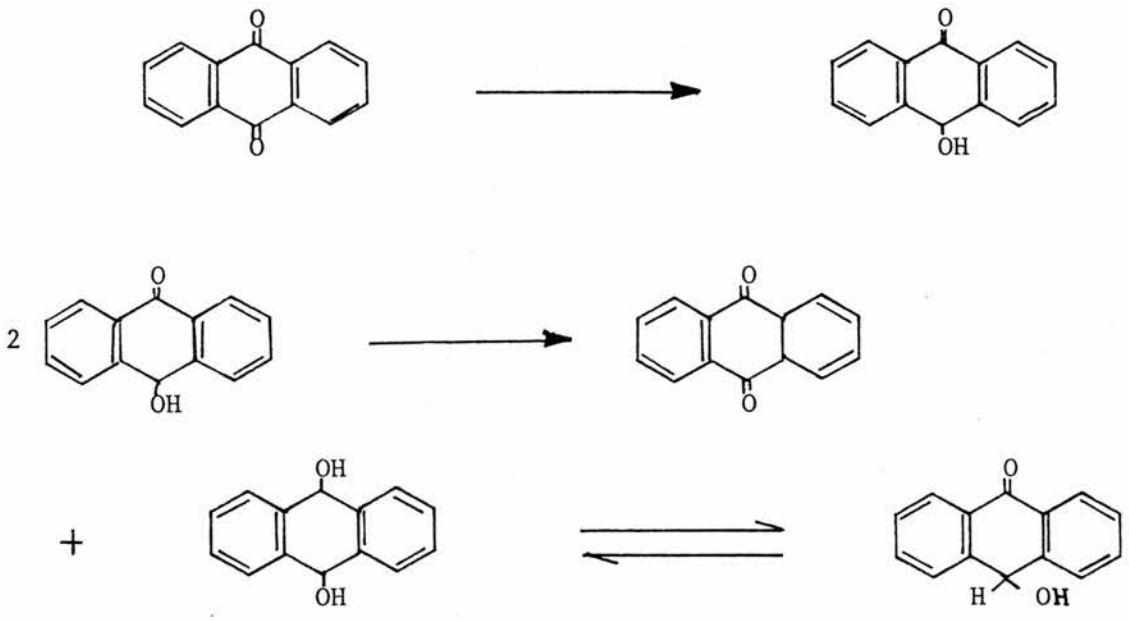

Figure 5.12. Photolysis of anthraquinone in ethanol.

The reactions described above in ethanol are in agreement with those observed by Herculese et al.,[84] and with other previous studies.[85-87] They are also consistent with the mechanism proposed at the beginning of the Chapter, which is illustrated in Figure 5.12.

Since 9,10 DHA and anthraquinone emit phosphorescence in the same region, 450-500nm, their emission spectra overlap and the most useful information was gained from the phosphorescence lifetime measurements and these also supported the above mechanism.

Prior to irradiation the emission observed at 500 and 410nm were both part of the same broad emission of anthraquinone and therefore had the same lifetime. Although the primary product of photolysis of

an ethanolic solution of anthraquinone is 9,10 DHA it has been shown by Herculese and Carlson,[85] that the concentration of 9,10 DHA becomes negligible after 20 minutes irradiation as it also undergoes photolysis under these conditions. The photolysis products found after 20 minutes irradiation included anthraquinone and a species with an emission at 410nm which was assigned to an isomer of oxanthrone whose precise structure was uncertain.

Anthraquinone is also a product of the disproportionation of the AQH$^{\bullet}$ radical and the observed emissions suggest that there was still a significant concentration of anthraquinone after 20 minutes irradiation and that the overlap of its emission with that of the oxanthrone isomer gave rise to the non-exponential nature of the decay at 410nm; at 500nm the emission was probably predominantly from the anthraquinone and hence remained unchanged and exponential after irradiation.

Heating of the irradiated sample produced no further change. This is not unexpected since the samples were heated in the dark and the reactions of these molecules are largely photochemical.

Photolysis of anthraquinone in a PMMA matrix clearly occurs by a different mechanism, the most obvious manifestation of this being the production of the red/brown colour, 485nm absorption, on irradiation. This colouration is absent in the monomer solution which may be indicative of some species, which is short-lived in solution, being stabilized or trapped in the matrix.

Hydrogen abstraction is well known in PMMA[63,12,91] and the first step in the photolysis of anthraquinone in PMMA is likely to be hydrogen abstraction by an anthraquinone molecule with the formation of the AQH$^{\bullet}$ radical. Deffner and Brunner[90] assigned the red/brown

colour, produced on irradiation of an alkaline ethanolic solution of anthraquinone containing PtO_2, to the AQH$^{\bullet}$ radical and since the possibility of disproportionation via diffusive encounters is greatly reduced in a PMMA matrix e.s.r. spectra were examined to determine if the red/brown colour originated from radicals of this nature being trapped in the matrix. The spectra, however, gave no support to this idea and established that the only radicals present in the irradiated samples were also present in an irradiated sample of pure PMMA and were characteristic of the matrix.[44] It was concluded from these spectra that the AQH$^{\bullet}$ radical was short-lived in the PMMA matrix and that the divergence in mechanism between ethanolic and PMMA solutions was likely to occur because the radical in the PMMA could undergo some reaction rather than diffuse through the matrix to encounter another AQH$^{\bullet}$ radical.

A mechanism for the photolysis of anthraquinone in PMMA has been proposed and is explained below, with supportive evidence from the present results.

Common to all anthraquinone photolysis in hydrogen donating media the reaction is initiated by hydrogen abstraction from the solvent by an excited state anthraquinone molecule with the production of AQH$^{\bullet}$ radicals.

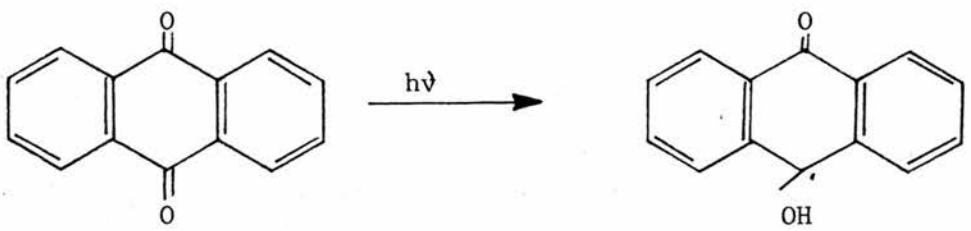

The e.s.r. spectra indicated that the radical was short-lived and since diffusion through the matrix is effectively prevented in the

lifetime of the radical the next step of the reaction must involve interaction with the PMMA to produce the red/brown substance which absorbs at 485nm. Continuous irradiation of the sample permits excitation of a radical which then abstracts a further hydrogen atom from the solvent to produce oxanthrone - the red/brown substance.

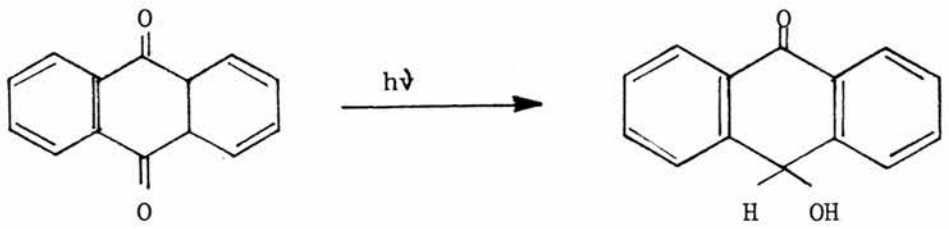

The most likely reason why oxanthrone rather than 9,10 DHA is the product of the hydrogen abstraction is that the PMMA inhibits the necessary rearrangement of the molecule. Emission from oxanthrone is known to be weak in comparison with the other emitting species and this was reflected in the emission spectra recorded at various times during the irradiation which only registered a decreasing concentration of anthraquinone.

$AQH^{\bullet}$ radicals which are not excited combine with PMMA radicals to regenerate anthraquinone.

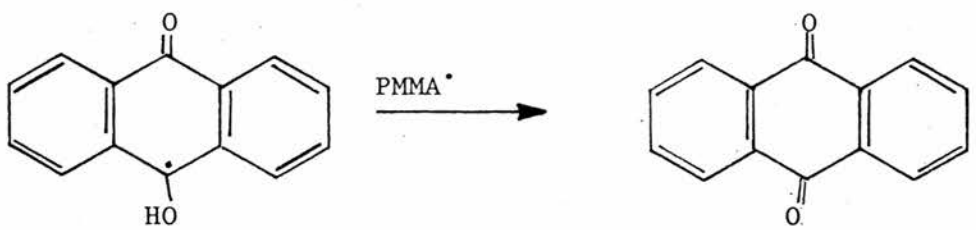

Anthraquinone is probably regenerated at some other stage of the reaction also because after heating a sample which had been irradiated

for 110 hours further irradiation produced more of the red/brown substance.

The next step in the mechanism is the rearrangement of oxanthrone to its tautomer 9,10 DHA

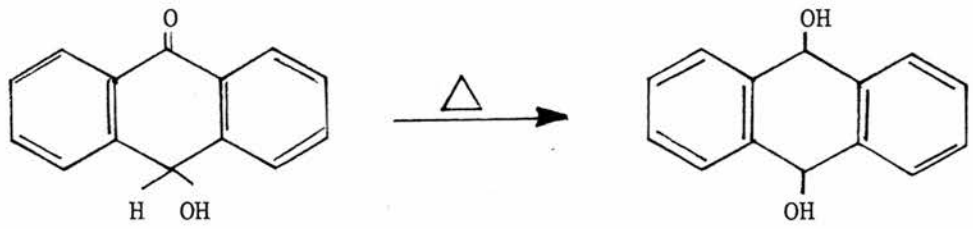

The emission spectrum after heating consisted of a single broad peak with a maximum at 460nm which is consistent with the formation of the strongly emitting 9,10 DHA.

This is a dark reaction which has a temperature dependent rate constant and an activation energy of 70-80 $kJmol^{-1}$. An activation energy of this magnitude would be expected since the rearrangement required for the tautomerism is inhibited in the rigid matrix.

The kinetics of the reaction of oxanthrone deviate from first order in the early part of the dark reaction, it was not possible to exclude oxygen from the samples and the deviation from first order kinetics may be due to reaction of the oxanthrone with oxygen which has diffused through the matrix. As previously mentioned the possibility of a second order component in the reaction kinetics could not be ruled out and this would be consistent with a diffusion controlled reaction between two oxanthrone molecules.

Phosphorescence lifetime measurements at 500nm and 410nm support the proposed reaction mechanism and products.

Prior to irradiation the lifetimes at both wavelengths were the

same and the emission was from anthraquinone alone, the values were in close agreement with those determined in ethanol solution.

Irradiation over a period of 20 minutes introduced non-exponential decay and caused a decrease in the lifetimes at both wavelengths. According to the proposed mechanism anthraquinone and oxanthrone were present at that stage of the reaction, with lifetimes of 2.7 and 2.2ms respectively. Although the decays were non-exponential the lifetimes determined from a least squares regression on the log intensity against time data, gave an indication of the lifetimes of the component emissions. At 500nm the lifetime was 2.5ms as expected since the emission was predominantly from anthraquinone and at 410 the lifetime was 2.3ms indicating a larger oxanthrone component.

Consistent with an overlap in the emissions from anthraquinone and 9,10 DHA the lifetimes at 500nm and 410nm were non-exponential after heating which is consistent with the proposed mechanism.

CHAPTER 6

TEMPERATURE DEPENDENCE OF PHOSPHORESCENCE OF EUROPIUM CHELATES

Lanthanide Chemistry

The lanthanides, or lanthanoids, are the fourteen elements following lanthanum in the periodic table and their electronic configurations are characterized by a progressive filling of the 4f shell.

The first three ionization potentials are relatively low so the elements are highly electropositive. Their chemistry is predominantly ionic and is determined primarily by the size of the M^{3+} ion.

Although the +3 oxidation state is the most stable in all the lanthanides, the +2 and +4 oxidation states are known for several of the elements and can, to a certain extent, be correlated with electronic structure and ionization potential. There appears to be a special stability associated with an empty, half-filled or full f-shell, e.g. Ce^{4+}, Eu^{2+}, Tb^{4+} and Yb^{2+} have f^o, f^7, f^7 and f^{14} electronic configurations respectively.

The lanthanides differ only in the number of 4f electrons and their chemistries are very similar. There are some variations in the properties of the same oxidation state caused by the decrease in ionic radius which occurs as the atomic number increases (the lanthanide

contraction). All the tripositive lanthanide ions, Ln^{3+}, form complexes with numerous coordination numbers with both inorganic and organic species.

Type of Bonding

Effective shielding, by the 5s and 5p electrons, tends to prevent the 4f orbitals from participating in bond formation so higher energy unfilled orbitals must be utilized, e.g. 5p and 6s. One consequence of this shielding is that complexes, stable relative to the hydrated cation, are only formed with strongly coordinating, electronegative atoms, e.g. oxygen and nitrogen. With these ligands the Ln^{3+} - ligand attractions are mainly electrostatic and the complexes are more closely related to those formed by the alkaline earth metals (e.g. Ca^{2+} and Ba^{2+}) than the d-shell transition metals, as might be expected, because the d orbitals are used in bond formation in the latter.

Ligands in which coordination takes place through oxygen atoms usually have the oxygen atom as part of a functional group such as:-

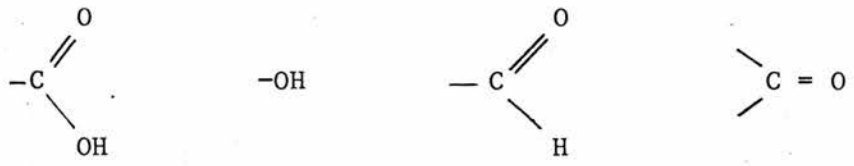

carboxylate hydroxyl aldehydic carbonyl

The numerous complexes formed between Ln^{3+} ions and ligands containing nitrogen or oxygen have been reviewed by Forster[92] and Moeller et al.[93] Many of these complexes are unstable with respect to

hydrolysis to the hydroxide and their preparation often requires anhydrous conditions.

Although many complexes are formed with monodentate ligands, greater stability, with respect to dissosiation into component molecules, is invariably achieved with bidentate ligands such as:-

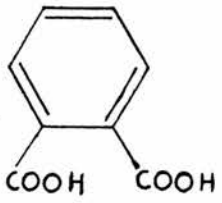

phthalic acid

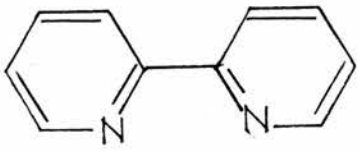

2,2´-dipyridyl

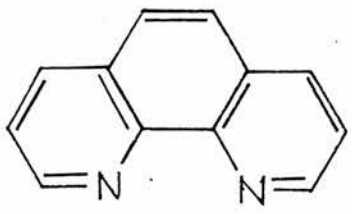

1,10-phenanthroline

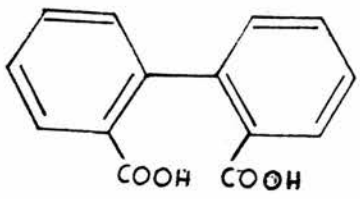

biphenyl dicarboxylic acid

β- diketonates

One particular class of bidentate ligands, the β-diketones or 1,3 alkyldiones, are known to complex with almost every metal and non-metal in the periodic table[94] and have general formula:-

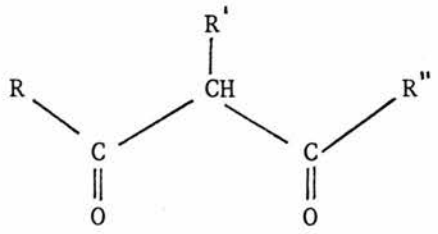

where R, R' and R'' may be alkyl or aryl.

Loss of a H^+ ion produces a β- diketonate anion and chelation occurs through the two oxygen atoms, with the formation of a six-membered ring:-

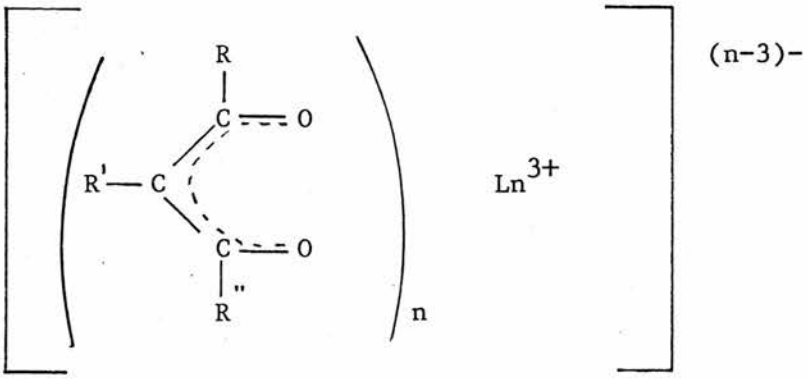

where n = 3 or 4.

Two classes of chelates are formed by β- diketonates which may be distinguished by the ratio of ligand to metal ion:-

(i) Neutral TRIS chelates where n = 3.

(ii) Anionic TETRAKIS chelates where n = 4.

In most cases, because of the lanthanide ions affinity for high coordination the tris complexes are usually isolated as solvates, and attempts to remove the solvent often leads to decomposition. The tetrakis chelates, because of their anionic nature, are isolated with a cation e.g. a protonated amine. A large number of both classes of

chelates are known and homologous series of tetrakis chelates can be produced by varying the cation.

The ligands and amine bases used to make the chelates investigated here are shown in Table 6.1 together with the abbreviations used in the following discussion.

systematic name	trivial name	abbreviation used
1,1,1-trifluoro-4-phenyl-2,4-pentanedione	benzoyltrifluoroacetone	Hbtfa
1,1,1,5,5,5-hexafluoro 2,4-pentanedione	hexafluoroacetone	Hhfaa
2,4-pentanedione	acetylacetonate	Haa
2-methyl,2-aminopropane	tertiarybutylamine	Bu^tNH_2
1-methylpyridine	αpicoline	αpic
piperidine	piperididine	pip
pyridine	pyridine	py
2-aminopyridine	2-aminopyridine	$2\text{-}NH_2py$
quinoline	quinoline	quin

Table 6.1. examples of β- diketonates and cations used to form Eu^{3+} chelates.

Coordination Numbers

In both ionic crystals and complexes the coordination number usually exceeds six; some compounds are known where the coordination number is six but solvation of the ions generally leads to coordination numbers of 7,8,9 or 10. The high coordination is due, in

part, to the relatively large ionic radius; the ionic radius of Ce^{3+} is 0.1034nm (compared to 0.063nm in Cr^{3+}).

Spectral Properties

Since the 4f electrons do not penetrate close to the nucleus, spin and orbital angular momentum may be treated by the Russell-Saunders coupling approximation which is not normally useful for heavy atoms. Spin-orbit coupling constants are relatively large (of the order of $1000cm^{-1}$) and the lanthanide ions have ground states with single, well defined values of angular momentum, J, with the next J state energy many times kT above in most cases, and hence, virtually unpopulated at room temperature.

Eu^{3+} is an exception to the general energy level pattern as the first, second and third excited J states are sufficiently close to the ground state to be appreciably populated at room temperature (see Figure 6.1 which shows the energy levels in Eu^{3+}, Tb^{3+}, Gd^{3+} and Sm^{3+}).

The most common type of transition giving rise to absorption and emission spectra are assosiated with rearrangements of the 4f electronic configuration. External forces have little influence on the 4f orbitals as the orbitals are effectively shielded by 5s and 5p shells, and therefore the states arising from the various 4f configurations are practically invariant for a given ion in all its compounds and are only split by external fields to the extent of ca. $100cm^{-1}$. Although the profile of emission from a Ln^{3+} ion is little affected by its chemical environment and absorption and emission bands are very narrow, the quantum yield of the transitions may vary considerably between compounds.

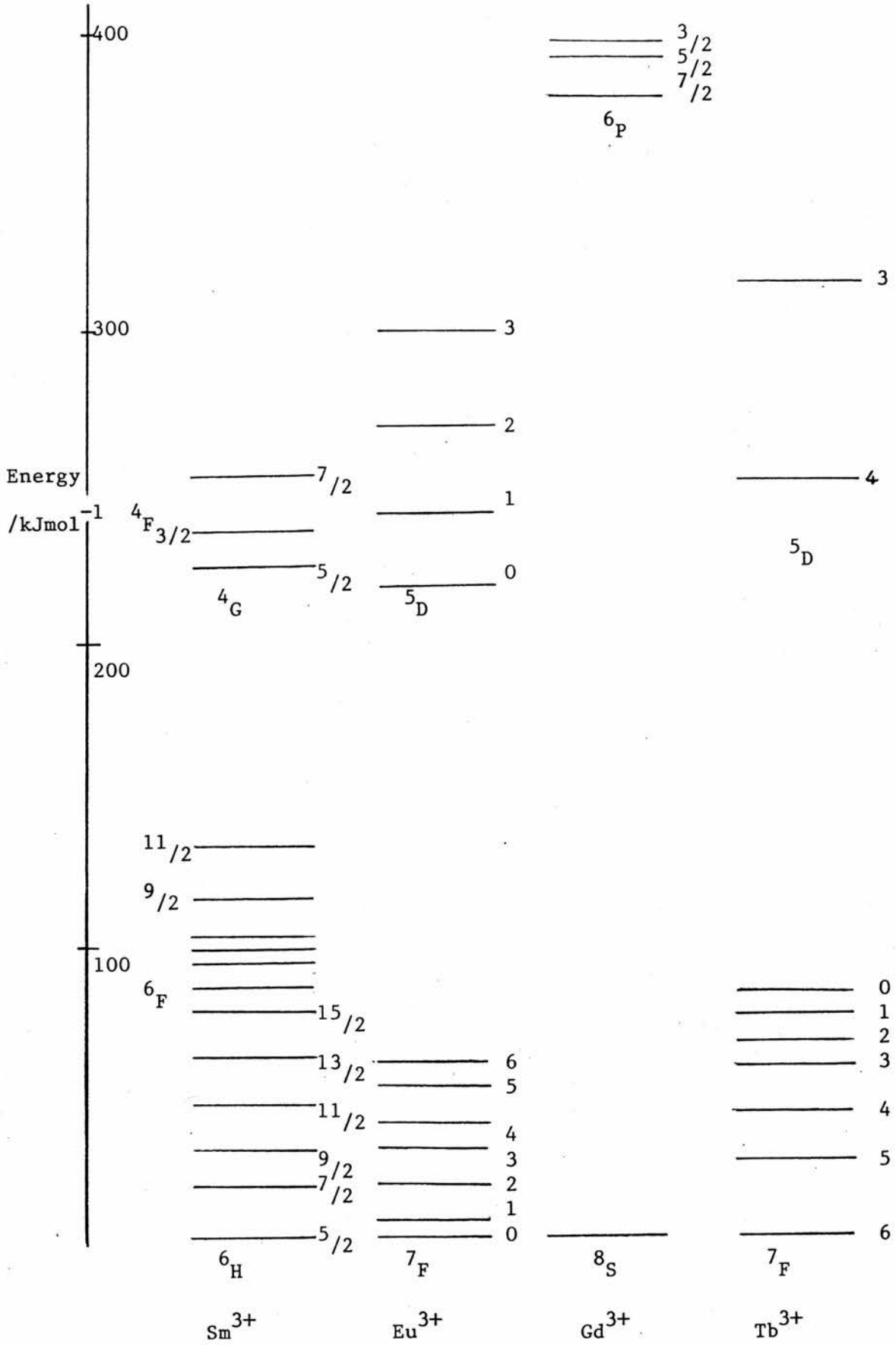

Figure 6.1 Energy levels for some rare-earth metal ions.

Chelate Emission

Weissman[95] first observed direct excitation of the organic ligand giving rise to emission characteristic of the metal ion.

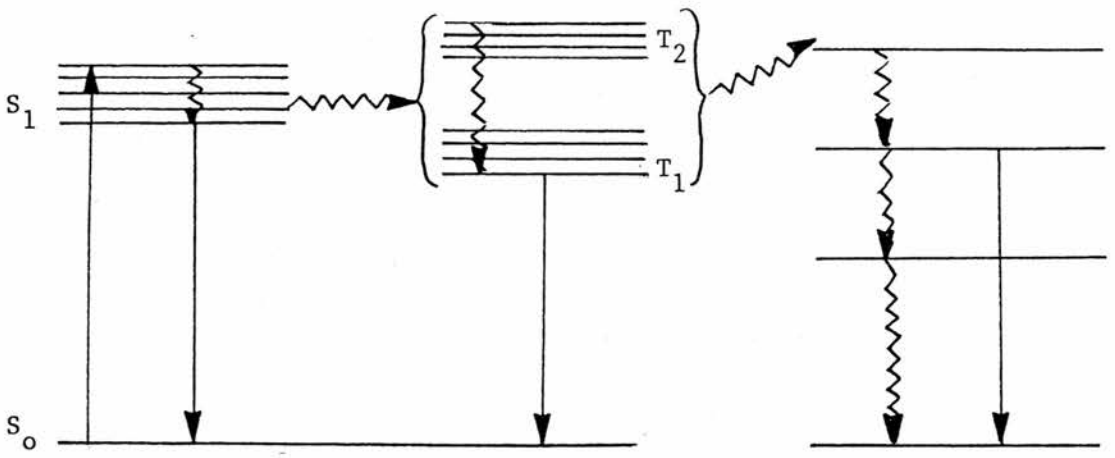

Figure 6.2. Representitive energy level diagram for a rare earth chelate having low-lying 4f electronic states.

The mechanism of this indirect population of the metal ion has been extensively investigated and reviewed by Crosby et al.,[96] and will be described here in terms of their diagram, Figure 6.2.

After absorption to the first excited state the chelate may undergo the several molecular radiative and non-radiative processes, described in Chapter 1, and in addition undergo a radiationless transition from the triplet manifold to a low-lying state derived from the 4f electronic configurations of the coordinated rare-earth ion. If the state is a resonance level then a radiative "line" emission, characteristic of the particular ion, may occur whereas deactivation of non-resonance states can only be non-radiative. Since the

radiative transition in the metal ion involves a change in spin multiplicity the emission is phosphorescence.

Consistent with this mechanism Crosby et al.,[96] classified the Ln^{3+} ions into three categories based on the phosphorescence properties of the chelates:-

(i) Ions which exhibit no metal-ion emission.

This category includes Gd^{3+} in which metal ion excitation is precluded by the fact that the lowest excited level of the ion lies above the triplet level of most ligands (ca. 32,000cm^{-1}), and Lu^{3+} in which the 4f shell is full and intra-4f transitions are not possible.

(ii) Ions which emit strongly.

This includes Eu^{3+}, Tb^{3+}, Sm^{3+} and Dy^{3+} where the acceptor energy levels are close to the donating triplet level of the ligand.

(iii) Ions which emit weakly.

This includes Pr^{3+}, Nd^{3+}, Ho^{3+}, Tm^{3+} and Yb^{3+} in which the energy levels are closely spaced which increases the probability of deactivation by a non-radiative, cascade, mechanism.

Characteristic metal-ion emission can only be sensitized if the resonance level lies below the donating level in the ligand and therefore depends upon the nature of the chelate, for example the luminescence of dysprosium trisbenzoylmethide consists of molecular fluorescence and phosphorescence whereas dysprosium trisbenzoylacetone emits primarily the blue line emission characteristic of Dy^{3+}.

Europium Chelates

The Eu^{3+} ion has a ^7F_o ground state and is known to emit strong metal-ion phosphorescence in many complexes with characteristic phosphorescence profiles which are characteristic in all

europium emission spectra and consist of a main peak at ca. 615nm, corresponding to the ^5D_o ---> $^7F_2$ transition and less intense peaks at ca.579 and 593nm corresponding to ^5D_o ---> ^7F_o and ^5D_o ---> $^7F_1$ transitions respectively.

Although the phosphorescence profiles vary little between the tetrakis chelates the relative intensities of the various emission lines vary considerably. In the solid state the intensities are primarily dependent upon the local symmetry about the Eu^{3+} ion, and therefore are affected by different substituents in the ligand[97] and by the cation.[98,99] Different ligand substituents alter the symmetry about the Eu^{3+} ion and the effective perturbation of the molecular field surrounding the ion; this results in a modification of the interaction of the 4f-shell and its environment and of the energy transfer processes leading to Eu^{3+} phosphorescence.[100]

The mechanism of excitation, via the triplet state proposed by Crosby, was questioned for some europium chelates by Kleinerman[101] who suggested that the mechanism was dependent upon the nature of the chelate and may, in some cases, involve direct transfer from the ligand singlet manifold.

Since Kleinerman's suggestion there has been much discussion and evidence produced for and against direct singlet excitation. Tanaka et al.,[102] showed that the rate of energy transfer from the ligand to the Eu^{3+} ion was slower, at 10^{-8}s, than previously estimated by El-Sayed et al.,[103] at 10^{-10}s., and they pointed out that energy transfer to the triplet manifold of the ligand was probable before Eu^{3+} excitation occured. Similar evidence was produced by Lyle et al.[104]

Supportive evidence for direct singlet excitation came from Dean

and Shepherd:[105] measurements of phosphorescence lifetimes in mixed lanthanide chelates at low temperature lead them to conclude that direct singlet transfer accounted for the major part of the inter-molecular transfer in (Eu,Gd)$(btfa)_4$pipH, and occurred at a rate considerably faster than inter-system crossing to the triplet, but was much less important in (Eu,Gd)$(hfaa)_4$pipH crystals.

Results

The phosphorescence decay of the ^5D_o ---> $^7F_2$ transition (at ca. 615nm) in several solid europium tetrekis chelates was measured and the lifetimes of the ^5D_o determined at 77K and at various temperatures up to 400K.

The lifetime at 77K was measured before and after the samples were heated to 400K and if the two values coincided it was assumed that the structure of the chelate had remained unchanged during the heating. This was not the case for several chelates and investigation of these was discontinued, e.g. Eu$(dbm)_4NEt_2H$ and Eu$(btfa)_4Et_3NH$.

All the chelates investigated exhibited temperature independent phosphorescence below 330K and the profile of emission intensity against time (Figure 6.3.) showed that the decay obeyed first order kinetics. Above 330K a temperature dependent process became a significant factor in the depopulation of the ^5D_o level and this was reflected by a decrease in the phosphorescence lifetimes, however the decay retained the first order characteristics (Figure 6.4). Variations in the temperature dependence profiles between the chelates were observed and are illustrated in Figure 6.5.

Activation energies and pre-exponential factors were calculated over the temperature range 330-400K from the Arrhenius equation using

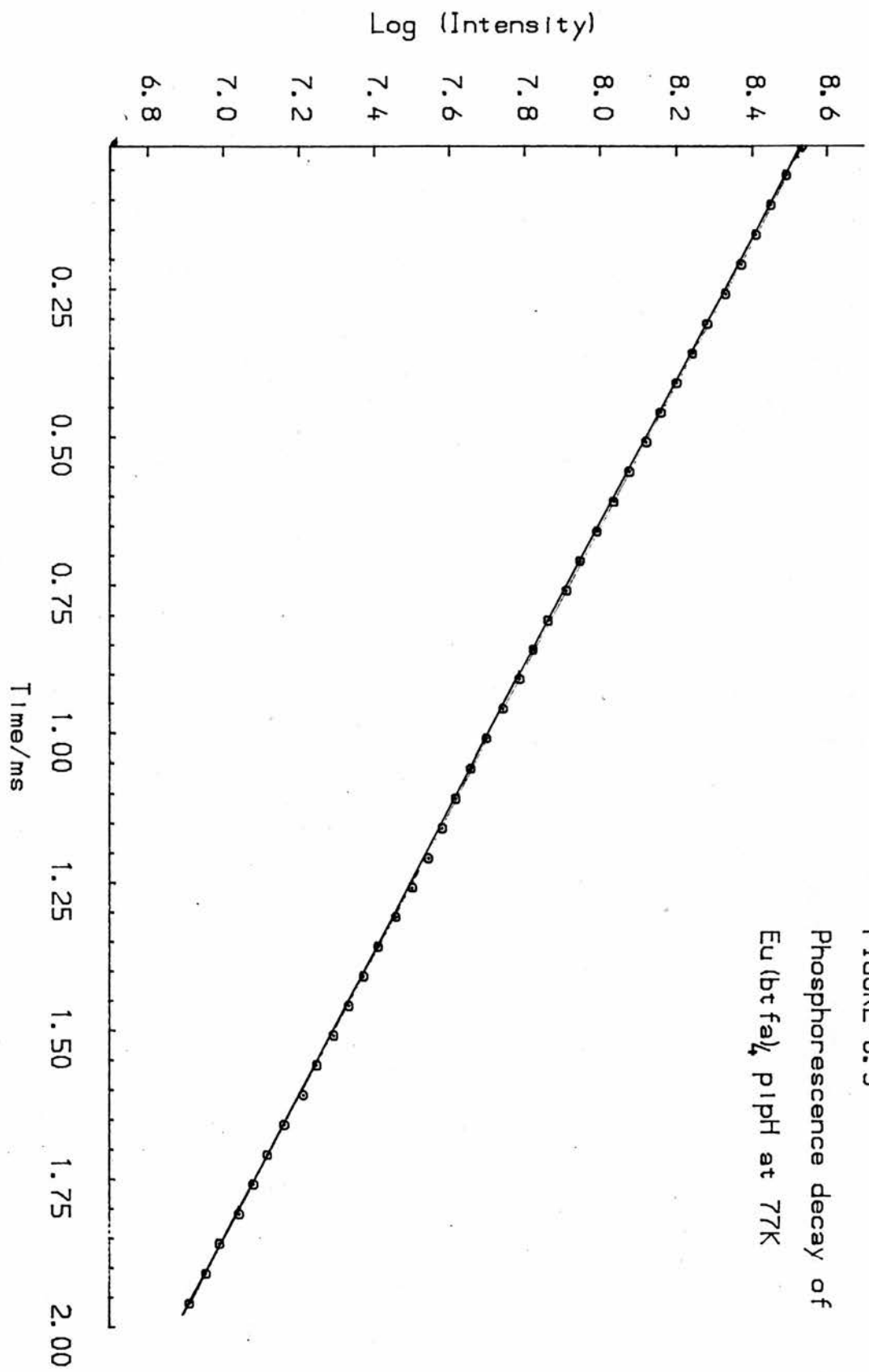

FIGURE 6.3

Phosphorescence decay of Eu(btfa)$_4$ pipH at 77K

FIGURE 6.4

Phosphorescence decay of $Eu(btfa)_4$ pipH at 383K

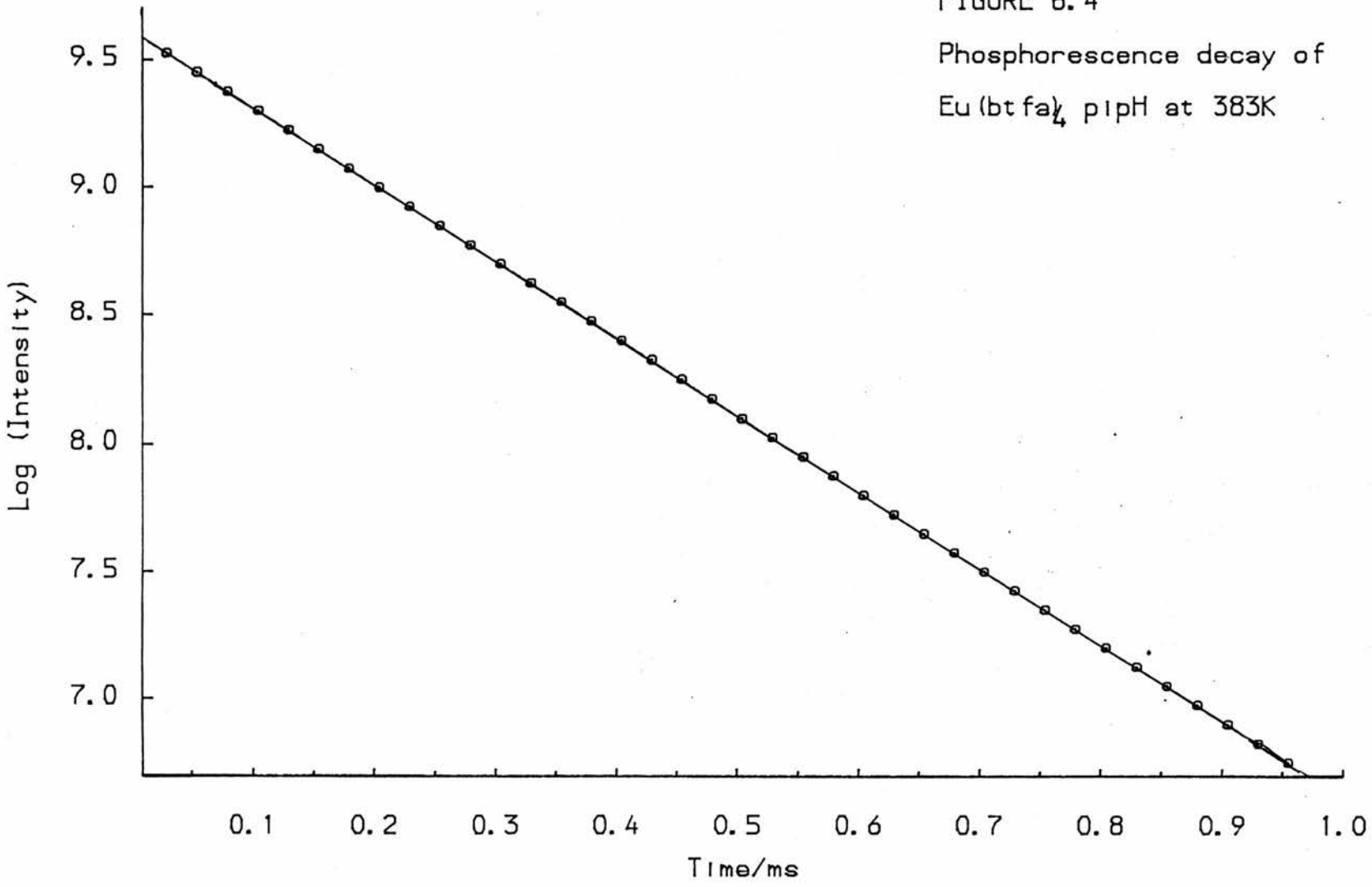

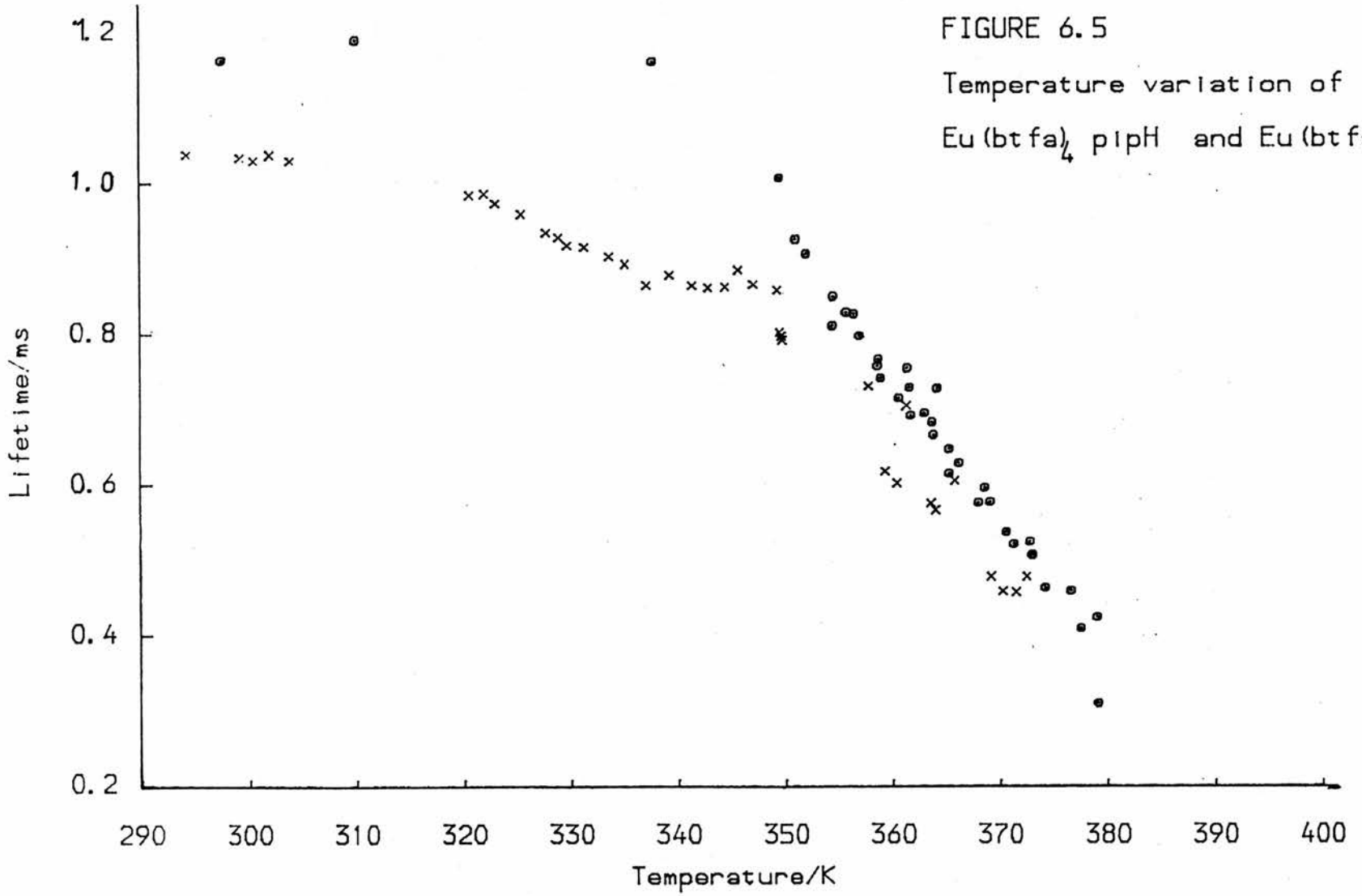

FIGURE 6.5

Temperature variation of lifetime

$Eu(btfa)_4$ pipH and $Eu(btfa)_4$ $Bu^t NH_3$

the method described in Chapter 2 for thermal deactivation. Figures 6.6 - 6.12 illustrate the linear relationship between 1/T and $(\frac{1}{\tau} - \frac{1}{\tau_{77}})$ and the activation energies and pre-exponential factors are summarized in Table 6.2.

This calculation is sensitive to the choice of τ_{77}. For example in solid $Eu(btfa)_4pipH$ if τ_{77} is taken as 1.18ms $E = 74.2kJmol^{-1}$ whereas $E = 72.7kJmol^{-1}$ if τ_{77} is taken as 1.2ms; the values used were the average of several experimentally determined values.

Although the lifetime of $Eu(hfaa)_4Bu^tNH_3$ was only measured at seven temperatures above 333K the activation energy and pre-exponential factor determined from this data were corroborated by the values found by Dean and Shepherd.[106]

chelate	ΔE /kJmol^{-1}	A /s^{-1}	R	τ_{77}
$Eu(btfa)_4pipH$	72.7	2×10^{13}	0.988	1.23
$Eu(btfa)_4pyH$	73.4	2×10^{13}	0.988	0.95
$Eu(hfaa)_4pyH$	83.6	4×10^{14}	0.986	1.29
$Eu(hfaa)_4{}^2NH_2pyH$	74.1	2×10^{13}	0.987	1.13
$Eu(hfaa)_4\alpha picH$	77.5	4×10^{14}	0.962	1.23
$Eu(btfa)_4quinH$	60.0	3×10^{11}	0.939	.051
$Eu(btfa)_4Bu^tNH_3$	50.2	2×10^{9}	0.942	1.04
$Eu(hfaa)_4Bu^tNH_3$	42.6	3×10^{8}	0.991	.055

Table 6.2. Activation energies, pre-exponential factors and 77K lifetimes of some europium chelates.

FIGURE 6.6

Eu(btfa)$_4$ pipH

Stern Volmer plot

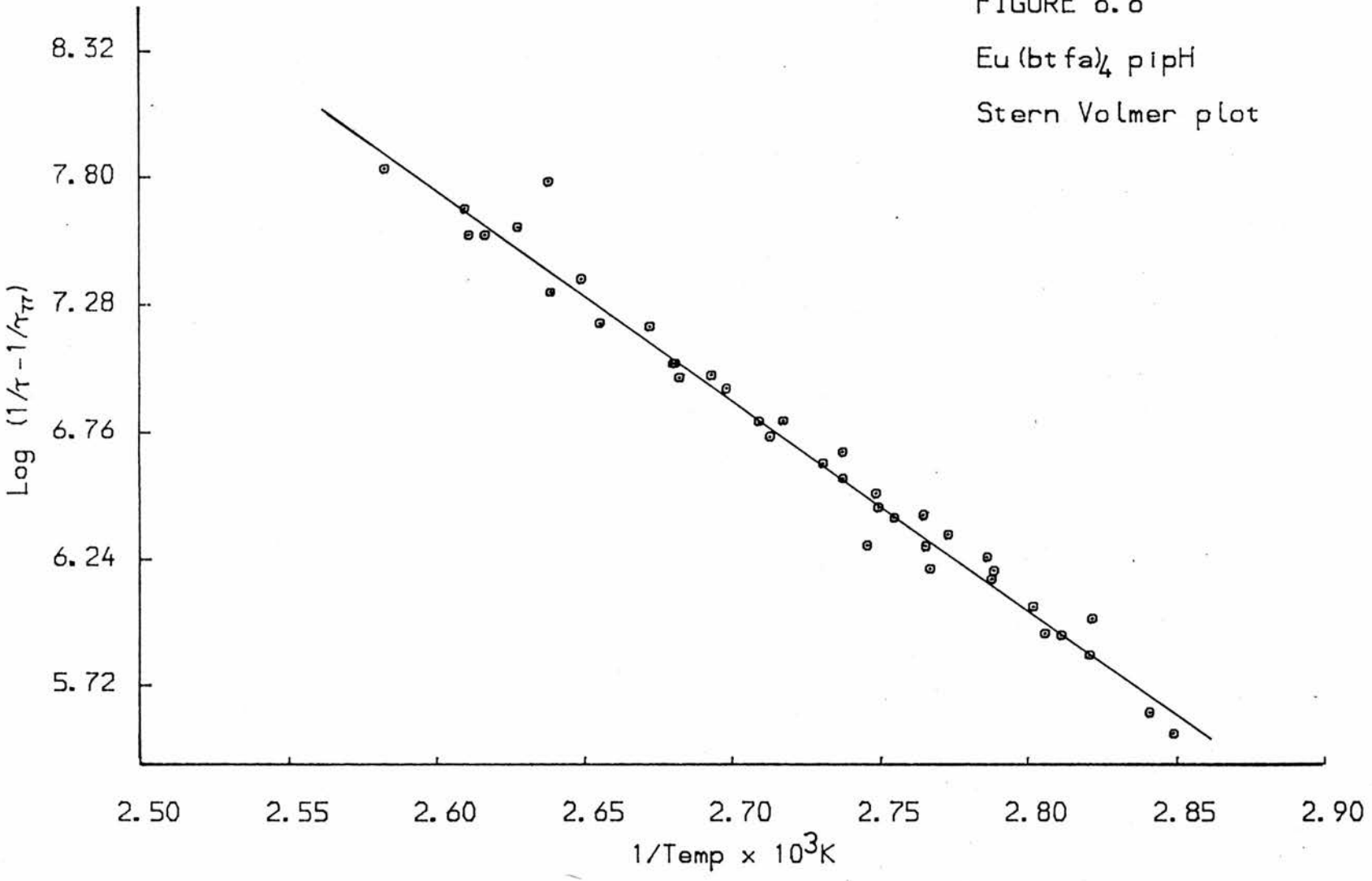

FIGURE 6.7

Eu(btfa)$_4$ pyH

Stern Volmer plot

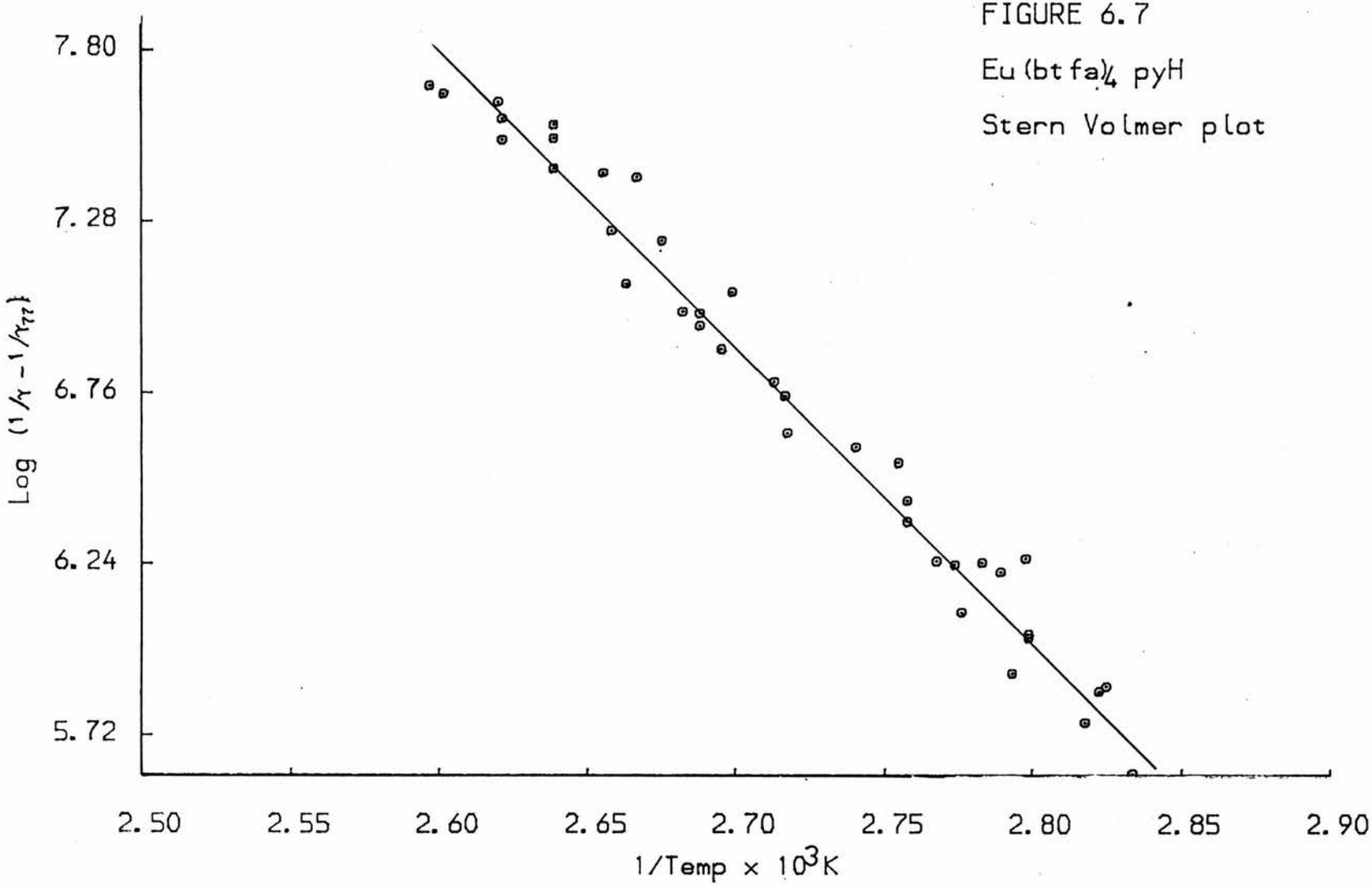

FIGURE 6.8

$Eu(btfa)_4 Bu^t NH_3$

Stern Volmer plot

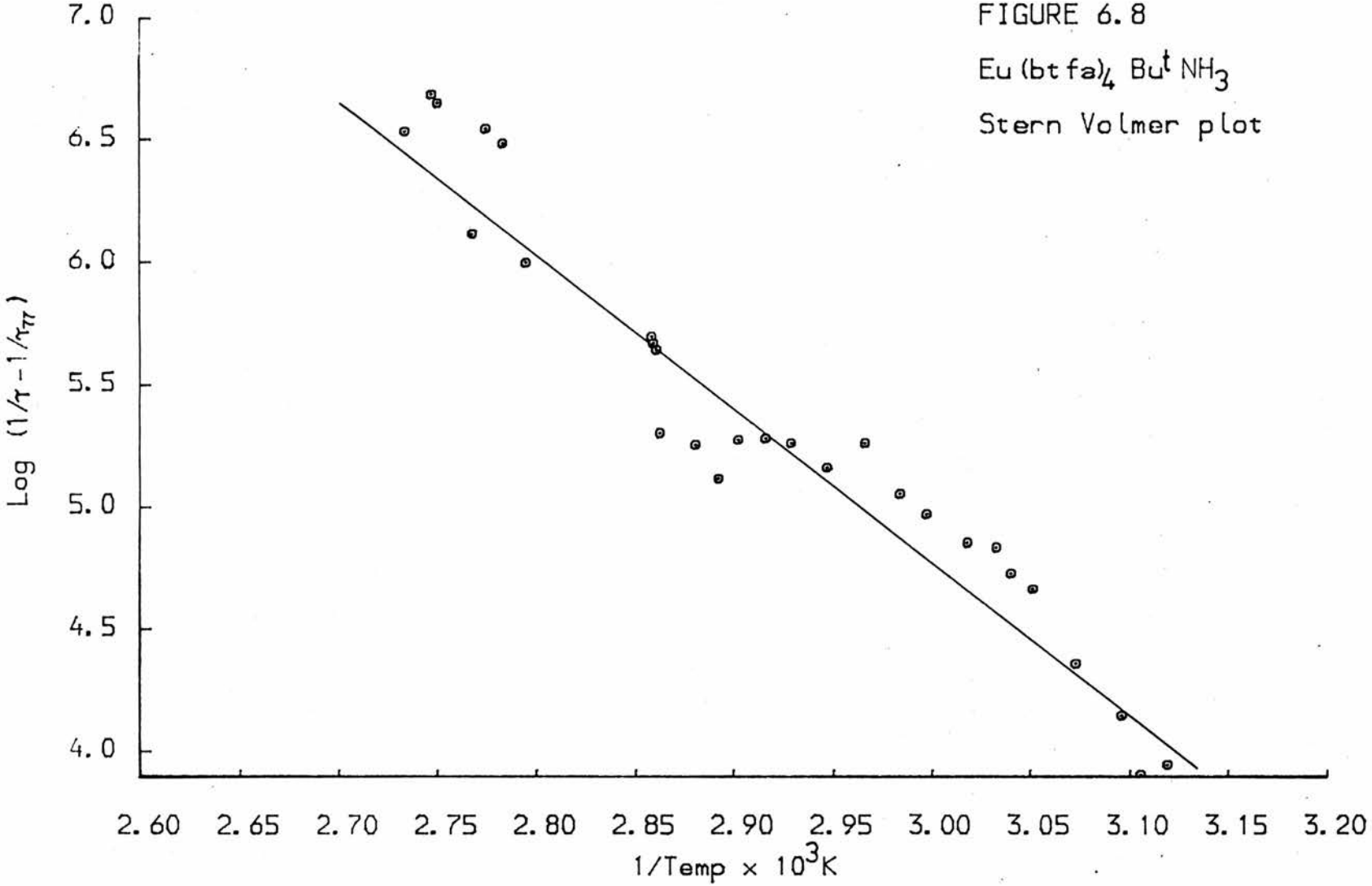

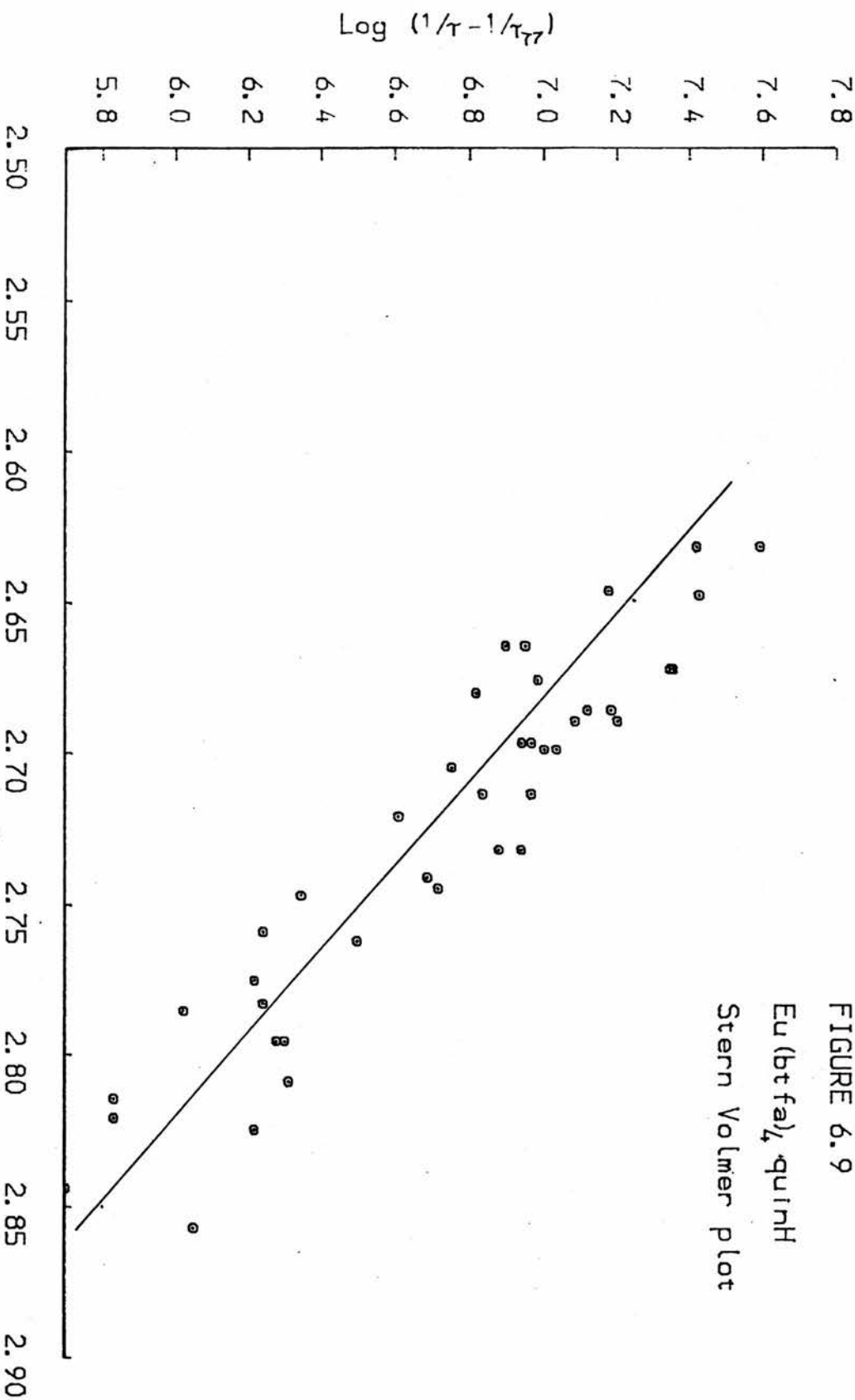

FIGURE 6.9

$Eu(btfa)_4$ quinH

Stern Volmer plot

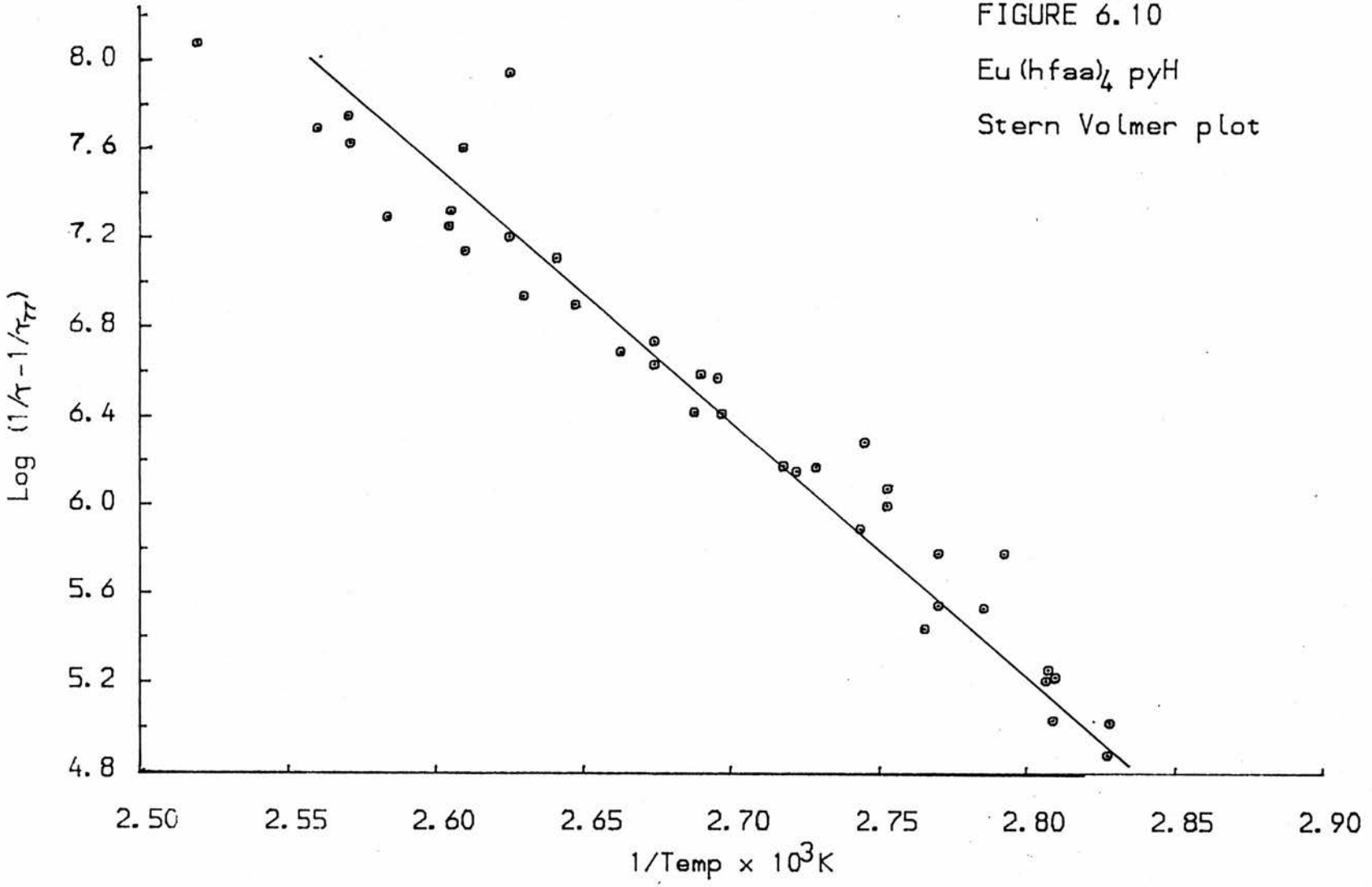

FIGURE 6.10

Eu(hfaa)$_4$ pyH

Stern Volmer plot

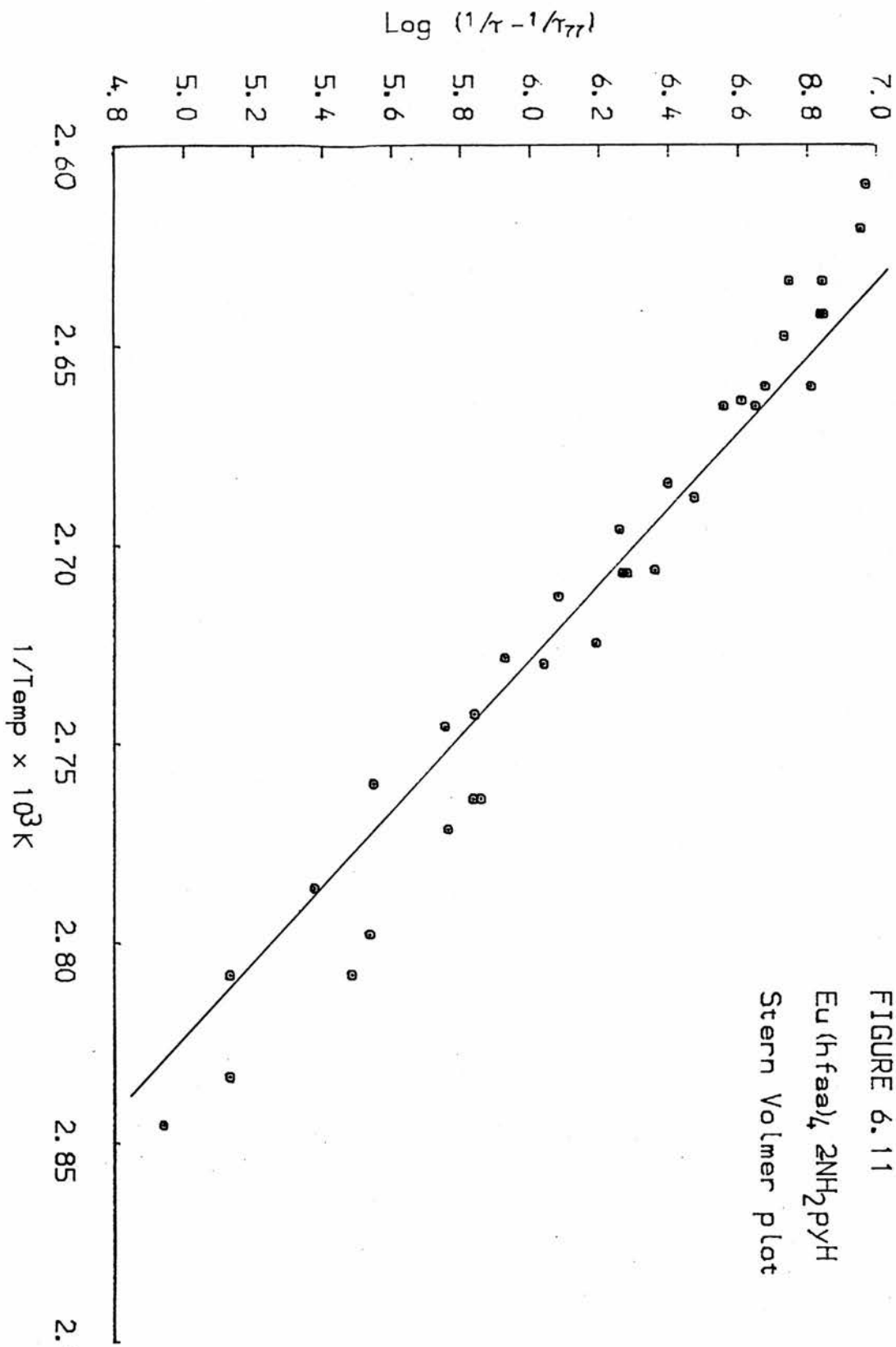

FIGURE 6.11

Eu (hfaa)$_4$ 2NH$_2$pyH

Stern Volmer plot

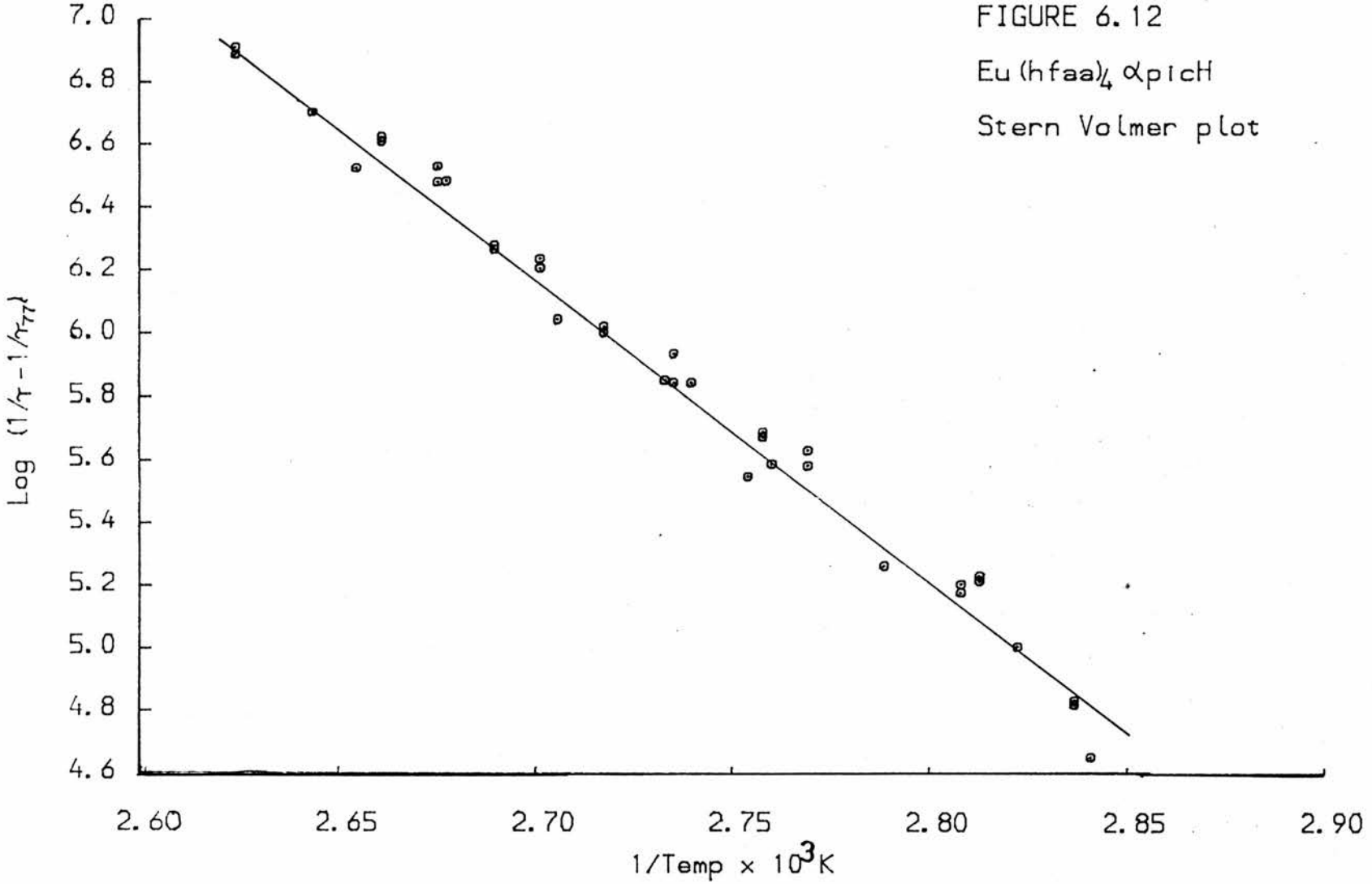

FIGURE 6.12

Eu (hfaa)$_4$ αpicH

Stern Volmer plot

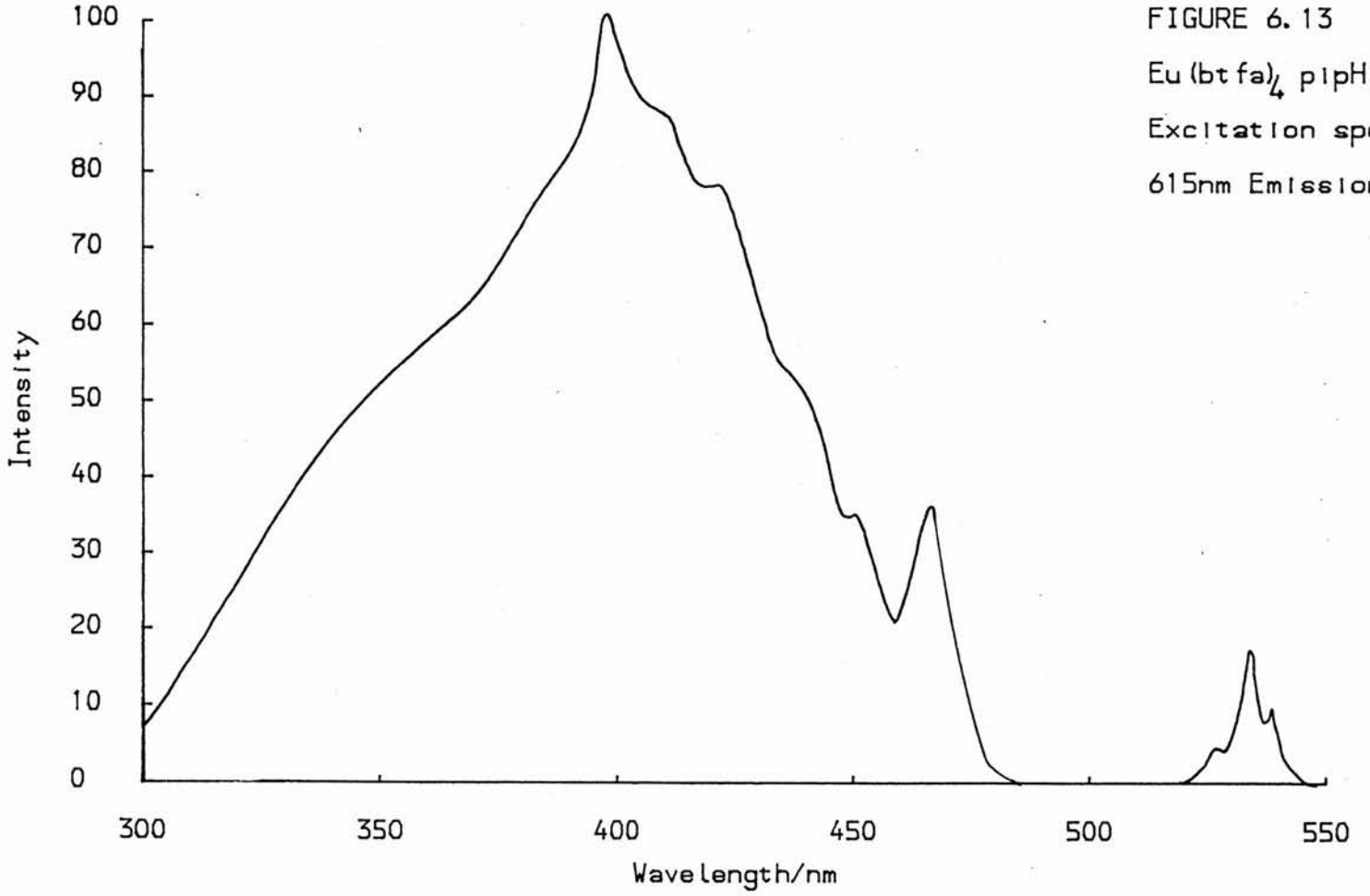

FIGURE 6.13

$Eu(btfa)_4$ pipH

Excitation spectrum

615nm Emission

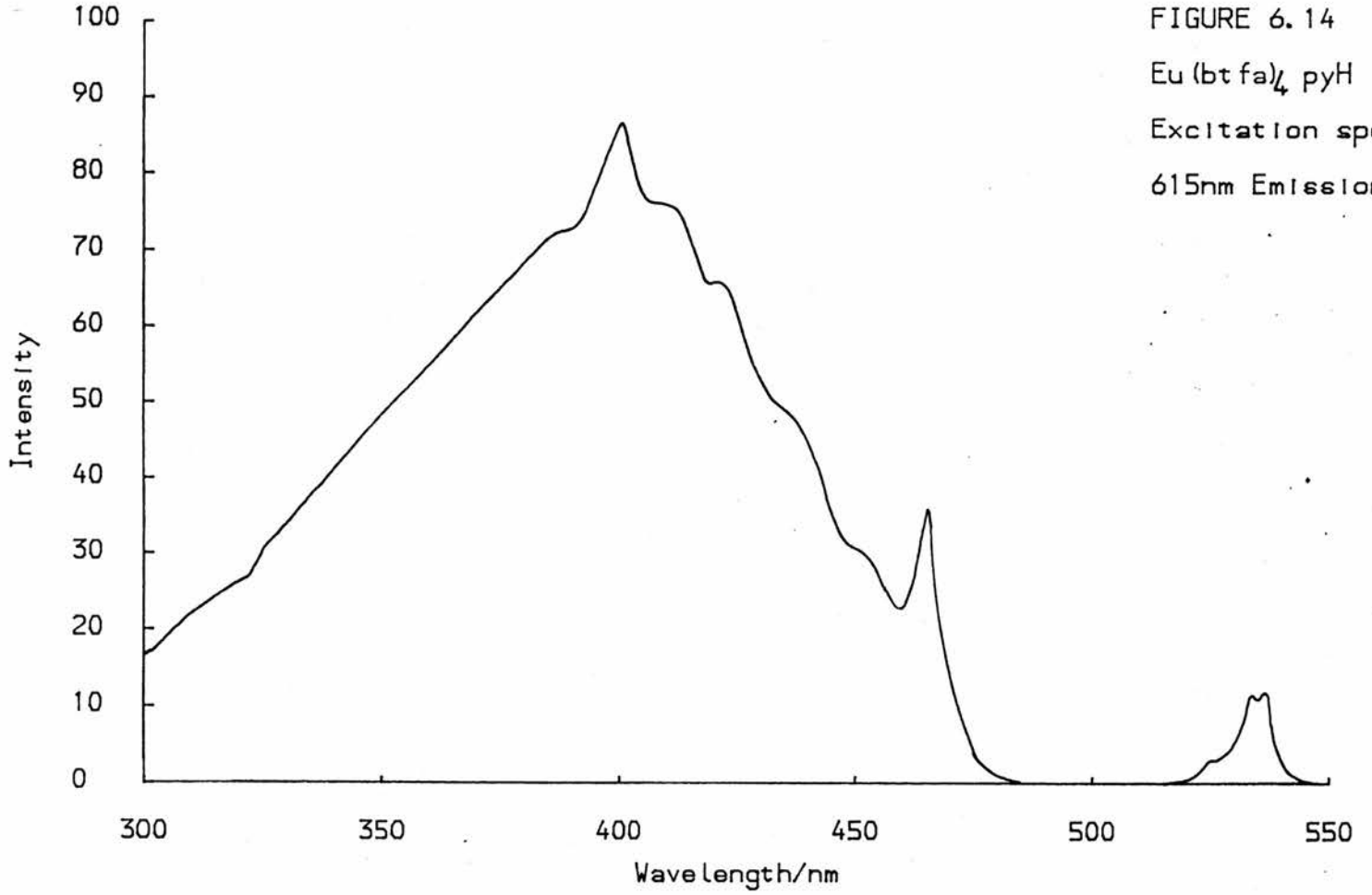

FIGURE 6.14

$Eu(btfa)_4 pyH$

Excitation spectrum

615nm Emission

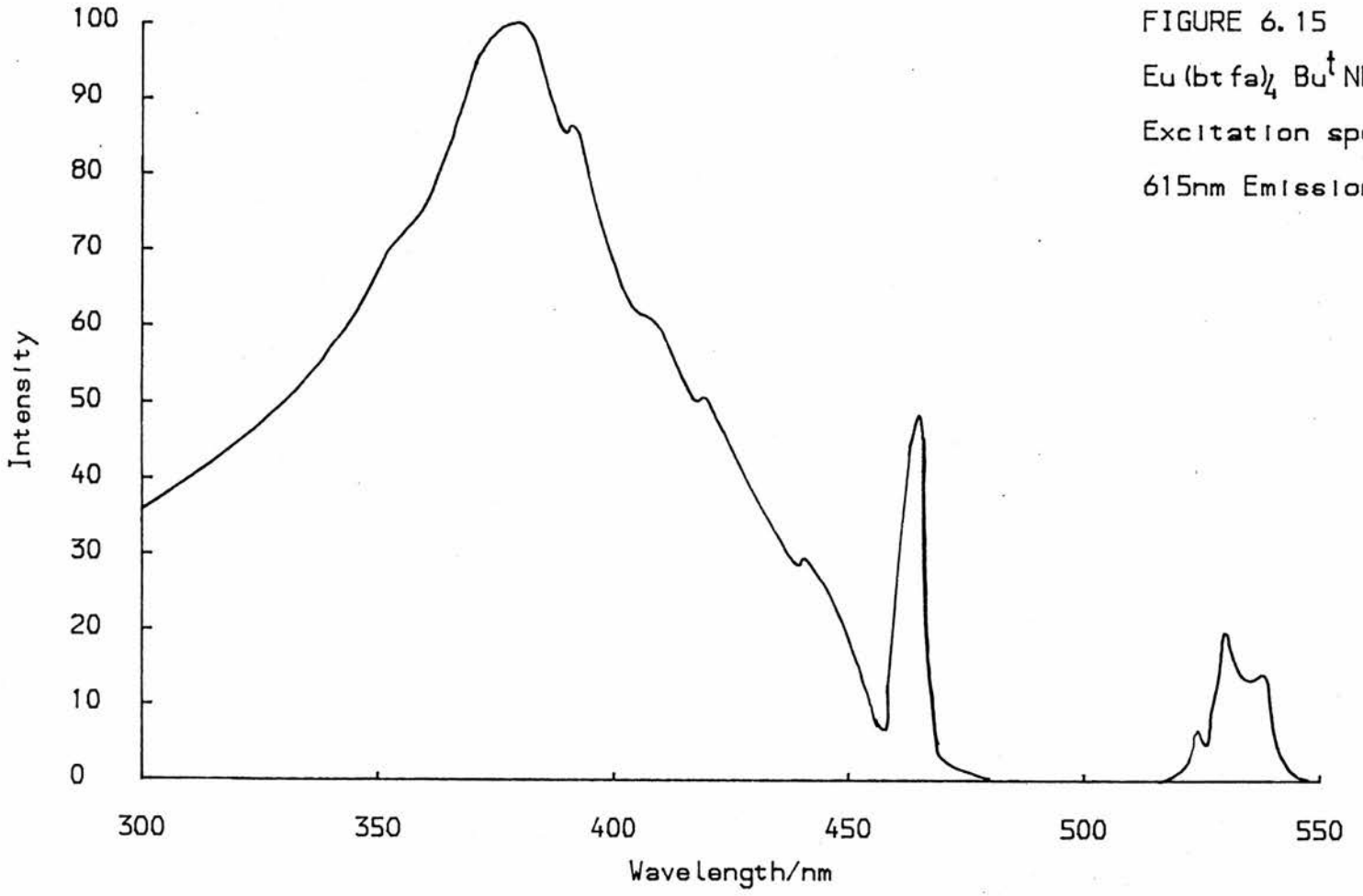

FIGURE 6.15

$Eu(btfa)_4\ Bu^tNH_3$

Excitation spectrum

615nm Emission

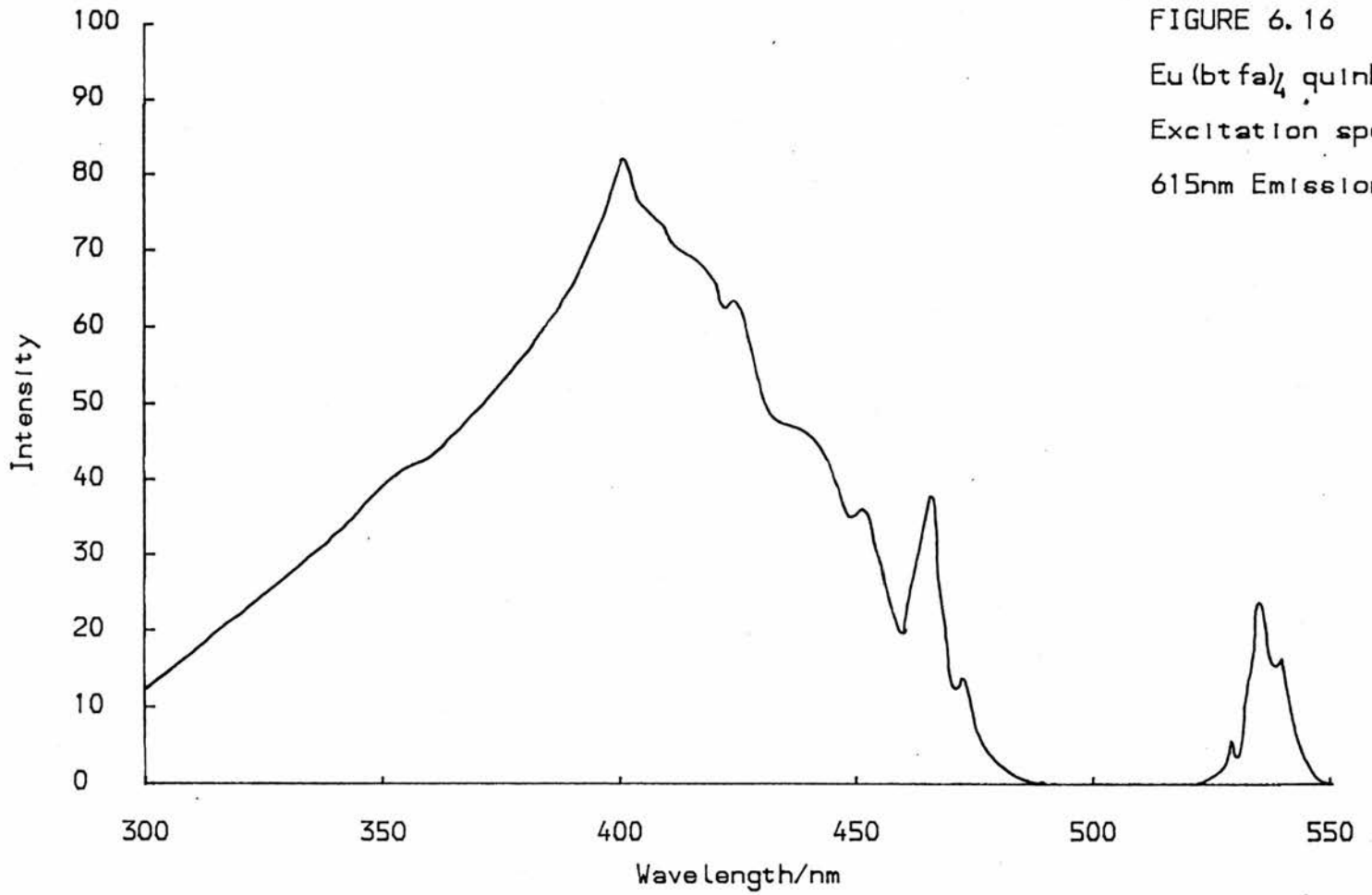

FIGURE 6.16

$Eu(btfa)_4$ quinH

Excitation spectrum

615nm Emission

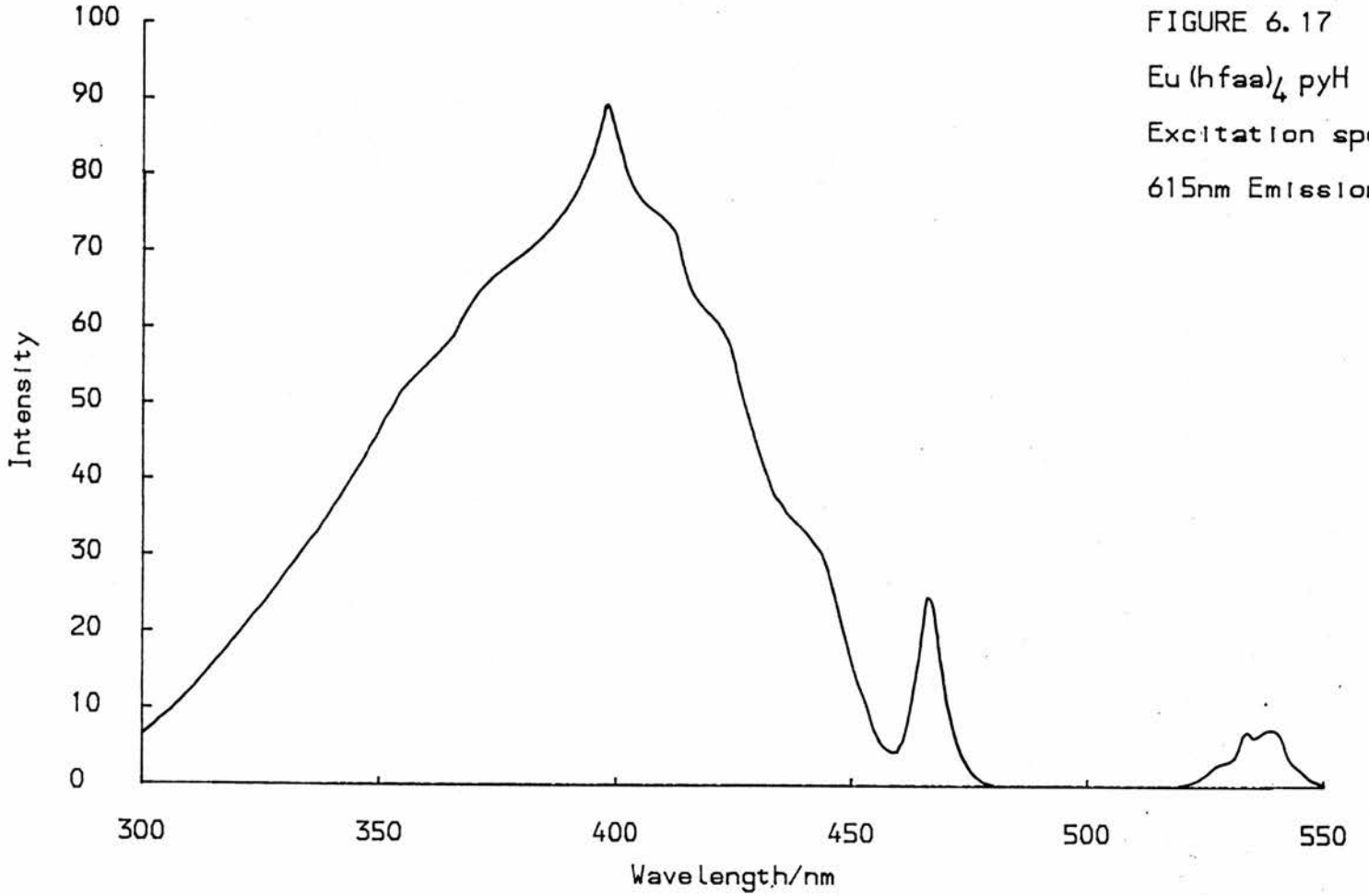

FIGURE 6.17

$Eu(hfaa)_4$ pyH

Excitation spectrum

615nm Emission

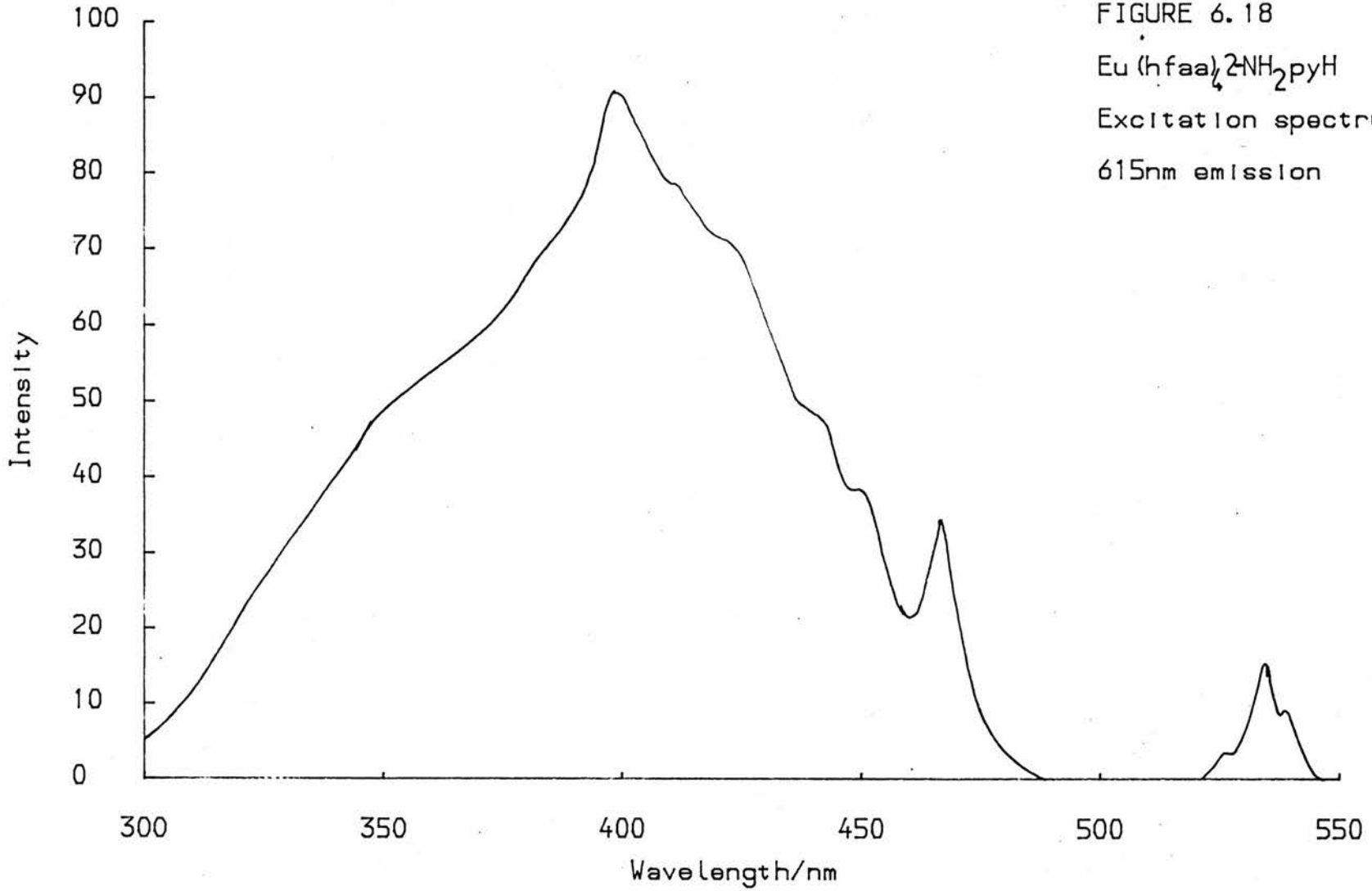

FIGURE 6.18

$Eu(hfaa)_4 2NH_2pyH$

Excitation spectrum

615nm emission

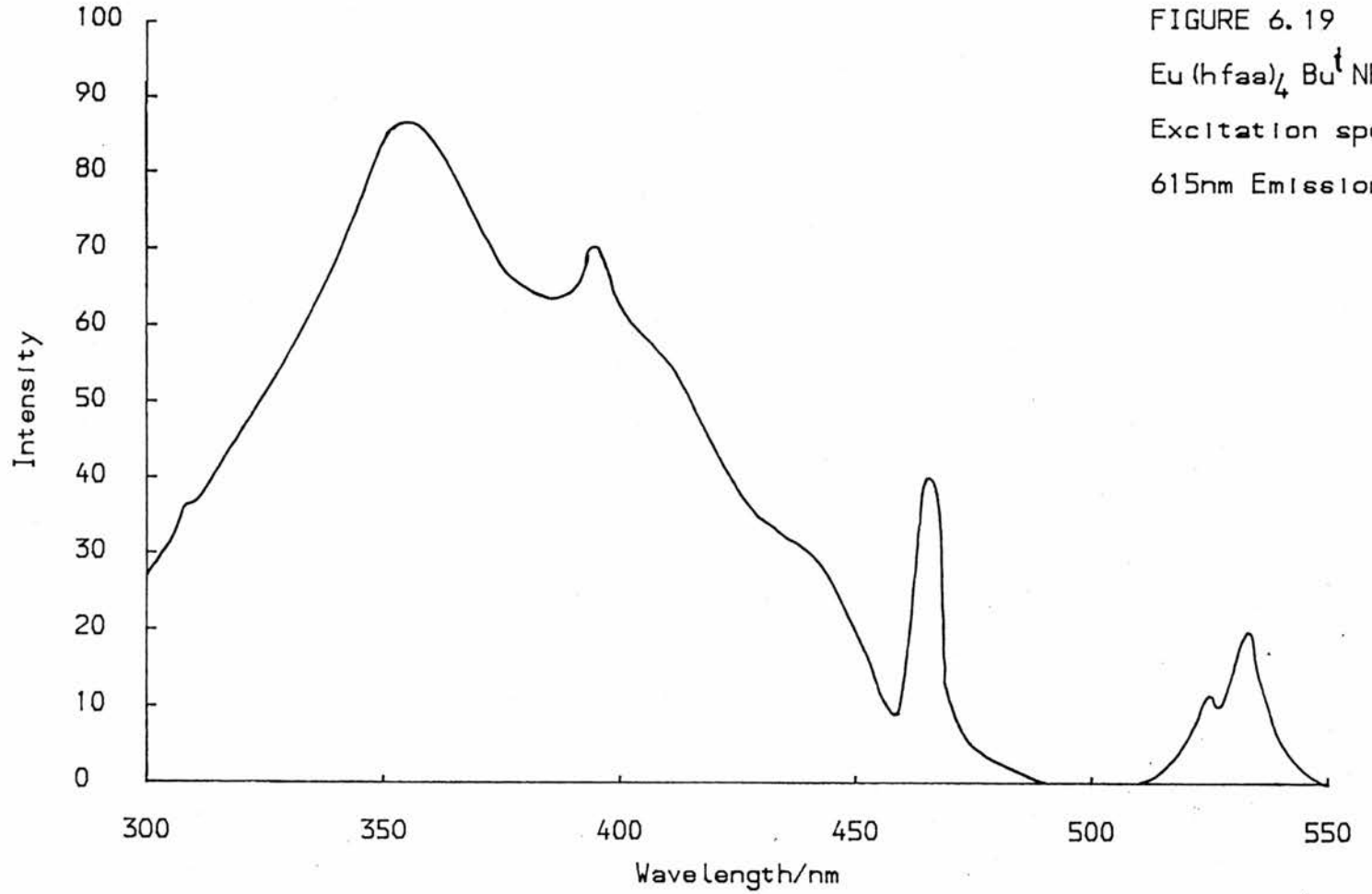

FIGURE 6.19

$Eu(hfaa)_4\ Bu^tNH_3$

Excitation spectrum

615nm Emission

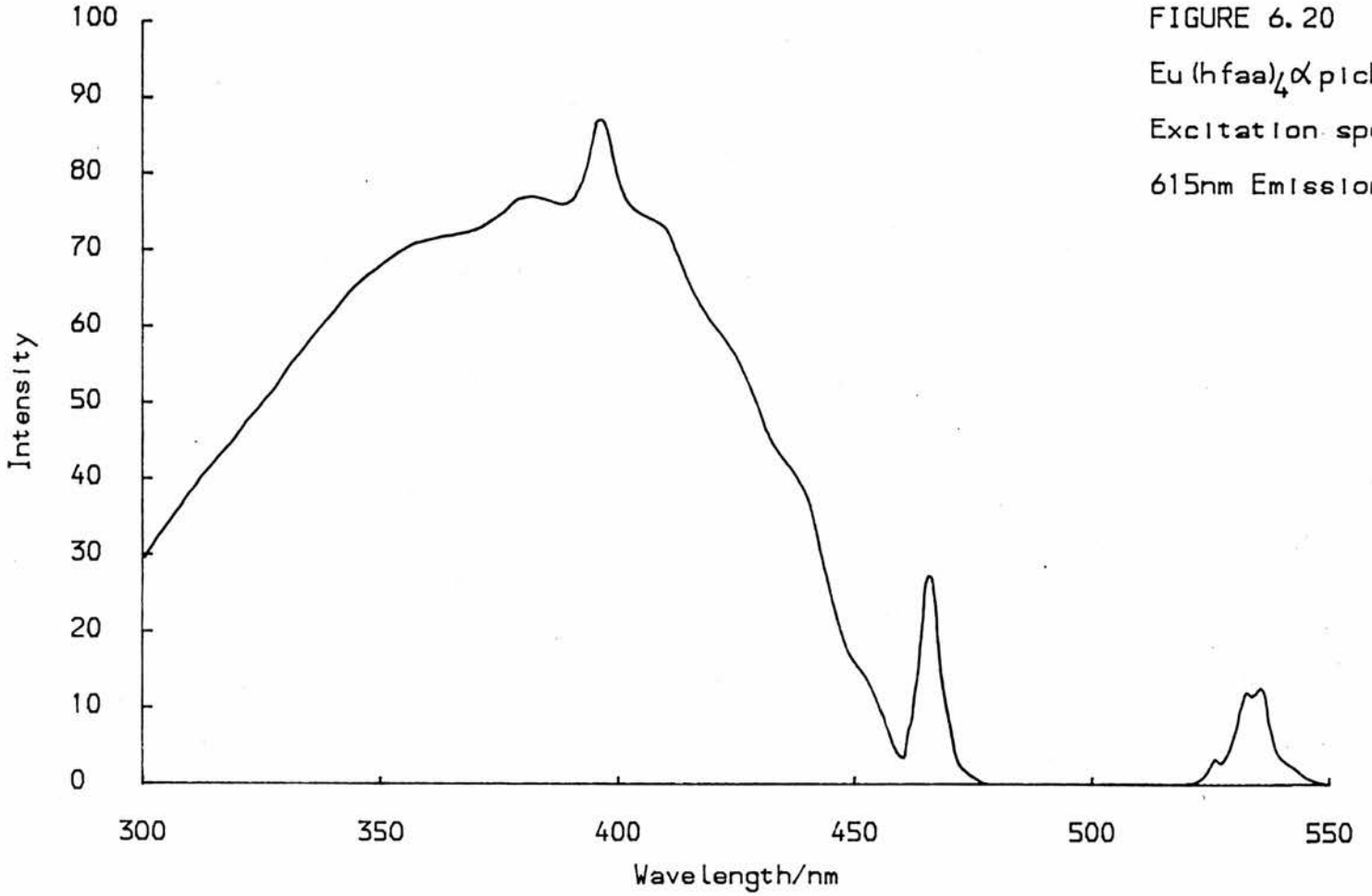

FIGURE 6.20

$Eu(hfaa)_4\alpha picH$

Excitation spectrum

615nm Emission

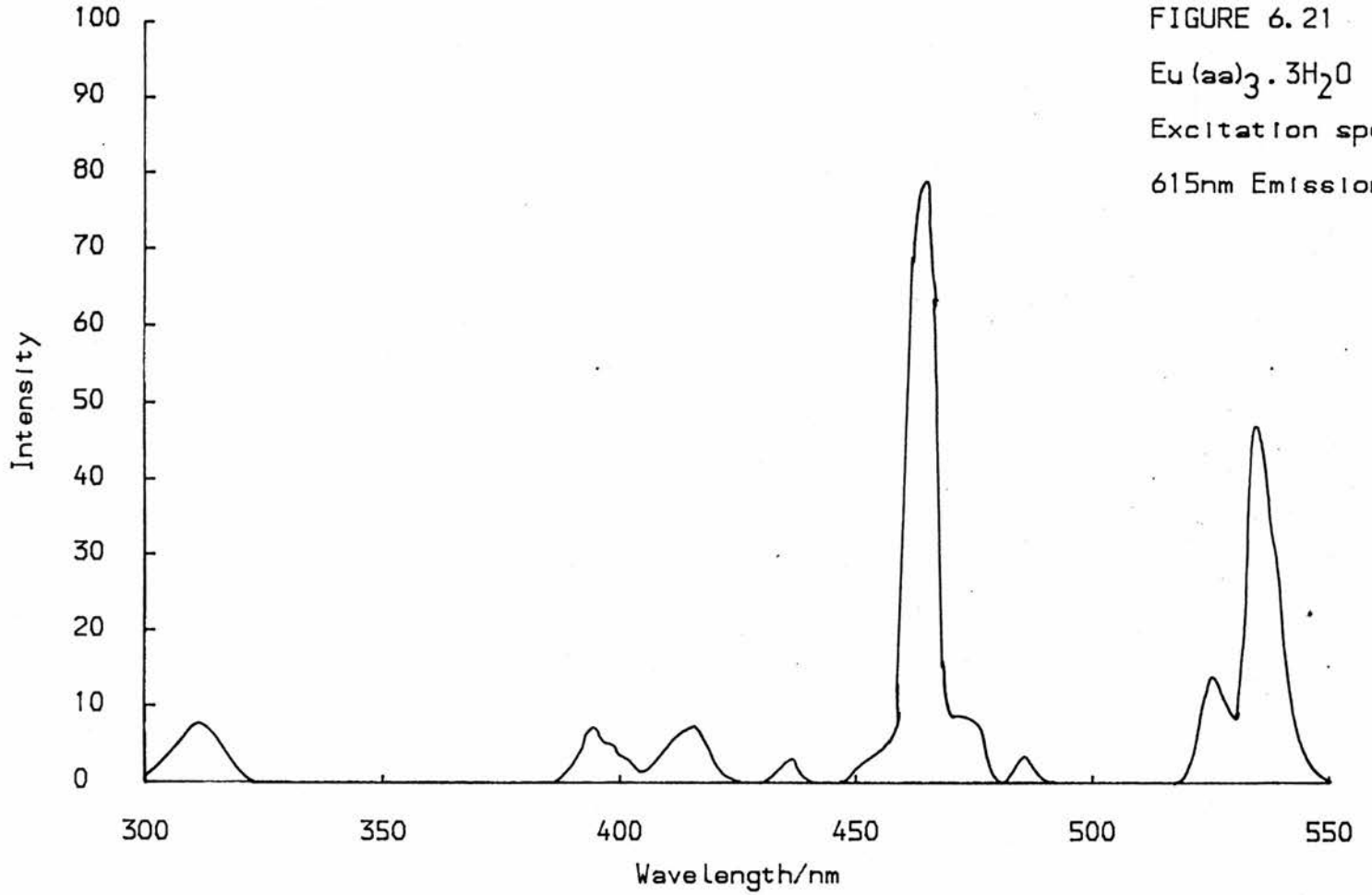

FIGURE 6.21

$Eu(aa)_3 . 3H_2O$

Excitation spectrum

615nm Emission

Excitation spectra of the ^5D_o ---> $^7F_2$ transition in the Eu^{3+} ion of several chelates with btfa and hfaa ligands were recorded and they all show strong sensitized emission via absorption to the ligand which is in the 350-450nm region (Figures 6.13 - 6.20). In contrast the emission from $Eu(aa)_3 3H_2O$ is much weaker as there is no excitation of the europium from the ligand, Figure 6.21.

The lifetime of the europium phosphorescence in $EuCl_3$ and $Eu(aa)_3 3H_2O$ were found to be temperature independent up to 400K at 0.13 and 0.3ms respectively.

Discusssion

Phosphorescence lifetimes have been shown to be temperature dependent in several lanthanide chelates, particularly those of Tb^{3+} and Eu^{3+}.[106-108]

Shepherd et al.,[107] observed temperature dependence of the $^5D_4$ emission in tris and tetrakis chelates of Tb^{3+}, between 77 and 323K, and attributed this to back donation of the energy to a low-lying triplet level in the ligand. Analogous back donation in Eu^{3+} chelates was discounted by Dawson et al.,[108] because the ^5D_o emitting level in europium is some $60kJmol^{-1}$ lower than the $^5D_4$ emitting level in terbium (see Figure 6.1). There have, however, been reports of thermal depopulation of the ^5D_o; to the $^5D_2$ level in some simple Eu^{3+} salts[109,110] and to the ligand triplet in the case of $Eu(hfaa)_4Bu^tNH_3$.[106]

From Table 6.2 it can be seen that the activation energies calculated from the experimental data fall into two categories:-

1. $\Delta E > 70kJmol^{-1}$, this includes $Eu(btfa)_4pipH$, $Eu(btfa)_4pyH$, $Eu(hfaa)_4pyH$, $Eu(hfaa)_4 2NH_2pyH$ and $Eu(hfaa)_4$ picH.

2. $\Delta E < 60 kJmol^{-1}$ which includes $Eu(btfa)_4 quinH$, $Eu(btfa)_4 Bu^t NH_3$ and $Eu(hfaa)_4 Bu^t NH_3$.

Exponential decay of the phosphorescence at all temperatures up to 400K suggests that the depopulation of the ^5D_o level takes place by a first order energy transfer process and evidence for the participation of the ligand energy levels as acceptors in the depopulation process arises from the excitation spectra and lifetimes of the ^5D_o emission in $Eu(aa)_3 3H_2O$ and $EuCl_3$. The absence of sensitized metal ion emission in both species and the temperature independent phosphorescence lifetimes up to 400K, suggests that the higher Eu^{3+} levels are not being populated to a significant extent below 400K. The inference from this is that the europium levels above the ^5D_o are unlikely to be involved in the thermally activated energy transfer process in the tetrakis chelates.

When considering possible acceptor levels in the ligand it must be pointed out that the ligand triplet levels have been shown to vary in the lanthanide chelates depending on their particular environments.[111] This variation is of the order of 5% and average values have been estimated for btfa[108] and hfaa[111] ligands at ca. $250 kJmol^{-1}$ and $262 kJmol^{-1}$ respectively and these values are used in the following discussion. The ^5D_o level in Eu^{3+} has been estimated at $208 kJmol^{-1}$.

A very good linear relationship between 1/T and $\log (\frac{1}{\tau} - \frac{1}{\tau_{77}})$ (Figures 6.6-6.12) implies that the energy transfer is predominantly to a single energy level. Transfer to the ligand triplet level would require an activation energy of ca. $42 kJmol^{-1}$ in btfa chelates and ca. $54 kJmol^{-1}$ in hfaa chelates and from Table 6.3 it can be seen that in the second category of chelates the activation energies are

consistent, within experimental error, with depopulation from the ^5D_o to the ligand triplet level.

chelate	$\Delta E + {}^5D_o$ /kJmol^{-1}
$Eu(btfa)_4pipH$	280.7
$Eu(btfa)_4pyH$	281.4
$Eu(hfaa)_4pyH$	291.6
$Eu(hfaa)_4 2NH_2pyH$	282.1
$Eu(hfaa)_4{}^{\alpha}picH$	285.5
$Eu(btfa)_4quinH$	268.0
$Eu(btfa)_4Bu^tNH_3$	253.1
$Eu(hfaa)_4Bu^tNH_3$	250.6

Table 6.3. $\Delta E + {}^5D_o$ (208kJmol^{-1})

The chelates in the first category, however, all have activation energies which require acceptor levels of significantly higher energy than the ligand triplet.

Although solid state excitation spectra are often misleading because of reflectance problems general information can be readily obtained. Reflectance can be cut down by mixing the solid sample with a non-reflecting solid such as NaCl and the spectra recorded by this method confirmed the general shape shown in Figures 6.13 - 6.20.

Although there is much dispute about the energy level which is

ultimately responsible for energy transfer to the metal ion there is agreement about the initial absorption to the ligand excited singlet state. This absorption appears in the excitation spectra as a broad band centred at ca. 400nm and indicates that the thermal deopoulation of the ^5D_o level to the ligand singlet would require an activation energy of ca. 72kJmol^{-1}.

Table 6.3 shows that the chelates in category one have activation energies which are consistent, within experimental error, with ^5D_o ---> S_1 transfer.

In the Arrhenius equation pre-exponential factors can be used to give an indication of the rate of the energy transfer process.[108] Shepherd et al., showed that in Tb^{3+} chelates the pre-exponential factors for the thermal deactivation of the $^5D_4$ to the ligand triplet varied between 10^4 and $10^7 s^{-1}$ and in $Eu(hfaa)_4Bu^tNH_3$[106] it was calculated to be 10^6 s^{-1}.

Table 6.2 shows that the pre-exponential factor for the chelates in the second category are of the same order as above and hence are consistent with having a ligand triplet level as the acceptor.

As with the activation energies, category one chelates show a higher pre-exponential factor those in category two. This indicates that the depopulation process in these chelates is faster than back donation to the ligand triplet state.

Energy transfer from the ligand leading to europium ion excitation has been estimated to have a rate which is slower than S_1 ---> T_1 inter-system crossing[102] whereas transfer from the ligand singlet has been shown to occur at a faster rate.[105] This implies that the transition probability for the S_1 ---> Eu^{3+} transition is greater than for the T_1 ---> Eu^{3+} transition and since the transition

probabilities are likely to be of the same order in excitation and back donation a faster rate would be expected for the process involving transfer to the ligand singlet.

If depopulation of the ^5D_o level is through the excited levels in the ligand then some variation in the activation energies and pre-exponential factors of the different chelates is inevitable because of the changes in the environment of the ligand and the resulting differences in the energy levels. Taking this variation into account the results in Table 6.2 show that generally the activation energies are lower in the btfa complexes than the hfaa complexes which is expected since the relevant energy levels are lower in btfa ligands than in hfaa ligands.

Further variation in activation energies of chelates with the same ligand, appears to be caused by the nature of the cation e.g. $Eu(btfa)_4pipH$ and $Eu(btfa)_4pyH$. The variations caused by the cation are not unexpected in the solid state since the arrangement of the ligands bonded to the europium ion is dependent on the nature of the crystal packing and this is affected by the size and shape of the cation.

Conclusions

The temperature dependence of the lifetime of the ^5D_o emitting level in europium chelates with btfa or hfaa ligands has been explained by thermal depopulation of the ^5D_o which takes place through the excited levels of the ligand.

The mechanism of this process has been shown to be dependent upon the nature of the ligand and the cation and may employ either the singlet or triplet level of the ligand.

The participation of the ligand singlet in the depopulation of the europium ion suggests that the excitation process may not be restricted to energy transfer from the ligand triplet but could also involve transfer from the excited singlet depending upon the nature of the ligand and the cation.

REFERENCES

1. R.P. Wayne. "Photochemistry". Butterworth, England, (1970)

2. C.A. Parker. "Photoluminescence of Solutions". Elsevier, England, 1968.

3. J.G. Calvert, J.N. Pitts Jnr. "Photochemistry" John Wiley & Sons N. York (1966)

4. G. Cario, K. Franck. Z.Physik. 1922,17, 202

5. J. Perrin, M. Choncroun. Compt. Rend. 1927,184,1097

6. J. Perrin, M. Choncroun. Compt. Rend. 1929,189,1213

7. A. Terenin, E. Putzeiko, I. Akimov. Disc. Farad. Soc. 1959,83,27.

8. J.E. Lennard-Jones. Trans. Farad. Soc. 1929,25,668

9. T. Forster. Z. Electrochem. 1952,56,716

10. D.L. Dexter. J. Chem. Phys. 1953,21,836

11. Kutsenova, Karputkhin. Vyosokomol. Soedin., Ser. B 1977, 19(5),334

12. W.H. Melhuish. Trans. Farad. Soc. 1966,62(2),3384

13. A.C. Newns. Trans. Farad. Soc. 1963,59,2153

14. G. Oster, G. Oster. "Luminescence of Organic and Inorganic Materials". ed. H.P. Kallman, G.M. Spruch 1962 N. York John Wiley & Sons.

15. R.E. Kellog. J. Chem. Phys. 1964,41,3046

16. R.F. Reid, I. Soutar. J. Polym. Sci; Polym. Phys. ed. 1978, 16,231

17. R.F. Cozzens, R.B. Fox. J. Chem. Phys. 1969,50,1532

18. J.R. MacCallum. Eur. Polym. J. 1981,17(3),209

19. R.B. Fox, T.R. Price, R.F. Cozzens, W.H. Echols. Macromolecules 1974,7(6),937

20. A. Terenin. Acta. Physiochem. 1943,18,210

21. G.N. Lewis, M. Kasha. J. Am. Chem. Soc. 1944,66,2100

22. D.S. McClure. J. Chem. Phys. 1949,17,905

23. J.C. Miller, J.S. Meek, S.J.Stickler. J. Am. Chem. Soc. 1977,99(25),8175

24. A. Jablonski. Z. Physik. 1935,38,94

25. C.A. Parker. Adv. Photochem. 1964,2,305

26. C.A. Parker, C.G. Hatchard. Trans. Farad. Soc. 1955,59,977

27. A.A. Lamola, G.S. Hammond. J. Chem. Phys. 1963,43,2129

28. R. Borkman, D. R. Kearns. Chem. Commun. 1966,14, 446

29. R. LaFara. "Computer Methods for Science and Engineering" Intertext, London 1973 p153.

30. M.A. West, K.J. McCallum, S.J. Formoshino, R.J.Woods. Trans. Farad. Soc. 1970,66,2135

31. F. El-Sayed, J.R. MacCallum, P.J. Pomery, T.M. Shepherd J. Chem. Soc., Farad. Trans. II 1979,75,79

32. M.B. Ledger, G. Porter. J. Chem. Soc. Farad. Trans. I. 1972,68,539

33. M. Berger, E. McAlpine, C. Steel. J. Am. Chem. Soc. 1978,100(16),5147

34. D.M. Mahoney. Int. Diss. Abs.(B) 1974

35. R.N. Graffin. Photochem. Photobiology. 1968,7,175

36. N.E. Geacintov, G. Oster, T. Cassen. J. Opt. Soc. Am. 1968,58,1217

37. P.F. Jones, S. Siegel. J. Chem. Phys. 1969,50,1134

38. B. Muel. Compt. Rend. 1962,225,3149

39. P. Pringsheim. "Fluorescence and Phosphorescence" Interscience N. York 1949. p295

40. A.C. Albrecht. Prog. Reaction Kinetics 1970,5,301

41. S. Kato, M. Koizumi. Bull. Chem. Soc. Jpn. 1957,30,27

42. G. Lisenko, G Kislyak. Ukr. Fiz. Zh. 1964,9(2),160

43. V. Pilipovitch, B. Svenshnikov. Soviet Phys. Doklady 1958,3,286

44. R.J. Abraham, H.W. Melville, D.W. Overnall, D.H. Whiffen. Trans. Farad. Soc. 1958,54,1133

45. A.H. Kalantar. J. Chem. Phys. 1968,72,2801

46. T. Azumi, S.P. McGlynn. J. Chem. Phys. 1963,38,2277

47. T. Azumi, S.P. McGlynn. J. Chem. Phys. 1963,39,1186

48. Tai-Shang Fang, L.A. Singer. Chem. Phys. Lett. 1978-79,60,117

49. V.L. Ermolaev. Uspekhi. Fiz. Nauk. 1963,3,80 (Eng)

50. W.E. Graves, R.H. Hofeldt, S.P. McGlynn. J. Chem. Phys. 1972,56(2),1309

51. J.L. Kropp, W.R.Dawson. J. Chem. Phys. 1967,71,4499

52. A.N. Jassim, J.R. MacCallum, T.M. Shepherd. Eu. Polym. J. 1981,17,125

53. T. Nakahira, S. Ishizuka, S. Iwabuchi, K. Kojima Macromol. Chem. Rapid. Commun. 1980,1(12),759

54. F. El-Sayed. Ph.D. Thesis 1979

55. A.M. Avdeenko, T.L. Dobrovoskaya, V.A. Kultchitsky, Yu.V. Naboikin, S.N. Patulov. J. Luminescence 1976,11,331

56. J.A. Bell, M. Berger, C. Steel. Chem. Phys. Lett. 1974,28(2),205

57. P.F. Jones, A.R. Calloway. J. Am. Chem. Soc. 1970,92,4497

58. P.F. Jones, A.R. Calloway. Chem. Phys. Lett. 1971,10(4),438

59. A. Beckett, G. Porter. Trans. Farad. Soc. 1963,59,2039

60. J.C. Scaiano. J. Photochem. 1973,2,81

61. M.W. Wolf, K.D. Legg, R.E. Brown, L.A. Singer, J.H. Parks J. Am. Chem. Soc. 1975,97,4490

62. J. Chilton, L.Giering, C. Steel. J. Am. Chem. Soc. 1976,98(7),1865

63. T.S. Godfrey. J.W. Hilpern, G. Porter. Chem. Phys. Lett. 1967,1,490

64. J.N. Pitts, R.L. Letsinger, R.P. Taylor, J.M. Patterson, G. Reckenwald, R.P. Martin. J. Am. Chem. Soc. 1959,81,1068

65. A. Becket, G. Porter. Trans. Farad. Soc. 1963,59,2039

66. G. Ciamiciam, P. Silber. Chem. Ber. 1900,33,2911

67. W.M. Moore, G.S. Hammond, R.P. Foss. J. Am. Chem. Soc. 1961,83,2798

68. G.S. Hammond, W.P. Baker, M.W. Moore. J. Am. Chem. Soc. 1961,83,2795

69. W.E. Backman. "Organic Synthesis" Vol II, Wiley N. York 1948. p71

70. G. Porter, M. Windsor. Mol. Spectroscopy 1955,6

71. G. Porter, M. Windsor. Proc. Roy. Soc. 1958,A245,238

72. G. Porter, F. Wilkinson. Trans. Farad. Soc. 1961,57,1686

73. D. McClure, P. Hanst. J. Phys. Chem. 1955,23,1772

74. N. Filipescu, F.L. Minn. J. Am. Chem. Soc. 1968,90,1544

75. G.O. Schench, M. Cziesla, K. Eppinger, G. Mathias, M. Pape Tett. Lett. 1967,193

76. P.J. Wagner. Mol. Photochem. 1969,1,71

77. S.G. Cohen, J.I. Cohen. Isr. J. Chem. 1968,6,757

78. Chr. Bräuchle, D.M. Burland, G.G. Bjorklund.
J. Phys. Chem. 1981,85(2),123

79. T-S. Fang, R.E. Brown, L.A. Singer. J. Chem. Soc. Chem. Commun.
1978,3,116

80. T-S. Fang, R.E. Brown, L.A. Singer. J. Phys. Chem.
1978,82(23),2489

81. D.J. Morantz, A.J.C. Wright. J. Chem. Phys. 1971,54(2),692

82. A.C. Somersall, E. Dan, J.E. Guillet. Macromolecules
1974,7,233

83. T.J. Chow. Ph.D. Thesis. Univ. Microfilms Int. 8016376

84. S.A. Carlson, D.M. Herculese. Photochem. Photobiol.
1973,17,123

85. S.A. Carlson, D.M. Herculese. Anal. Chem. 1973,45(11),1794

86. S.A. Carlson, D.M. Herculese. Anal. Chem. 1974,46,674

87. K. Tickle, F. Wilkinson. Trans. Farad. Soc. 1965,61,1981

88. H.H. Dearman. A. Chan. J. Chem. Phys. 1966,44(1),416

89. J.H. Sharp, T. Kuwana, A. Osborne, J.N. Pitts Jnr.
Chem. and Ind. 1962,508

90. U. Deffer, E. Brunner. Z. Phys. Chem. (Frankfurt am Main)
1966,51(5-6),290

91. J.B Farmer, C.L. Gardner, C.A. McDowell. J. Chem. Phys. 1961,34,1058

92. R.J. Forster. Coord. Chem. Rev. 1973,10,195

93. T. Moeller, D.F. Martin, L.C. Thompson, R. Ferrus, G.R. Feistel
W.J. Randall. Chem. Rev. 1965,65,1

94. D. Gibson, J. Lewis, C. Oldam. J. Chem. Soc. (A) 1966,1453

95. S.I. Wiessman. J. Chem. Phys. 1942,10,214

96. G.A. Crosby, R.E. Whan, J.J. Freeman. J. Phys. Chem.
1962,66,2493

97. R.F. Charles, E.P. Reidel. J. Inorg. Nucl. Chem. 1967,29,715

98. L.R. Melby, N.J. Rose, E. Abramson, J.C. Caris. J. Am. Chem. Soc. 1964,86,5117

99. H. Bauer, J. Blanc, D.L. Ross. J. Am. Chem. Soc. 1964,86,5125

100. N. Filipescu, W.F. Sager, F.A. Serafin. J. Phys. Chem. 1965,69,1092

101. M. Kleinerman. J. Chem. Phys. 1969,51,2307

102. Tanaka, Yamaguchi, Shiokawa, Yamanka. Bull. Chem. Soc. Jpn. 1970,43,549

103. M.L. Bhaumik, M.A. El-Sayed. J. Chem. Phys. 1965,42,787

104. S.J. Lyle, J.E. Newbery, A.D. Witts. J. Chem. Soc. Dalton 1972,1726

105. C.R.S. Dean, T.M. Shepherd. Chem. Phys. Lett. 1975,32(3),480

106. C.R.S. Dean, T.M. Shepherd. J. Chem. Soc. Farad. II 1975,71,146

107. T.D. Brown, T.M. Shepherd. J. Chem. Soc. Dalton 1972 , 1616

108. W.R. Dawson, J.L. Kropp, M.W. Windsor. J. Chem. Phys. 1966,45,2410

109. W.R. Dawson, J.L. Kropp. J. Opt. Soc. Am. 1965,55(7),822

110. W.R. Dawson, J.L. Kropp. J. Chem. Phys. 1966,45(7),2419

111. T.D. Brown, T.M. Shepherd. J. Chem. Soc. Dalton 1973 , 336

APPENDIX I. COMPUTER PROGRAM TRIP

```
10C     NON-EXPONENTIAL PHOSPHORESCENCE DECAY FITTING ROUTINES
20C             DOUBLE EXPONENTIAL KINETICS
30C               D.A.G. 10/12/1980
40C
50C
60C      DATA REQUIRED:- TITLE---20A4
70C                      SWEEP TIME IN SEC---F10.0
80C                      DATA----F8.0
90C                       0.0 MARKS END OF DATA
100C
110C
120     DIMENSION ITIT(20)
130     DIMENSION V(50),VC(50)
140     READ(2,30)ITIT
150 30 FORMAT(20A4)
160     READ(2,40)ST
170 40 FORMAT(F10.0)
180     ST=ST/40.0
190     DO 100 J=1,50
200     READ(2,50)V(J)
210 50 FORMAT(F8.0)
220     IF(V(J).EQ.0.0)GO TO 110
230     N=J-1
240 100 CONTINUE
250 110 CONTINUE
260C
270C
280C         TITLE, SWEEP TIME AND DATA READ
290C
300C
310     DO 140 J=1,N
320     VC(J)=EXP(V(J))
330 140 CONTINUE
340     WRITE(6,500)
350     WRITE(6,500)
360     WRITE(6,145)ITIT
370 145 FORMAT(20A4)
380     WRITE(6,148)
390 148 FORMAT("-----------------------------------",/)
400     WRITE(6,175)ST
410 175 FORMAT(1H ,"SPACING OF POINTS = ",E12.6,"S")
420     WRITE(6,150)
430 150 FORMAT(/,"DOUBLE EXPONENTIAL FITTING ROUTINE")
440     WRITE(6,160)
450 160 FORMAT("--------------------------------")
460     WRITE(6,170)
470 170 FORMAT("VALUE OF A")
480     READ(5,180)A
490 180 FORMAT(F5.0)
500     WRITE(6,200)
510 200 FORMAT("VALUE OF K1")
520     READ(5,210)W1
530 210 FORMAT(F7.0)
540     WRITE(6,220)
550 220 FORMAT("VALUE OF K2")
560     READ(5,230)W2
570 230 FORMAT(F7.0)
580     WRITE(6,240)
590 240 FORMAT(5X,"A",7X,"K1",10X,"K2",8X,"ERROR",/)
600C
```

```
610C
620C     TITLE WRITTEN, VALUES OF K1, K2, AND A READ
630C
640C
650      D=A
660      E=W1
670      F=W2
680      Z=VC(1)
690      WRITE(6,300)D,W1,W2,ER
700      DO 270 J=1,N
710      VC(J)=VC(J)/Z
720  270 CONTINUE
730  250 I=0
740  260 CONTINUE
750C
760C
770C       **FITTING ROUTINE**
780C
790C
800      S1=0.0
810      S2=0.0
820      S3=0.0
830      S4=0.0
840      S5=0.0
850      S6=0.0
860      F1=0.0
870      F2=0.0
880      F3=0.0
890      T=0.0
900      I=I+1
910      DO 280 J=1,N
920      YA=EXP(-E*T)-EXP(-F*T)
930      IF(T.NE.0.0) GO TO 290
940      YA=0.0
950  290 YB=-D*T*EXP(-E*T)
960      YC=(D-1.0)*T*EXP(-F*T)
970      DY=VC(J)-(D*YA+EXP(-F*T))
980      S1=S1+YA*YA
990      S2=S2+YA*YB
1000      S3=S3+YA*YC
1010      S4=S4+YB*YB
1020      S5=S5+YB*YC
1030      S6=S6+YC*YC
1040      F1=F1+YA*DY
1050      F2=F2+YB*DY
1060      F3=F3+YC*DY
1070      T=T+ST
1080 280 CONTINUE
1090      D1=S4*S6-S5*S5
1100      D2=S2*S6-S3*S5
1110      D3=S2*S5-S3*S4
1120      D4=S1*S6-S3*S3
1130      D5=S1*S5-S2*S3
1140      D6=S1*S4-S2*S2
1150      DH=S1*D1-S2*D2+S3*D3
1160      DD=(F1*D1-F2*D2+F3*D3)/DH
1170      DE=-(F1*D2-F2*D4+F3*D5)/DH
1180      DF=(F1*D3-F2*D5+F3*D6)/DH
1190      D=D+DD
1200      E=E+DE
```

```
1210     F=F+DF
1220     ER=ABS(DD/D)+ABS(DE/E)+ABS(DF/F)
1230     W1=E
1240     W2=F
1250     A=D
1260     WRITE(6,300)A,W1,W2,ER
1270 300 FORMAT(F8.2,2X,F8.3,2X,F10.3,2X,E12.6)
1280   * IF(ER.LT.0.000001)GO TO 370
1290     IF(I.LT.100)GO TO 260
1300     WRITE(6,500)
1310     WRITE(6,360)
1320 360 FORMAT("NO CONVERGANCE AFTER 100 ITERATIONS")
1330     GO TO 600
1340 370 WRITE(6,500)
1350     WRITE(6,380)I
1360 380 FORMAT("CONVERGANCE AFTER ",I3," ITERATIONS")
1370C
1380C
1390C      **END OF FITTING ROUTINE**
1400C
1410C
1420     WRITE(6,400)W1
1430 400 FORMAT(1H0,"K1= ",F10.4)
1440     WRITE(6,410)W2
1450 410 FORMAT(1H0,"K2= ",F10.4)
1460 500 FORMAT(/,/,/,/)
1470     WRITE(6,520)
1480 520 FORMAT(1H ,/,5X,"EXPT",8X,"CALC",4X,"%DIFF",7X,"EXPT(LN)",
1490    &2X,"CALC(LN)",3X,"%DIFF",/)
1500     T=0.0
1510     A=A*EXP(V(1))
1520     B=EXP(V(1))-A
1530     DO 550 J=1,N
1540     CALC=A*EXP(-W1*T)+B*EXP(-W2*T)
1550     CALG=ALOG(ABS(CALC))
1560     VLG=V(J)
1570     DIF=100.0*(EXP(V(J))-CALC)/EXP(V(J))
1580     DFLG=100.0*(VLG-CALG)/VLG
1590     T=T+ST
1600     Z1=EXP(V(J))
1610     WRITE(6,530)Z1,CALC,DIF,VLG,CALG,DFLG
1620 530 FORMAT(1H ,F10.2,1X,F10.2,2X,F9.5,3X,F7.4,3X,F7.4,3X,F9.5)
1630C
1640C
1650C       EXPERIMENTAL AND CALCULATED DATA WRITTEN
1660C
1670C
1680 550 CONTINUE
1690 600 STOP
1700     END
```

*

APPENDIX II. COMPUTER PROGRAM DEX

```
10C     NON-EXPONENTIAL PHOSPHORESCENCE DECAY FITTING ROUTINES
20C           TRIPLET-TRIPLET ANNIHILATION
30C              D.A.G. 10/12/1980
40C
50C
60C      DATA REQUIRED:- TITLE---20A4
70C                      SWEEP TIME IN SEC---F10.0
80C                      DATA ----F8.0
90C                       0.0 MARKS END OF DATA
100C
110C
120     DIMENSION ITIT(20)
130     DIMENSION V(50),VC(50)
140     READ(2,30)ITIT
150 30 FORMAT(20A4)
160     READ(2,40)ST
170 40 FORMAT(F10.0)
180     ST=ST/40
190     DO 100 J=1,50
200     READ(2,50)V(J)
210 50 FORMAT(F8.0)
220     IF(V(J).EQ.0.0)GO TO 110
230     N=J-1
240 100 CONTINUE
250 110 CONTINUE
260C
270C
280C       TITLE, SWEEP TIME AND DATA READ
290C
300C
310     DO 140 J=1,N
320     VC(J)=EXP(V(J))
330 140 CONTINUE
340     WRITE(6,500)
350     WRITE(6,500)
360     WRITE(6,145)ITIT
370 145 FORMAT(20A4)
380     WRITE(6,148)
390 148 FORMAT("-------------------------------------",/)
400     WRITE(6,170)ST
410 170 FORMAT(1H ,"SPACING OF POINTS = ",E12.6,"S")
420     WRITE(6,150)
430 150 FORMAT(/,"TRIPLET-TRIPLET ANIHLATION FITTING ROUTINE")
440     WRITE(6,160)
450 160 FORMAT("-----------------------------------------")
460     WRITE(6,200)
470 200 FORMAT("VALUE OF K1")
480     READ(5,210)W1
490 210 FORMAT(F7.0)
500     WRITE(6,220)
510 220 FORMAT("VALUE OF K2")
520     READ(5,230)W2
530 230 FORMAT(F7.0)
540     WRITE(6,240)
550 240 FORMAT(3X,"START",5X,"K1",10X,"K2",8X,"ERROR",/)
560C
570C
580C       TITLE PRINTED, INITIAL VALUES OF K1 AND K2 READ
590C
600C
```

```
      D=1/VC(1)
      WRITE(6,300)D,W1,W2,ER
  250 I=0
  260 CONTINUE
C
C
C        **FITTING ROUTINE**
C
C
      E=W2/W1
      F=W1
      S1=0
      S2=0
      S3=0
      S4=0
      S5=0
      S6=0
      F1=0
      F2=0
      F3=0
      T=0.0
      I=I+1
      DO 280 J=1,N
      YA=EXP(F*T)
      YB=YA-1
      YC=(D+E)*T*YA
      DY=(1/VC(J))-(((D+E)*YA)-E)
      S1=S1+YA*YA
      S2=S2+YA*YB
      S3=S3+YA*YC
      S4=S4+YB*YB
      S5=S5+YB*YC
      S6=S6+YC*YC
      F1=F1+YA*DY
      F2=F2+YB*DY
      F3=F3+YC*DY
      T=T+ST
  280 CONTINUE
      D1=S4*S6-S5*S5
      D2=S2*S6-S3*S5
      D3=S2*S5-S3*S4
      D4=S1*S6-S3*S3
      D5=S1*S5-S2*S3
      D6=S1*S4-S2*S2
      DH=S1*D1-S2*D2+S3*D3
      DD=(F1*D1-F2*D2+F3*D3)/DH
      DE=-(F1*D2-F2*D4+F3*D5)/DH
      DF=(F1*D3-F2*D5+F3*D6)/DH
      D=D+DD
      E=E+DE
      F=F+DF
      ER=ABS(DD/D)+ABS(DE/E)+ABS(DF/F)
      W1=F
      W2=E*F
      TA=1/D
      WRITE(6,300)TA,W1,W2,ER
  300 FORMAT(F8.2,2X,F9.3,2X,F10.6,2X,E12.6)
      IF(ER.LT.0.000001)GO TO 370
      IF(I.LT.100)GO TO 260
      WRITE(6,500)
```

```
      WRITE(6,360)
  360 FORMAT("NO CONVERGANCE AFTER 100 ITERATIONS")
      GO TO 600
  370 WRITE(6,500)
      WRITE(6,380)I
  380 FORMAT("CONVERGANCE AFTER ",I3," ITERATIONS")
C
C
C       **END OF FITTING ROUTINE**
C
C
      WRITE(6,400)W1
  400 FORMAT(1HO,"K1= ",F10.5)
      WRITE(6,410)W2
  410 FORMAT(1HO,"K2=",F10.6)
  500 FORMAT(/,/,/,/)
      WRITE(6,520)
  520 FORMAT(1H ,/,5X,"EXPT",8X,"CALC",4X,"%DIFF",7X,"EXPT(LN)",
     &2X,"CALC(LN)",3X,"%DIFF",/)
      T=0.0
      W3=W2/W1
      W4=1/TA+W3
      DO 550 J=1,N
      CALC=1/(W4*EXP(W1*T)-W3)
      CALG=ALOG(ABS(CALC))
      VLG=ALOG(ABS(VC(J)))
      DIF=100*(VC(J)-CALC)/VC(J)
      DFLG=100*(VLG-CALG)/VLG
      T=T+ST
      WRITE(6,530)VC(J),CALC,DIF,VLG,CALG,DFLG
  530 FORMAT(1H ,F10.2,1X,F10.2,2X,F9.5,3X,F7.4,3X,F7.4,3X,F9.5)
C
C
C       EXPERIMENTAL AND CALCULATED DATA WRITTEN
C
C
  550 CONTINUE
  600 STOP
      END
```

*